CHAPTER 4

RESULTS AND DISCUSSION

Part I Preformulation study of lycopene and carriers

1. Preliminary physicochemical properties of lycopene

1.1. Lycopene identification

Lycopene identification gave the results as following;

1.1.1. UV-visible (UV/Vis) analysis

Three absorption peaks were recorded at 445, 475, and 503 nm of which the maximum absorption peak is 475 nm (Figure 4-1-1). For a calibration curve, the dilutions of different concentrations of lycopene were prepared from a stock solution and assayed in triplicate from 300 to 600 nm. The calibration curve was obtained by plotting the absorbance of lycopene solution *versus* their concentration (µg/mL) and performing linear regression analyzes. Equation of the type $y = m \times x$ were obtained, where y is the absorbance, x the concentration of lycopene solution (µg/mL) and m the slope. The linearity (R^2=0.9973) of the method observed from UV/Vis spectroscopy was confirmed over the tested concentration range (2-12 µg/mL). An example for a calibration curve obtained during the validation process is shown in Figure 4-1-2.

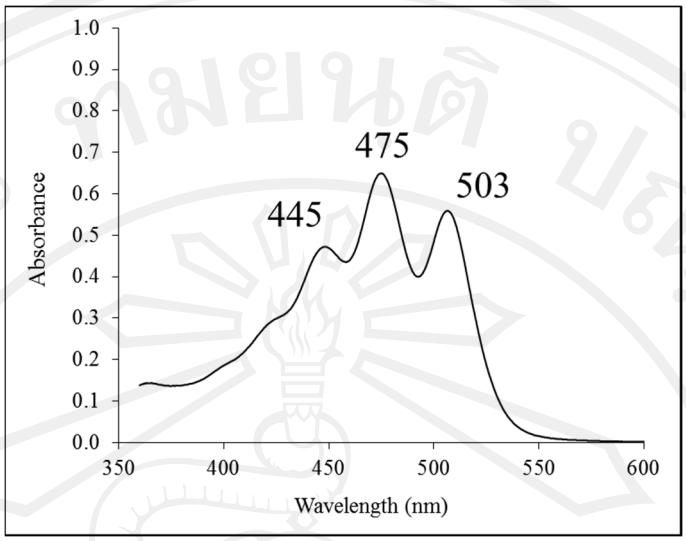

Figure 4-1-1 UV/Vis spectrum of lycopene standard solution.

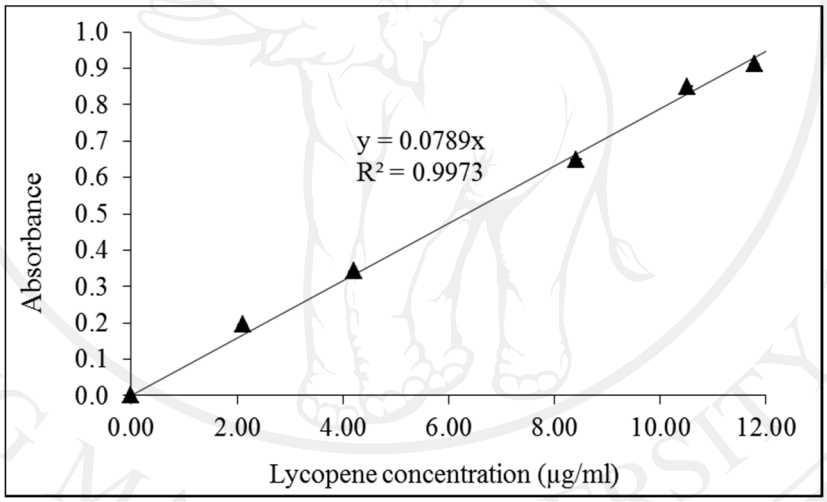

Figure 4-1-2 Calibration curve of lycopene by UV/Vis analysis.

1.1.2. HPLC analysis

The linearity of an analytical method is its ability to obtain test results which are directly proportional to the concentration of the analyte in the sample. Dilutions of different concentrations of lycopene were prepared from a fresh stock solution and assayed in triplicate. The calibration curve was obtained by plotting the area under the curve (AUC) of lycopene solution *versus* their concentration (µg/mL) and performing linear regression analyzes. Equation of the type $y = m \times x$ were obtained, where y is

the AUC, *x* the concentration of lycopene solution and *m* the slope. The linearity (R^2=0.9988) of the method observed from HPLC analysis was confirmed over the tested concentration range (1-5 µg/mL). An example for a calibration curve obtained during the validation process is shown in Figure 4-1-3. Under the tested conditions, lycopene was eluted at retention time of about 11.4 min. A chromatogram of lycopene solution is shown in Figure 4-1-4. The method specifications for HPLC analysis are listed in Table 4-1-1.

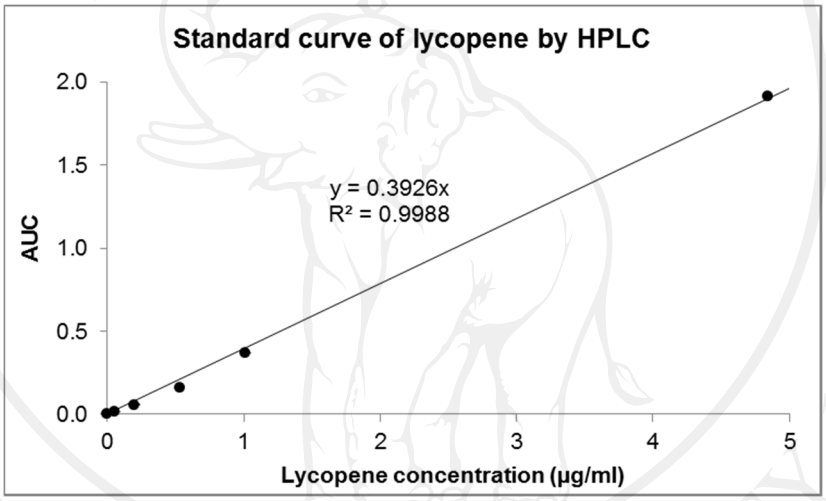

Figure 4-1-3 Calibration curve of lycopene by HPLC analysis.

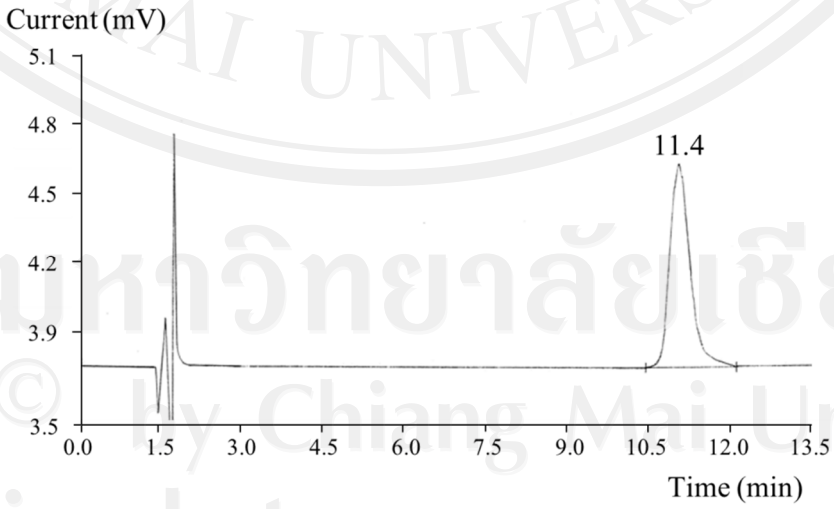

Figure 4-1-4 HPLC chromatogram of standard lycopene solution at 1 µg/mL.

Table 4-1-1 The resulted suitable HPLC condition.

Parameter	Specification
Column	Eurosphere-100 C18 (5 µm) endcapped 250x 4.6 mm column
Mobile phase	MeOH/THF/Water = 60/33/7 %v/v
Sample solvent	THF
Flow rate	1.5 mL/min
Temperature	25ºC
Detector	UV visible at 475 nm
Injection volume	20 µL
Specificity	Retention time about 11.4 min
Measurement time cycle	13.5 min
Linearity	$R^2 = 0.9988$
LOD	0.058 µg/mL
LOQ	0.2 µg/mL
Accuracy (intraday assay)	93.97 %
RSD (intraday assay)	2.03 %
Range	0.2 – 4.8 µg/mL

1.2. Solubility

To load lycopene in the NLC with a dose as high as possible, a lipid screening was performed by determining the solubility of lycopene in melted solid lipids. Table 4-1-2 shows the solubility in different solid lipids. Orange wax was superior to enhance solubility of lycopene when compared to mango butter, having 2.53 folds

higher solubility at room temperature. The solubility of lycopene in the melted beeswax was lower by 2.82 folds, by 5.88 folds lower for cetylpalmitate, and by 9.45 folds lower for Dynasan^{TM} 118.

Table 4-1-2 Solubility of lycopene in melted solid lipids at room temperature after heating at 80°C.

Solid solvent	Solubility (mg/g)
Orange wax	12.00
Mango butter	4.75
Beeswax	4.25
Cetylpalmitate	2.04
Dynasan 118	1.27

Besides solid lipids, the liquid lipids, surfactants, and organic solvents were also investigated as possible solvents. Table 4-1-3 showed the different solubility of lycopene in liquid lipids, surfactants, and organic solvents. Due to the lipophilic character of lycopene, solubility in polar solvents such as water, PBS pH 7.4, Transcutol^{TM} P and glycerin was not possible.

Table 4-1-3 Solubility of lycopene in organic solvents at room temperature and in liquid lipids and surfactants at room temperature after heating at 80°C.

Liquid solvents	Solubility (mg/mL)
Rice bran oil	4.175
Pomergranate seeds oil	4.045
Sesame oil	0.760

Table 4-1-3 (Cont.)

Liquid solvents	Solubility (mg/mL)
Myristol™ 318	0.745
Safflower oil	0.420
Cranberry oil	0.399
Broccoli oil	0.396
Lorbeer tree oil	0.388
Chloroform	0.380
Miglyol™ 812	0.265
Tetrahydrofuran (THF)	0.230
Olive oil	0.212
Soybean oil	0.197
Triolein	0.145
Oleic acid	0.119
Labrasol™	0.093
Avocado oil	0.087
Hexane	0.080
Macadamia oil	0.075
Toluene	0.073
Almond oil bitter	0.060
Tween™ 80	0.056
Acetone	0.048
Lycosol™	0.040

Table 4-1-3 (Cont.)

Liquid solvents	Solubility (mg/mL)
Isopropyl myristate	0.038
Span™ 80	0.037
Triton™ X100	0.035
Propylene glycol	0.017
Mineral oil	0.015
Acetonitrile	6.67×10^{-3}
Methanol	4.36×10^{-3}
95% Ethanol	4.00×10^{-3}
Dimethyl sulfoxide (DMSO)	2.70×10^{-3}
Water	Insoluble
PBS pH 7.4	Insoluble
Transcutol P	Insoluble
Glycerine	Insoluble

1.3. Thermal analysis

Figure 4-1-5 shows a DSC thermogram of lycopene compound obtained by heating and cooling the sample from 0°C to 200°C and 200°C to 0°C. The endothermic peak with a peak maximum at 171.03°C, obtained in the heating curve only, indicates the melting point of lycopene compound. The exothermic peak with a peak maximum at 135.19°C, obtained in the cooling curve only, indicates the re-crystallization temperature of lycopene compound.

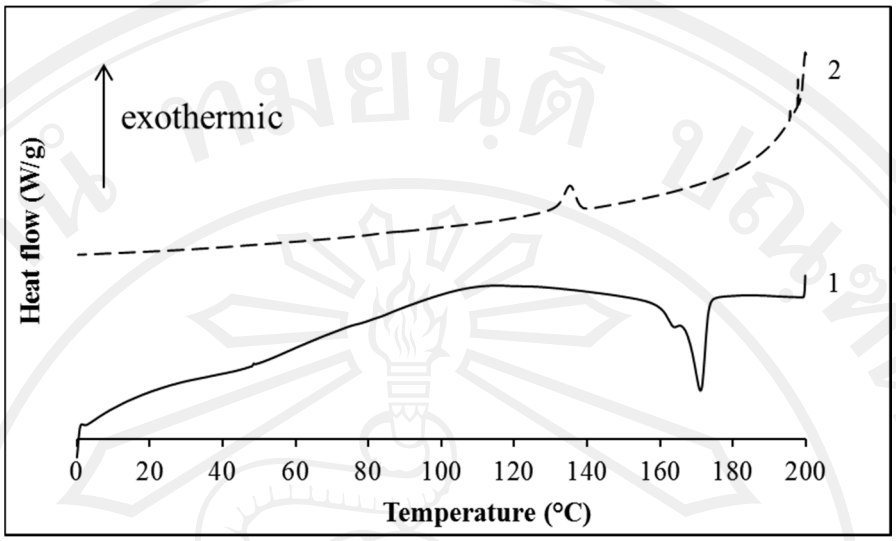

Figure 4-1-5 DSC heating (1) and cooling (2) curves of lycopene compound.

1.4. Crystalline characterization

Figure 4-1-6 showed the diffraction pattern of a crystalline phase consisting of a series of peaks. A series of sharp peaks reflected that many small crystals are exposed to the X-ray beam. WAXS pattern of lycopene exhibits sharp peaks at 2θ scattered angles 2.64°, 5.16°, 21.44°, 24.40°, and 29.32°, indicating the crystalline nature of this active compound.

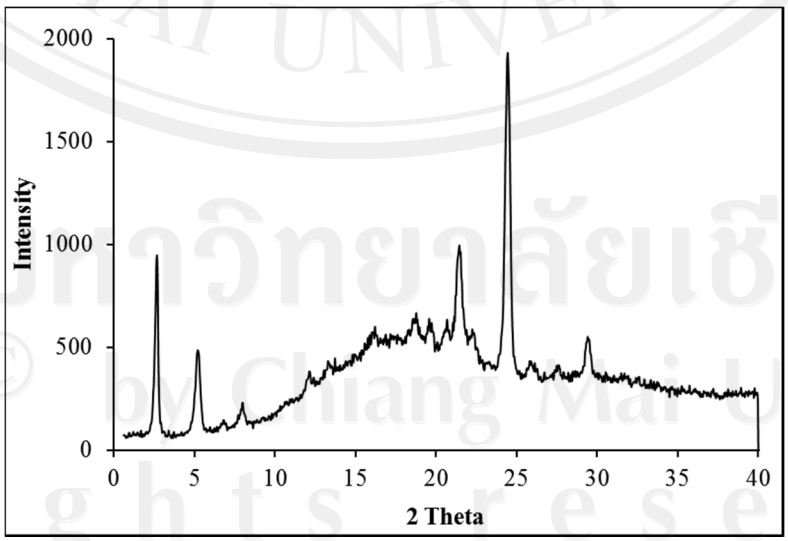

Figure 4-1-6 WAXS pattern of lycopene powder.

1.5. Morphology

Lycopene is extracted from *Lycopersicon esculentum* milled from fruit parts. It is red-brown crystal powder with characteristic odor. The purity of lycopene that is used in this study is 90.25%, and a density is between 45-55 g/100 mL (Lycopene COA, 2009). Figure 4-1-7 shows the appearance of lycopene powder captured by a digital camera. It presents in dark reddish-brown powder form. Lycopene dispersed in rice bran oil responded as a red plain texture under LM as demonstrated in Figure 4-1-8 (A) which reveals that lycopene is responsible for red pigments. However, the crystalline characteristics of lycopene can be seen under PLM as the bright sparkle brighten from the dark background as shown in Figure 4-1-8 (B). The crystal of lycopene was seen by long deep red needles shape. This finding (the crystalline nature of lycopene) was later confirmed by DSC and WAXS data.

Figure 4-1-7 Physical appearance of lycopene powder.

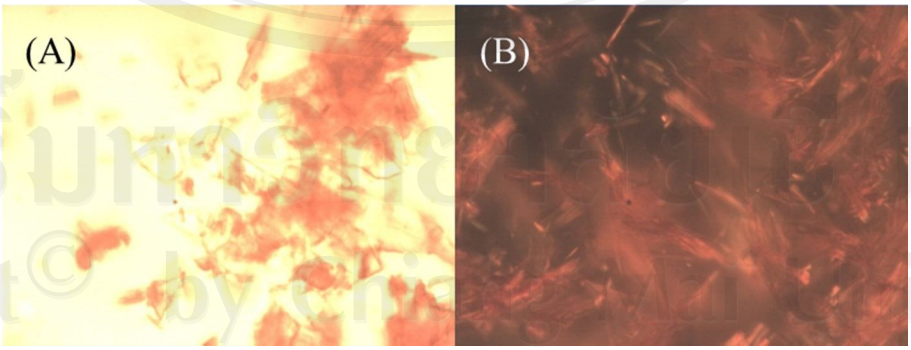

Figure 4-1-8 LM picture (A) and PLM picture (B) of lycopene powder suspended in rice bran oil with magnification of 100x10 folds.

1.6. Biological action (antioxidant activities)

1.6.1. ABTS assay

As the reaction between ABTS solution and potassium persulfate react stoichiometrically at a ratio of 1:0.5, respectively, the absorbance was unable to reach the maximum and unstable until more than 6 h has elapsed. Therefore, the mixture must be stand for 12-16 h in the dark at room temperature before use to complete the oxidation reaction of ABTS (Re and others, 1999). The oxidation of ABTS with potassium persulfate generated a stable ABTS radical monocation ($ABTS^{\bullet+}$) which has a blue-green chromophore absorption at 734 nm. Figure 4-1-9 helps to understand the formation of $ABTS^{\bullet+}$. The mechanism of free radical scavenging by antioxidants is *via* hydrogen donation. By this action, the antioxidants convert free radicals to more stable products which lead to the termination of the oxidation process. Hence, the antioxidant capacity is determined by the decolorization of ABTS solution, which means, the decreasing of absorbance measured at 734 nm indicates the reduction of $ABTS^{\bullet+}$ radical. In this study, a suitable period of time for the reaction was also studied.

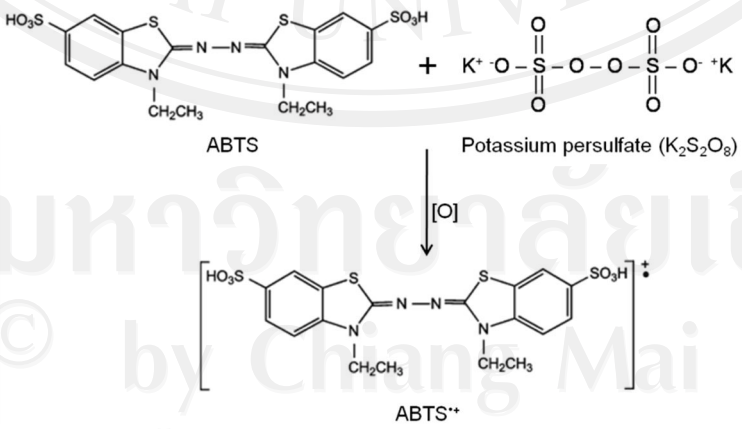

Figure 4-1-9 Formation of $ABTS^{\bullet+}$ (Moon and Shibamoto, 2009) with some modifications.

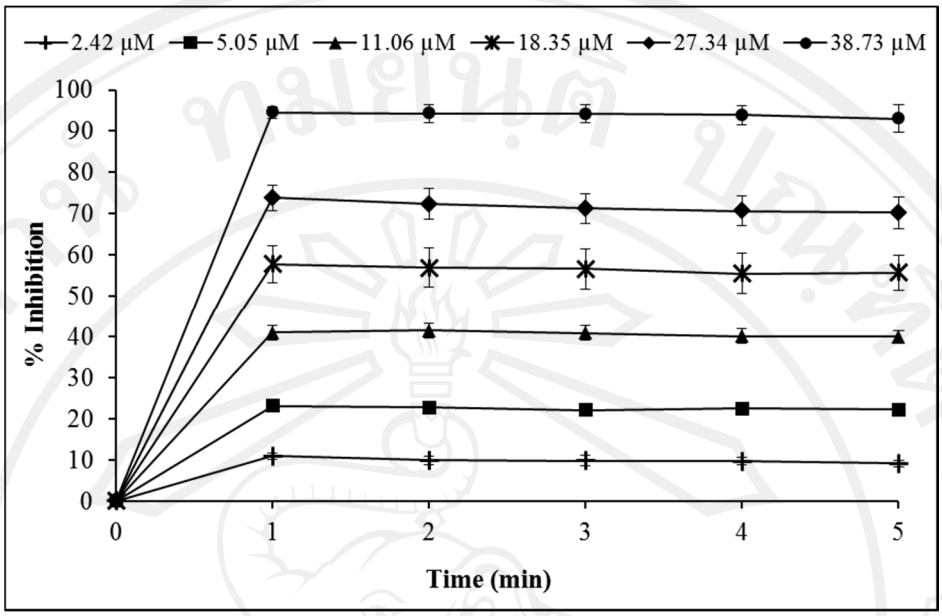

Figure 4-1-10 %Inhibition of standard Trolox™ solution which varies the concentrations and reaction time.

The solvent for lycopene is acetone which is very volatile and this makes the volume of different time point is not equal, thus the absorbance is changed by changing of the volume. The specific time of reaction is assumed to have the equal volume. However, in this observed, %inhibition is constant at reaction time of 3 min (Figure 4-1-10). Thus, the specific reaction time of 3 min was selected for further investigation. Calibration curve of Trolox™ (Figure 4-1-11) is used for calculation of TEAC value. This value is defined as a concentration of a Trolox™ solution whose the antioxidant capacity is equivalent to 1 mg of tested sample. The plot of %inhibition *versus* the concentration showed a linear regression with $y = 4.2841x$ ($R^2 = 0.9965$). The TEAC value of lycopene is 2646.219±3.802 µM which means the antioxidant capacity of 1 mg of lycopene is equivalent to 2646.219±3.802 µM Trolox™ solution concentration. In comparing of TEAC, the higher TEAC value

indicates the higher antioxidant capacity. The IC_{50} value of lycopene is 0.022±0.000 mg/ml which means lycopene 0.022 mg/mL could scavenge $ABTS^{\bullet+}$ radical in the solution by 50%.

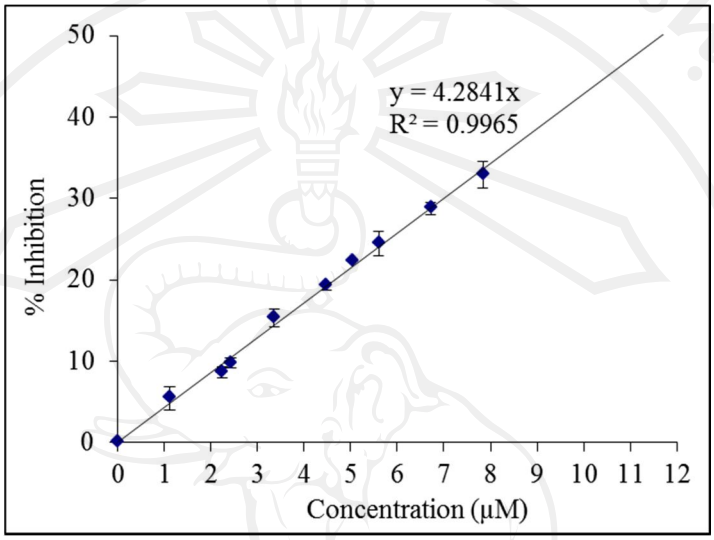

Figure 4-1-11 Standard calibration curve of Trolox™ solution at concentration of 2-39 µM at reaction time of 3 min.

1.6.2. DPPH assay

This assay is one of the most popular antioxidant assay world widely used due to its simple and highly sensitive. DPPH radical (organic nitrogen radical) is one of few stable radicals which are commercially available on the market. DPPH radical strongly absorbs at 517 nm (purple). In this study, the absorbance was measured at 540 nm due to the limitation of an instrument to reflect the amount of DPPH radical remaining in the solution. Figure 4-1-12 helps to understand more in mechanism of action by antioxidants in DPPH assay. At initial, a stable radical is purple and absorb at 517 nm. Antioxidants tested by this assay must have a hydrogen atom donor property. When an unpaired electron of DPPH is accepted hydrogen atom from

antioxidants, DPPH became to a reduced form (DPPH-H) resulting in changing color of DPPH radical from purple to yellow solution. Measuring the absorbance at 517 nm can indicate the disappearance of DPPH radical in the tested sample and reflect the amount of DPPH radical remaining, which is proportional to an antioxidant power (Antolovich and others, 2002). The radical scavenging activity was expressed as the IC_{50} which is defined as a concentration of tested samples required for scavenging DPPH radical in the solution by 50% (Tachakittirungrod and others, 2007a). The IC_{50} value of lycopene was found to be 0.078 ± 0.001 mg/mL which means 0.078 ± 0.001 mg/mL of lycopene is required for scavenging DPPH radical in the solution by 50%. As described definition, the lower of IC_{50} value is, the higher potential antioxidant of scavenging DPPH radical will be, which means, less amount of antioxidant will be used for scavenging 50% of DPPH radical in the solution. The mechanism of antioxidant activities of lycopene is *via* the free radical scavenging by hydrogen atom donation.

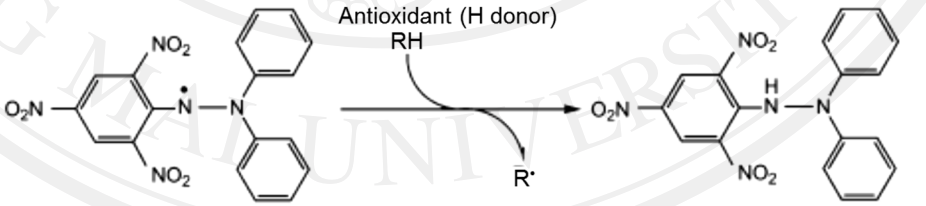

Figure 4-1-12 Mechanism of action by antioxidants on DPPH radical in DPPH assay (Moon and Shibamoto, 2009) with some modifications.

1.7. Stability of lycopene

As an acyclic chemical structure of lycopene presented in Figure 2-7, lycopene possesses symmetrical planarity and has no vitamin A activity, and as a highly

conjugated polyene, it is particularly susceptible to oxidative degradation. Physical and chemical factors known to degrade other carotenoids, including elevated temperature, exposure to light, oxygen, extremes in pH, and molecules with active surfaces that can destabilize the double bonds, were applied to lycopene as well. Figure 4-1-13 represents the degradation of lycopene when exposed to light and oxygen for 7 days. The color of lycopene changes from deep dark red to light orange-yellow color. It has been known for many years that carotenoids ‘‘bleach’’ i.e., lose their color, when exposed to radicals or to oxidizing species. The bleaching process of lycopene involves interruption of the conjugated double bond system either by cleavage or by addition to one of the double bonds (Krinsky and Yeum, 2003). The WAXS pattern of degraded lycopene (Figure 4-1-14) was totally different compared to the original one. The typically sharp peaks at 2θ scattered angles 2.64°, 5.16°, 21.44°, 24.40°, and 29.32° were disappeared. This result also demonstrated the lost of its properties i.e. its crystalline characteristic.

Figure 4-1-13 Outer appearance of original lycopene powder (A) and degraded lycopene powder (B) under exposed to light and oxygen after 7 days at room temperature.

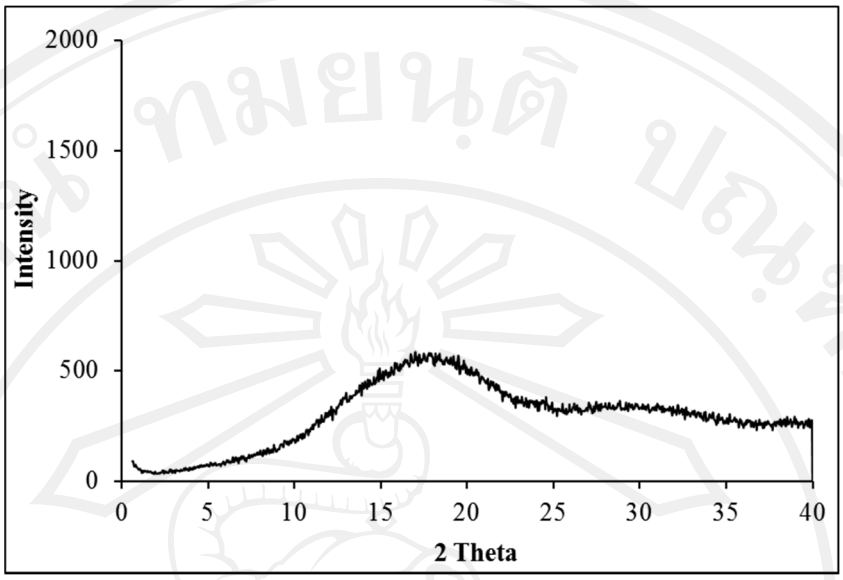

Figure 4-1-14 WAXS pattern of degraded lycopene powder.

2. Preliminary physicochemical properties of carriers (solid lipids and liquid lipids)

2.1. Physicochemical properties of solid lipids

2.1.1. Orange wax

The orange wax was selected to represent the solid lipid in this study because its benefits to skin and its multi-functional properties which make it suitable for cosmetic applications. It is a solid biodegradable lipid from the fruit peel of Citrus. It is acceptable for cosmetic use in the United States, Europe, and Japan. It was reported to have many activities such as sunscreen-enhancing, antioxidant, antimicrobial and anti-inflammatory properties (Reynhardt and Riederer, 1991; Puleo and Rit, 1992). The main constituents of orange wax are unsaturated monoesters, hydroxy-monoesters, free fatty acids (C12-C26), hydrocarbons (C21-C33), sterol esters, free sterols, free alcohols, carotenoids, glycolipids, phospholipids, and flavonoids (Puleo and Peters, 1994). Orange wax can be classified as a skin friendly solid lipid material since its lipid composition is similar to that of skin. It is light reddish-brown to orange

in color, depending on the level of refinement (Figure 4-1-15). The external structure of orange wax texture observed by LM showed various small sizes of granule-like spherical shape without crystalline structure as presented in Figure 4-1-16 (A). An anisotropic molecular organization material showing birefringent under PLM indicates the crystalline characteristic formation (Whittaker and others, 1989). In contrast, the majority materials without crystalline forms showed no birefringent and appeared dark screen under the PLM. The optical properties of the birefringent materials provide a means of assessing their molecular organization. In the present study, under PLM, the crystalline nature of orange wax was noticed as the bright sparkle brightens from the dark background as shown in Figure 4-1-16 (B). This result demonstrated the crystalline nature of this lipid. These findings were later confirmed by DSC and WAXS analysis.

Figure 4-1-15 Physical appearance of orange wax.

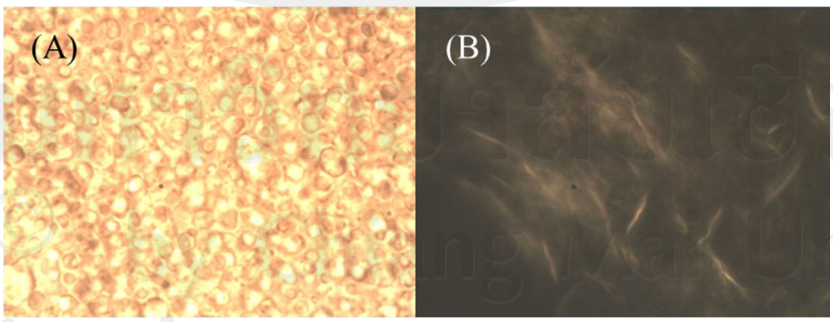

Figure 4-1-16 LM picture (A) and PLM picture (B) of orange wax with magnification of 100x10 folds.

Figure 4-1-17 shows a DSC thermogram of orange wax obtained by heating and cooling the sample twice from 20°C to 80°C and 80°C to 20°C. Table 4-1-3 provides a summary of the obtained thermal events. The endothermic broaden peak with a peak maximum at 50.66°C, obtained in the first heating curve indicates the melting point of orange wax was between 35°C and 60°C. In the second heating curve the same polymorph of this wax was obtained. In both cooling curves the re-crystallization of this modification took place. The obtained data reviewed that this wax can return to solid after heat process was ceased and could be used as a solid lipid substance again.

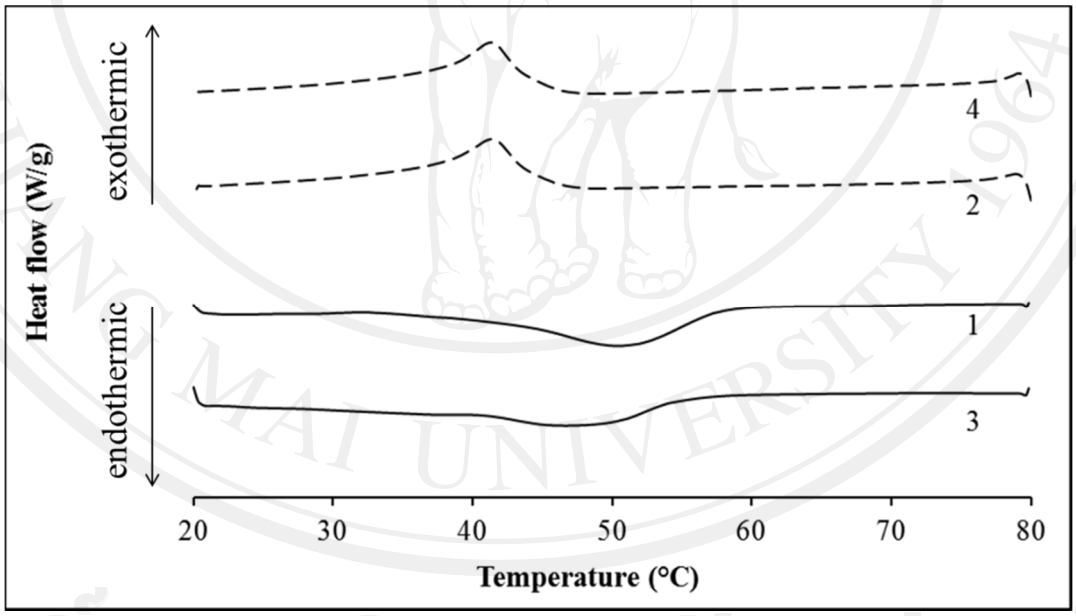

Figure 4-1-17 DSC 1st heating (1), 1st cooling (2), 2nd heating (3) and 2nd cooling (4) curves of orange wax.

Table 4-1-4 Thermal events observed in DSC analysis of orange wax shown in Figure 4-1-17.

Peak No.	Action	Thermal effect	Onset (°C)	Melting point/ Crystallinity temp(°C)	Enthalpy (J/g)	Area (mJ)
1	1st heating	endothermic	40.24	50.66	14.24	19.62
2	1st cooling	exothermic	44.72	41.35	12.32	16.97
3	2nd heating	endothermic	35.91	47.33	14.10	19.43
4	2nd cooling	exothermic	44.51	41.35	12.28	16.92

The WAXS pattern of orange wax was shown in Figure 4-1-18. Orange wax revealed the typical reflections at 21.32º and 23.12º corresponded to the d-spacing values of 0.41 and 0.38 nm, respectively. According to Larsson short spacings of the triglycerides (Larsson, 1966), these results can be applied with and described as the lattice spacings of 0.42-0.43 nm and 0.37-0.40 nm correspond to β′ modification with orthorhombic perpendicular subcell unit.

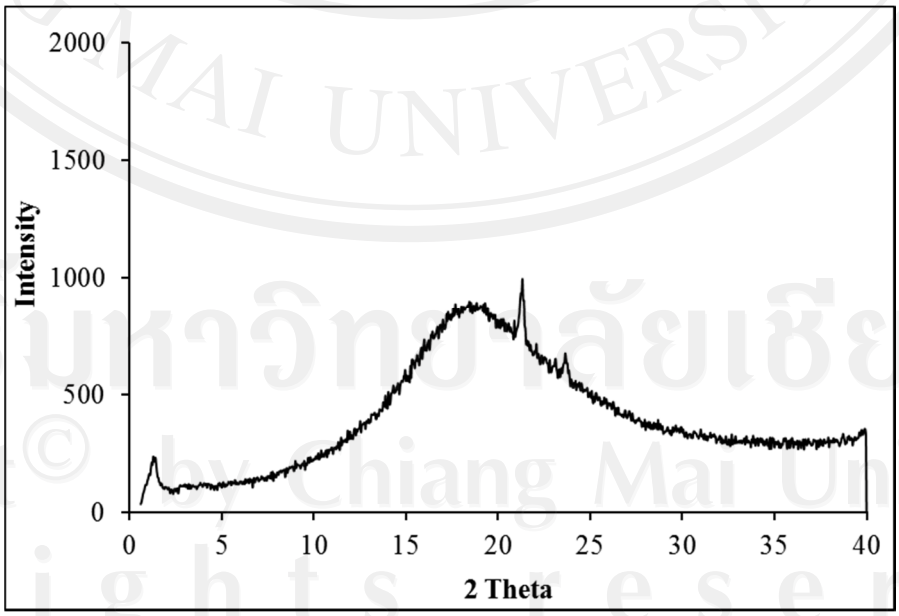

Figure 4-1-18 WAXS pattern of orange wax.

2.1.2. Mango butter

The appearance of mango butter is a soft pale yellow semi-solid fat with slightly fatty odor (Figure 4-1-19). Figure 4-1-20 revealed many obviously small crystals from mango butter. It can be categorized as a crystalline substance. This crystalline nature was later confirmed by DSC and WAXS. After incorporated lycopene into mango butter, the growth of crystals was observed in Figure 4-1-21. Its crystals are bigger and sharpen.

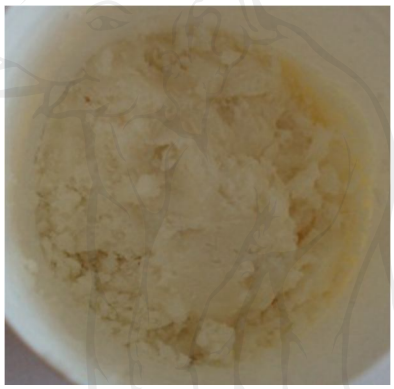

Figure 4-1-19 Physical appearance of mango butter.

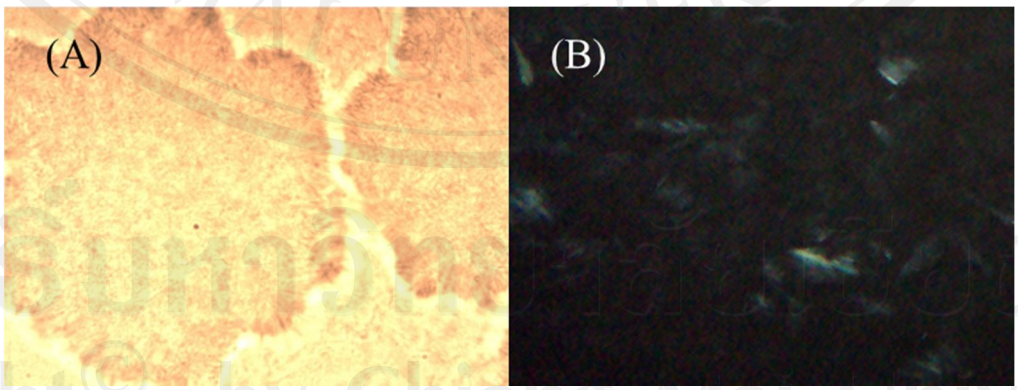

Figure 4-1-20 LM picture (A) and PLM picture (B) of mango butter with magnification of 100x10 folds.

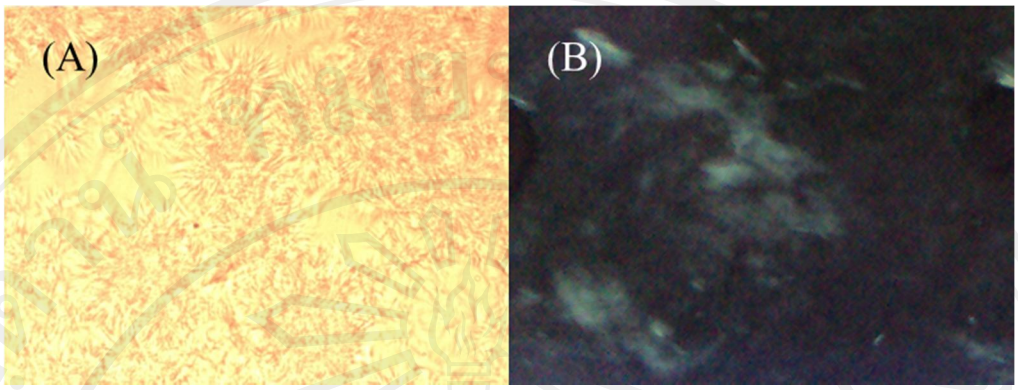

Figure 4-1-21 LM picture (A) and PLM picture (B) of the mixture of mango butter and lycopene with magnification of 100x10 folds.

Figure 4-1-22 showed the thermograms of fusion for mango butter and the crystallization thermograms of the same fat after being heated until complete fusion and then cooled down until complete crystallization twice from -100°C to 100°C and 100°C to -100°C. According to Hagemann (1988), vegetable origin lipids (fatty acids, acylglycerides, fats and oils) present polymorphism, and in general, and with more frequency, solidify in three different crystalline forms: α, β' and β, with correspondingly higher fusion temperatures. Polymorph α (lowest fusion point) is generally present after rapid cooling processes from melted fat. Form β', with a higher melting or fusion point than the previous one, is generated through solidification of fat under certain conditions of temperature or due to transition from the α form. Polymorph β, the most stable crystalline form, is produced from the other two forms by incubating at slightly higher fusion temperatures than for the α form. Mango butter is capable of existing in 6 polymorphic forms noted from I to VI in increasing order of melting points, applied with the nomenclature of Wille and Lutton (1966). In the first heating run, it is shown that, during fusion, there is melting point of Form IV (β'') at

22°C, Form V (β') at 30°C and Form VI (β) at 39ºC. In the second heating run mango butter revealed the melting point of the unstable gamma form (Form I) at -4ºC, the alpha form (Form II) at 9ºC, Form III at 17ºC and Form IV at 22ºC. The melting points of Form V and VI were disappeared after the first run. According to some authors (Wille and Lutton, 1966; Schlichter-Aronhime and Garti, 1988; Schlichter-Aronhime and others, 1988), Form III corresponds to a mixture of Forms II and IV and is not a separate crystalline variety. In several research studies, mango butter was reported that some of its characteristics showed resemblance to that of cacao butter. According to Sinko (2006) DSC of cacao butter, these results can be applied with and described that if mango butter is heated to the point at which it is completely liquefied (about 45ºC), the nuclei of the stable beta crystals are destroyed and the mass does not crystallize. From the stand point of production of SLN and/or NLC, they must be solid at room and body temperature to maintain their properties. Therefore, mango butter should be excluded from this study based on this primary screening and due to the limited solubility of lycopene in it.

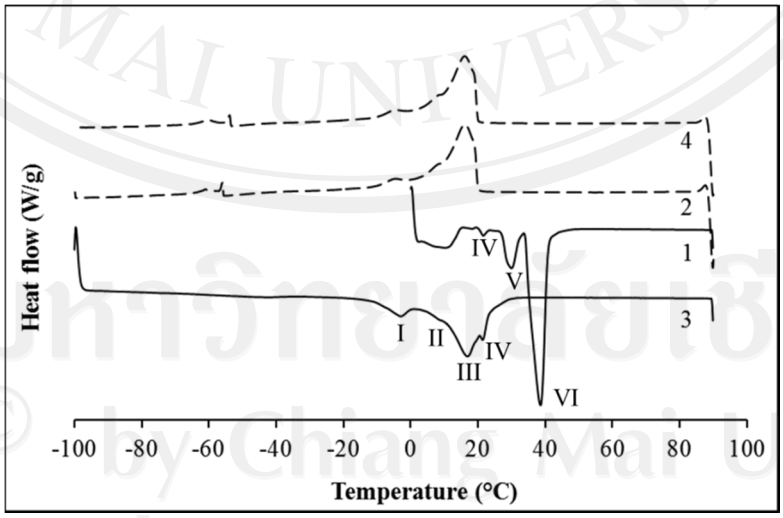

Figure 4-1-22 DSC 1st heating (1), 1st cooling (2), 2nd heating (3), and 2nd cooling (4) curves of mango butter (I-VI are existing polymorph forms).

Mango butter exhibits series of sharp peak at 2θ scattered angles 2.68°, 6.72°, 16.24°, 19.24° and 24.12° as seen in Figure 4-1-23. This result was in good agreement with PLM and DSC analysis and indicated the crystalline nature of mango butter.

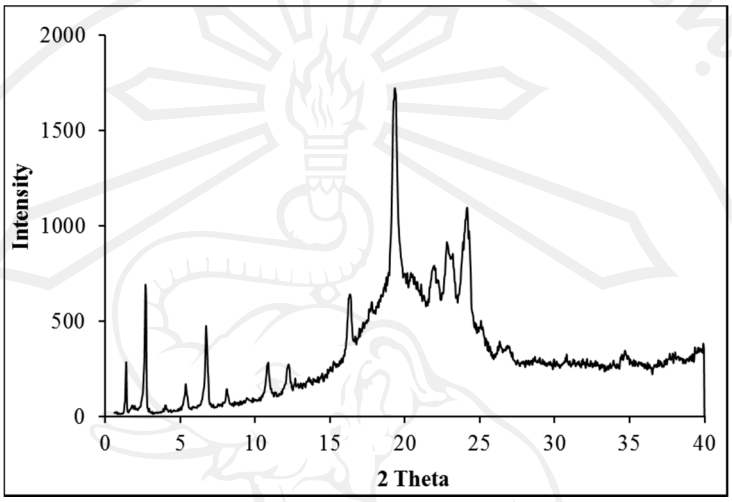

Figure 4-1-23 WAXS pattern of mango butter.

2.1.3. Beeswax

Figure 4-1-24 (A) and (B) showed morphology images of beeswax under LM and PLM, respectively. Adding the lycopene into beeswax, the crystalline characteristic of the lipid was clearly improved as seen in Figure 4-1-25. The red-brown color came from the color of lycopene.

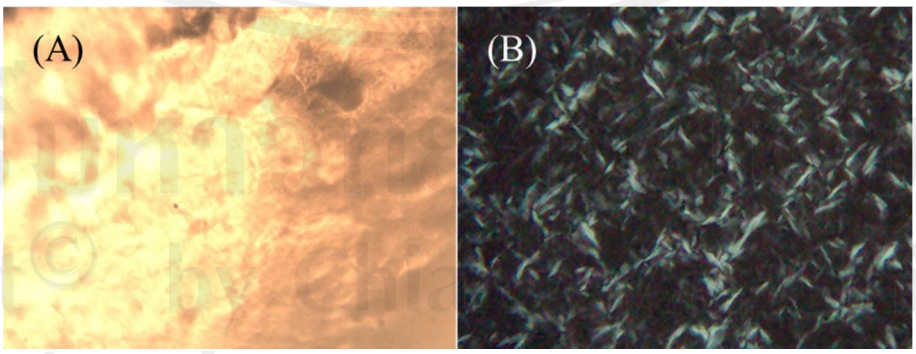

Figure 4-1-24 LM picture (A) and PLM picture (B) of the mixture of beeswax with magnification of 100x10 folds.

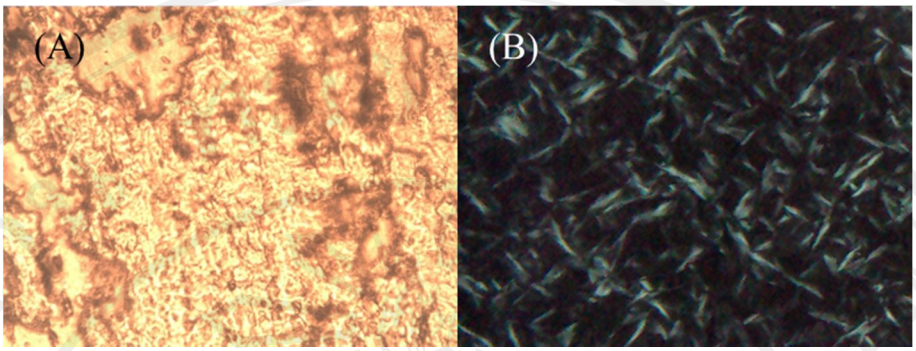

Figure 4-1-25 LM picture (A) and PLM picture (B) of the mixture of beeswax and lycopene with magnification of 100x10 folds.

Figure 4-1-26 shows DSC spectrums of beeswax obtained by heating and cooling the sample twice from -10°C to 100°C and 100°C to -10°C. Table 4-1-5 provides a summary of the obtained thermal events. As energy is applied to the sample, the curve is linear as long as the sample remains in the same phase (at baseline). Once the applied energy starts affecting intermolecular bonds, the curve leaves the baseline, representing the onset of melting of the material (phase change). Melting occurs over a temperature range and once the transition to the higher energy phase is complete, the curve returns to baseline. The endothermic broaden peak with a peak maximum at 64.06°C, obtained in the first heating curve indicates the melting point of beeswax between 40°C and 67°C. In the second heating curve the same polymorph of this wax was obtained. In both cooling curves re-crystallization of this modification took place. The obtained data reviewed that this wax can be solid after heat process and could be used as a solid lipid substance.

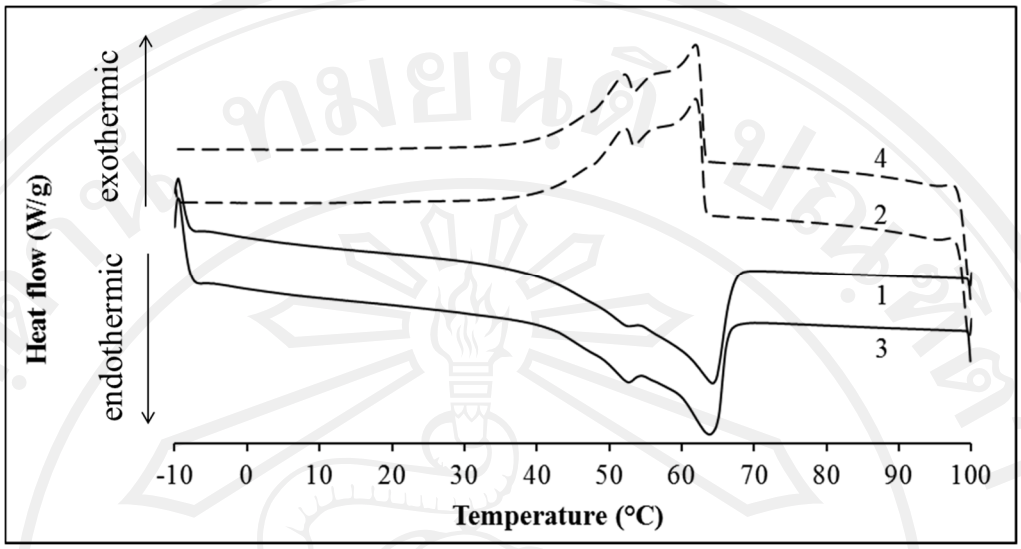

Figure 4-1-26 DSC 1st heating (1), 1st cooling (2), 2nd heating (3), and 2nd cooling (4) curves of beeswax.

Table 4-1-5 Thermal events observed in DSC analysis of beeswax shown in Figure 4-1-26.

Peak No.	Action	Thermal effect	Onset (°C)	Melting point/ Crystallinity temp(°C)	Enthalpy (J/g)	Area (mJ)
1	1st heating	endothermic	51.13	64.06	195.97	227.32
2	1st cooling	exothermic	63.35	61.92	179.46	208.17
3	2nd heating	endothermic	53.32	63.73	185.37	215.03
4	2nd cooling	exothermic	63.31	61.92	182.95	212.22

Beeswax exhibits sharp peaks at 2θ scattered angles 21.24° (d = 0.41 nm) and 23.64° (d = 0.38 nm) as seen in Figure 4-1-27. These results can be applied with and described as the lattice spacings of 0.42-0.43 and 0.37-0.40 nm correspond to β′ modification with orthorhombic perpendicular subcell unit due to Larsson short

spacings of the triglycerides (Larsson, 1966). The crystalline characteristic of beeswax from WAXS corresponded with PLM and DSC analysis.

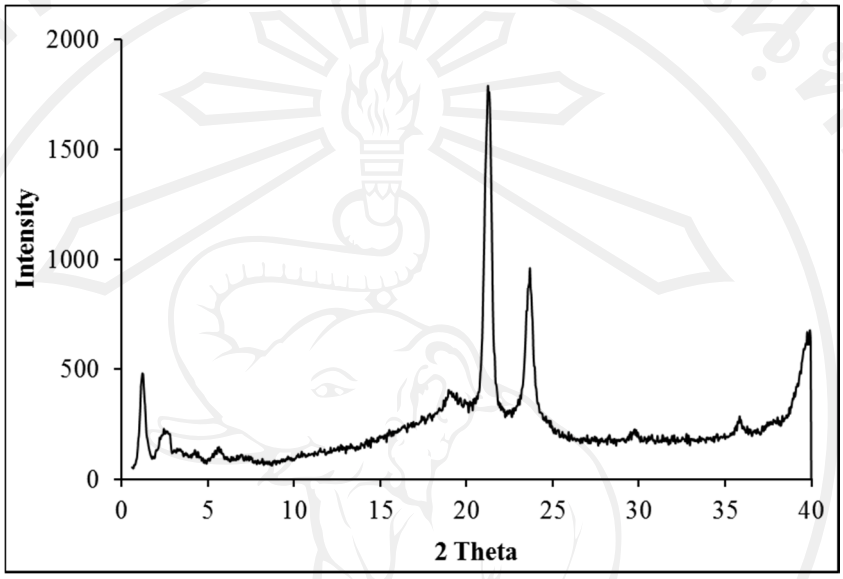

Figure 4-1-27 WAXS pattern of beeswax.

2.2. Physicochemical properties of liquid lipids

2.2.1. Thermal analysis

The DSC thermograms of the mixtures of orange wax and different liquid lipids were shown in Figure 4-1-28 revealed the melting point of these mixtures during 44-48°C. Surprisingly, admixing orange wax with rice bran oil and pomegranate seeds oil showed very broaden peaks which indicated extremely high solubility and compatibility of oils and orange wax. Based on these data and due to the solubility test, rice bran oil, pomegranate seeds oil and sesame oil were right selection for further studies.

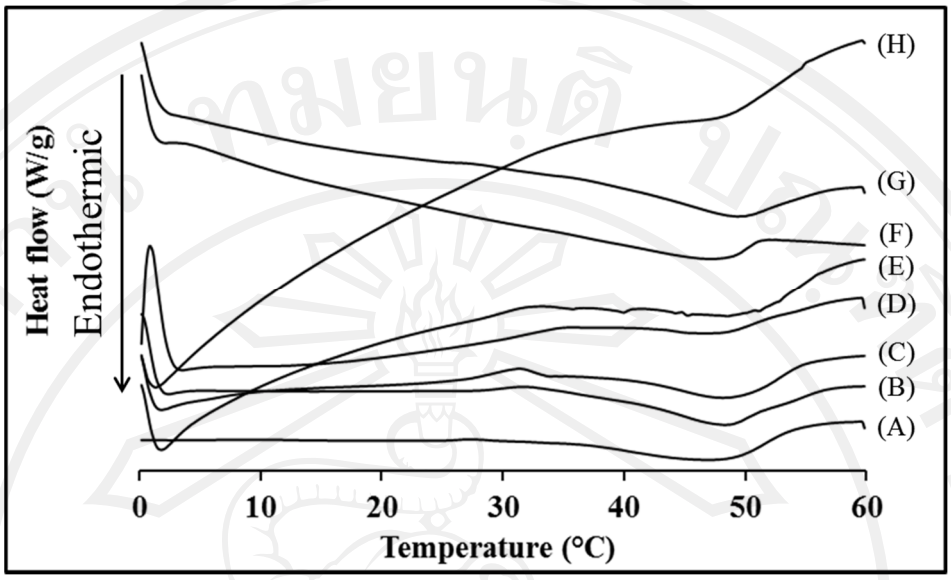

Figure 4-1-28 DSC thermograms of the mixtures of orange wax (90%) and different liquid lipids (10%); lycosol (A), broccoli (B), lorbeer tree (C), sesame (D), safflower (E), rice bran (F), pomegranate seeds (G), cranberry (H).

2.2.2. Antioxidant activities

2.2.2.1. ABTS assay

TEAC values presented in Table 4-1-6 demonstrated that all liquid lipids showed the free radical scavenging activities, but at the different levels. Among 3 selected original liquid lipids, rice bran oil possessed the highest antioxidant capacity through a highest TEAC value of 41.466 ± 1.638 μM/mg. After the incorporation of lycopene, the TEAC values of sesame oil and rice bran oil were increased, but except for pomegranate seeds oil which was decreased. When incorporating lycopene 0.069 %w/w into rice bran oil, the TEAC value was 1.001 times higher than the expected value due to the additional effect. When incorporating equal amount of lycopene into sesame oil, the TEAC value was 1.739 times higher than the expected value due to the

synergistic effect. The TEAC value of pomegranate seeds oil after incorporation of lycopene was 0.895 times lower than the expected value which may be due to the antagonistic effect.

Table 4-1-6 Summarization of TEAC values of different liquid lipids and liquid lipids contain the equal specific amount of lycopene.

Liquid lipids	TEAC (μM/mg)	
	absent of lycopene	present of lycopene
Sesame oil	4.623 ± 0.068	11.207 ± 0.209
Pomegranate seeds oil	20.423 ± 0.604	19.902 ± 3.961
Rice bran oil	41.466 ± 1.638	43.297 ± 0.583

The IC_{50} values of liquid lipids and liquid lipids containing lycopene were summarized in Table 4-1-7.

Table 4-1-7 Summarization of IC_{50} values by ABTS assay of different liquid lipids and liquid lipids contain the equal specific amount of lycopene.

Liquid lipids	IC_{50} (mg/mL)	
	absent of lycopene	present of lycopene
Sesame oil	12.626 ± 0.185	5.208 ± 0.098
Pomegranate seeds oil	2.859 ± 0.085	3.022 ± 0.677
Rice bran oil	1.414 ± 0.045	1.348 ± 0.018

It was found that the IC_{50} values for inhibition of $ABTS^{\bullet+}$ radical from the lowest derived from rice-lycopene, rice bran oil, pomegranate seeds oil, pomegranate

seeds-lycopene, sesame-lycopene, and sesame oil which were 1.348±0.018, 1.414±0.045, 2.859±0.085, 3.022±0.677, 5.208±0.098, and 12.626±0.185 mg/mL, respectively. When comparing pure lycopene with the liquid lipids, the highest antioxidant capacity against $ABTS^{\bullet+}$ radicals was from lycopene. Lycopene alone expressed very low IC_{50} value and also decreased IC_{50} values of liquid lipids (except for pomegranate seeds oil). Thus, it was clearly seen that lycopene could help to promote the antioxidant activities of liquid lipids observed from the decreasing of IC_{50} values. Among 3 studied liquid lipids (rice bran oil, sesame oil, pomegranate seeds oil), rice bran oil posed the highest antioxidant activity against $ABTS^{\bullet+}$ free radical. The rice bran oil, in general, showed high antioxidant activities due to the gamma-oryzanol compound contribute to antioxidant activity in rice bran oil (Vorarat and others, 2010).

2.2.2.2. DPPH assay

The IC_{50} values of different liquid lipids and liquid lipids contain lycopene were summarized in Table 4-1-8. The highest antioxidant capacity against DPPH radicals was from pomegranate seeds oil containing lycopene. For pomegranate seeds oil and rice bran oil, lycopene decreased the IC_{50} values in all of them. In contrast to these liquid lipids, lycopene in sesame oil increased IC_{50} value higher than IC_{50} value of sesame oil alone. However, the evidence in decreasing IC_{50} values of pomegranate seeds oil and rice bran oil indicated the enhancement of antioxidant activities of the original liquid lipids.

Table 4-1-8 Summarization of IC_{50} values by DPPH assay of different liquid lipids and liquid lipids contain the equal specific amount of lycopene.

Liquid lipids	IC_{50} (mg/mL)	
	absent of lycopene	present of lycopene
Sesame oil	15.965 ± 0.490	18.282 ± 0.112
Pomegranate seeds oil	4.544 ± 0.034	3.846 ± 0.287
Rice bran oil	6.208 ± 0.100	5.927 ± 0.311

<u>Part II</u> Optimization of formulations

1. Effect of surfactant

1.1. Effect of surfactant on contact angle

In the process of NLC production, the spreading of surfactant on the surface of oil droplet of lipid is one of the main reactions required for desirable NLC. One impact for this interaction is a contact angle, an angle of which creates at the point where the three phases composed of gas, liquid and solid meet (Xie and others, 2002). It is known that contact angle influences the spreading of liquid onto the solid substrate (Decker and others, 1999; Kwok and Neumann, 1999). In a meanwhile, there are very few systematic investigations of quantitative relation between surfactant solution and the spreading behavior on the solid lipids.

Five different surfactant solutions dropped on the solid surface composed of orange wax and lycopene oil solution demonstrated the different contact angle as shown in Figure 4-2-1. It was obviously seen that the smallest contact angle of 38° was obtained from C-1216 followed closely by Plantacare™ 1200 which showed the contact angle of 39°. The other three surfactants; C-1816, C-1616, and C-1815, exhibited their contact angle values higher than 45°. Considered the properties of surfactant, it was found that they are similar in basic properties. All five surfactants are non-ionic sugar ester. Four surfactants (C-1216, C-1616, C-1816, and Plantacare™ 1200) have the similar HLB value of 16, but except for C-1815 which have an HLB value of 15. No different contact angle between C-1815 and C-1816 indicated that HLB did not show the influence on the contact angle. Plantacare™ 1200 and C-1216, which had the same lipophilic tail, showed no different on the

contact angle as well. Therefore, the different contact angle obtained from these surfactants was considered to be due to the number of carbon atoms existing in the hydrophobic chain of each molecule.

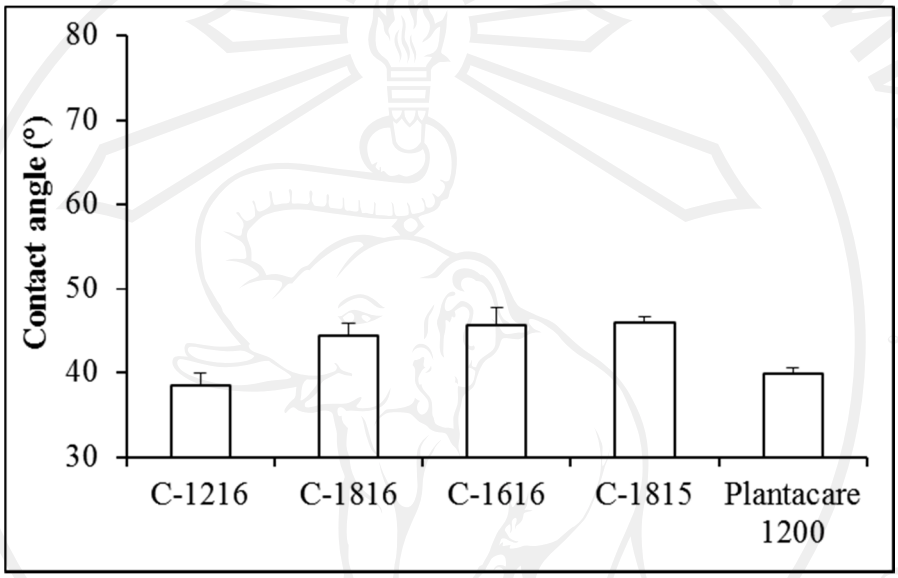

Figure 4-2-1 Contact angle between surfactant solutions and lipid surface of orange wax and lycopene mixture.

The chemical structure of C-1216 (sucrose laurate) and Plantacare™ 1200 (lauryl glycoside) as shown in Figure 4-2-2 indicates that these two surfactants have 12 carbon atoms in a molecule whereas the other surfactants such as sucrose stearate (C-1815 and C-1816) and sucrose palmitate (C-1616) possess 18 and 16 carbon atoms, respectively. It was considered that the surfactant with shorter hydrocarbon chain length of C12 was more appropriate to the surface of lycopene-orange wax than that of C15-C18. The contact angle was depended only on the number of carbon atoms existing in the hydrophobic chain.

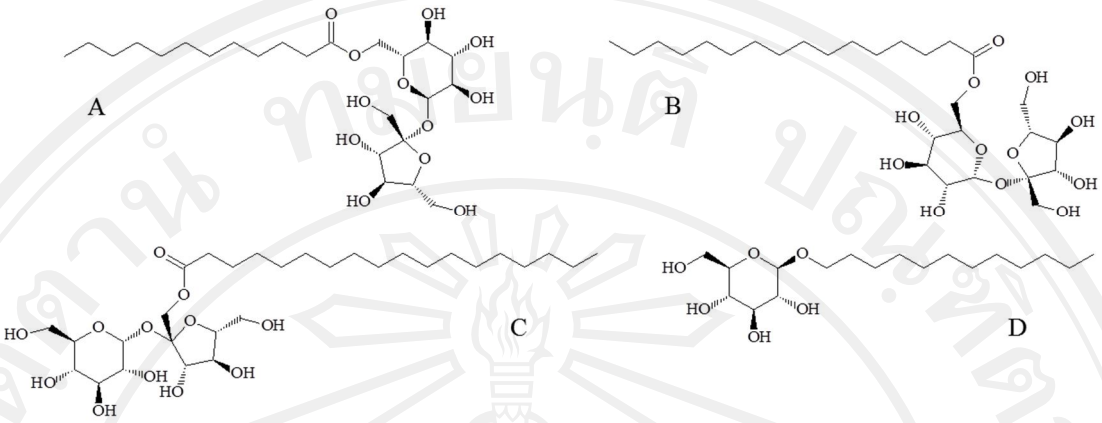

Figure 4-2-2 Chemical structures of sucrose laurate (A), sucrose palmitate (B), sucrose stearate (C), and lauryl glucoside (D).

1.2. Effect of surfactant on the particle size

The lycopene-loaded NLC formulations of five different surfactants were produced. The development of lycopene-loaded NLC in this study was expected to promote an additional biological action of both orange wax and lycopene as well as to enhance their bioavailability *via* NLC system. Moreover, lycopene was used as the oil solution in order to reduce the degree of crystalline organization of orange wax in lipid matrix after the process of NLC production. The results of this study revealed that the different five surfactants produced lycopene-loaded NLC with different size as shown in Figure 4-2-3. It was found that only two surfactants, C-1216 and Plantacare^{TM} 1200, could yield the extremely smallest size NLC with average particle size (z-ave) of approximately 170-190 nm. The NLC particles obtained from C-1616, C-1816, and C-1815 were obviously greater with z-ave of higher than 900 nm. Considering this effect with the contact angle values obtained from five surfactants previously mentioned, it was found that the contact angle value and the particle size of the NLC were closely related.

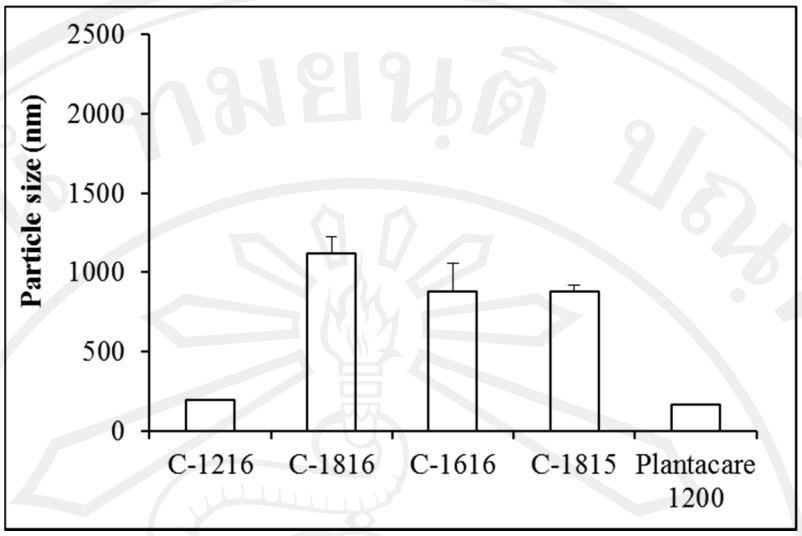

Figure 4-2-3 Particle size of lycopene loaded NLC stabilized by different surfactants.

The results demonstrated that the small particle size of lycopene-loaded NLC was obtained from the surfactants with small contact angle of less than 40°. According to the famous Young equation (Good, 1993), surfactant with lower surface tension gives the smaller contact angle. Moreover, a surfactant solution with lower surface tension can reduce more surface or interfacial free energy. Considered the data obtained from this experiment, it could be presumed that the small particle size of the lycopene loaded NLC obtained from the small contact angle surfactant was due to the high capacity in decreasing interfacial free energy between the two immiscible lipid and aqueous phases during emulsion forming process.

When compared the particle size of formulation using Plantacare^{TM} 1200 with the particle size of formulation using C-1216, it was found that Plantacare^{TM} 1200 gave the smaller particle size. Since the different between these 2 surfactants was only the hydrophilic head group, the smaller particle size of Plantacare^{TM} 1200 was due to the smaller surfactant's molecular size.

When the particle size of formulation using C-1216, C-1616 and C-1816 were compared, it was found that an increase in the particle size could be observed with the increasing number of C atom (longer C chain length) since these surfactants had the same hydrophilic head group. The different size of lipophilic tails lead to different in particle diameter. The longer lipophilic tail gave the bigger in particle size of formulation.

When the particle size of formulation using C-1815 was compared with C-1816, the particle size of C-1815 was different from the particle size of C-1816. These 2 surfactants had the different HLB values, therefore, the HLB of surfactant showed an influence on the particle size.

1.3. Effect of surfactant on the physical stability of the NLC

The NLC formulations obtained from C-1216 and Plantacare™ 1200 surfactants were further evaluated for their particle size, polydispersity index (PdI), and zeta potential (ZP) because they showed the lowest contact angle value and high ability to produce the smallest size lycopene loaded NLC. The results demonstrated that the mean particle size of the freshly prepared NLC of both formulations was not significantly different with z-ave approximately 170-190 nm. However, the PdI and ZP values of these particles were different. The PdI of lycopene loaded NLC obtained from C-1216 was 0.3 whereas that of Plantacare™ 1200 was 0.1. The ZP of the NLC obtained from C-1216 was -52 mV whereas that obtained from Plantacare™ 1200 was -62 mV. Keeping these formulations at 25°C for 30 days caused the ZP of the NLC obtained from C-1216 decreased to -47 mV whereas no significantly change of ZP in the NLC obtained from Plantacare™ 1200 as seen in Figure 4-2-4.

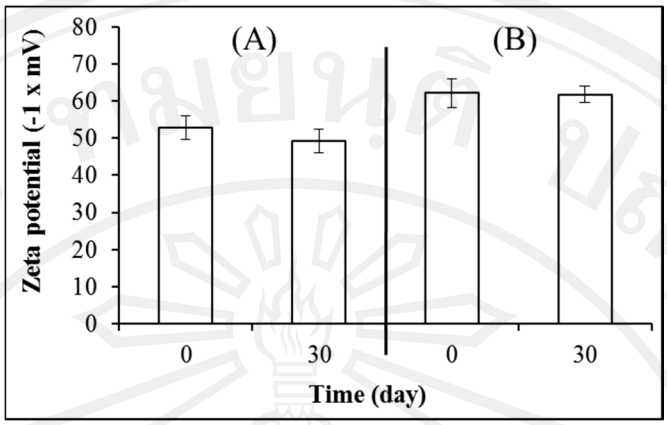

Figure 4-2-4 Effect of storage time on ZP of lycopene-loaded NLC stabilized by C-1216 (A) and Plantacare™ 1200 (B).

The particle size and PdI of the lycopene loaded NLC were observed in day 7, day 14, and day 30 in comparison with the time of freshly prepared (day 0). The results are shown in Figures 4-2-5 and 4-2-6, respectively. It was found that the particle size of the NLC obtained from C-1216 was increased obviously during 30 days of storage at room temperature whereas the size and PdI of that obtained from Plantacare™ 1200 showed no significantly changed. Therefore, the lycopene loaded NLC obtained from Plantacare™ 1200 revealed more stable than that from C-1216. The good narrow size distribution with constant small particle size of the NLC obtained from Plantacare™ 1200 throughout the period of 30 days might be due to the strong effect of Plantacare™ 1200 to produce extremely high ZP at the surface of the NLC system. The high ZP of the Plantacare™ 1200 based NLC was considered to be due to the hydroxyl ions caused by Plantacare™ 1200 molecules surrounding around the surface of the NLC nanoparticles. The high ZP resulted from the electrical charge on this particle surface repulsed with the charge from other particles, and therefore made a stable NLC system. This is the reason why the lycopene loaded NLC

stabilized by Plantacare™ 1200 showed higher stability overtime than those made from C-1216. The results of this investigation demonstrated the influence and mechanism of the surfactant on enhancing of NLC stability.

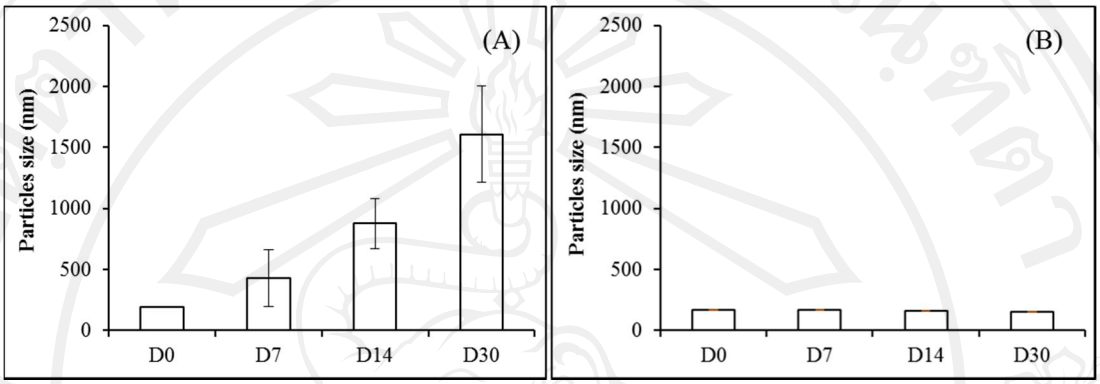

Figure 4-2-5 Effect of storage time on particle size of lycopene loaded NLC stabilized by C-1216 (A) and Plantacare™ 1200 (B).

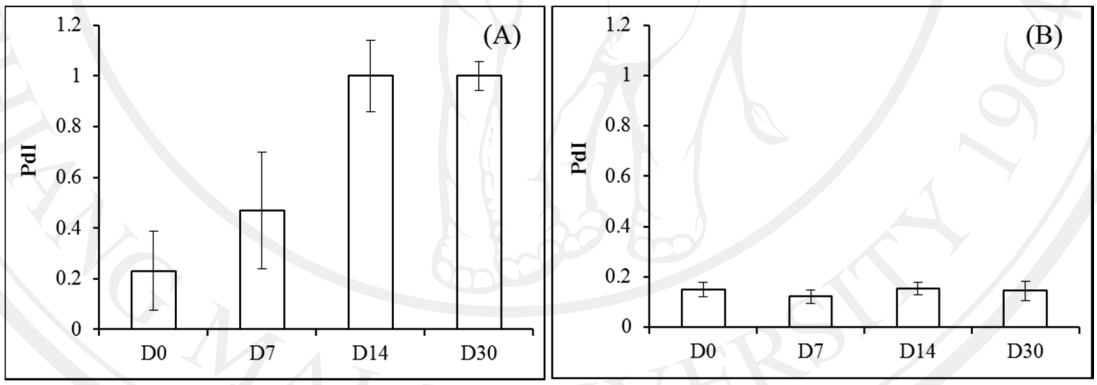

Figure 4-2-6 Effect of storage time on PdI of lycopene loaded NLC stabilized by C-1216 (A) and Plantacare™ 1200 (B).

From these results, it could be concluded that among 3 sucrose surfactants (C-1216, C-1616, C-1816), C-1216 yielded the smallest particle size due to its shortest C atom in molecule. Looking closely into the structure, two possible reasons are predicted. They are corresponding to the C atom in lipophilic tail and the head group size. The shorter C-chain lenght, the smaller the particle size obtained. Plantacare™

1200 yielded the smaller particle size than that of C1216 due to the smaller head group of glucose. Therefore, the size of hydrophilic head group and the amount of C atom in lipophilic tail show the great impacts on particle size obtained.

In this study, even though ZP values were so high, the observation by visualization found that the long-term stability of lycopene-loaded NLC stabilized by Plantacare^{TM} 1200 was quite poor. It lost integrity and aggregated after 2 months. According to very high ZP measured, a better stability was expected. However, these instabilities can be explained by bridging phenomena that some fatty acids and longer chain alcohols can cause (Kutz, 2001). Moreover, it might be due to destabilizing effects not accessible by a ZP measurement.

1.4. Chemical stability of the lycopene

The chemical stability of lycopene in the solution and in comparison with that loaded in the NLC was studied. The results revealed that lycopene in the solution decreased rapidly during the first 4 h of storage and further gradually decomposed as demonstrated in Figure 4-2-7 (A). The plot of log lycopene *versus* the storage time showed a linear regression with $y = 1.674 – 0.072x$ ($R^2 = 0.995$). It was found that the degradation profile of lycopene was extremely retarded when incorporated in the NLC stabilized by C-1216 and Plantacare^{TM} 1200 as shown in Figure 4-2-7 (B) and 4-2-7 (C), respectively. The plot of log lycopene during the storage time showed a linear regression with $y = 1.596 – 0.006x$ ($R^2 = 0.992$) and $y = 1.599 – 0.004x$ ($R^2 = 0.997$) for C-1216 and Plantacare^{TM} 1200 systems, respectively. These results suggested that lycopene in the samples followed a first order chemical degradation. The first order kinetic calculation demonstrated that the half life of lycopene in the solution was 9.6 h

whereas that entrapped in the NLC was 117.5 and 192.5 h stabilized by C-1216 and Plantacare™ 1200, respectively. This result revealed that lycopene was more chemically stable when was entrapped in the NLC.

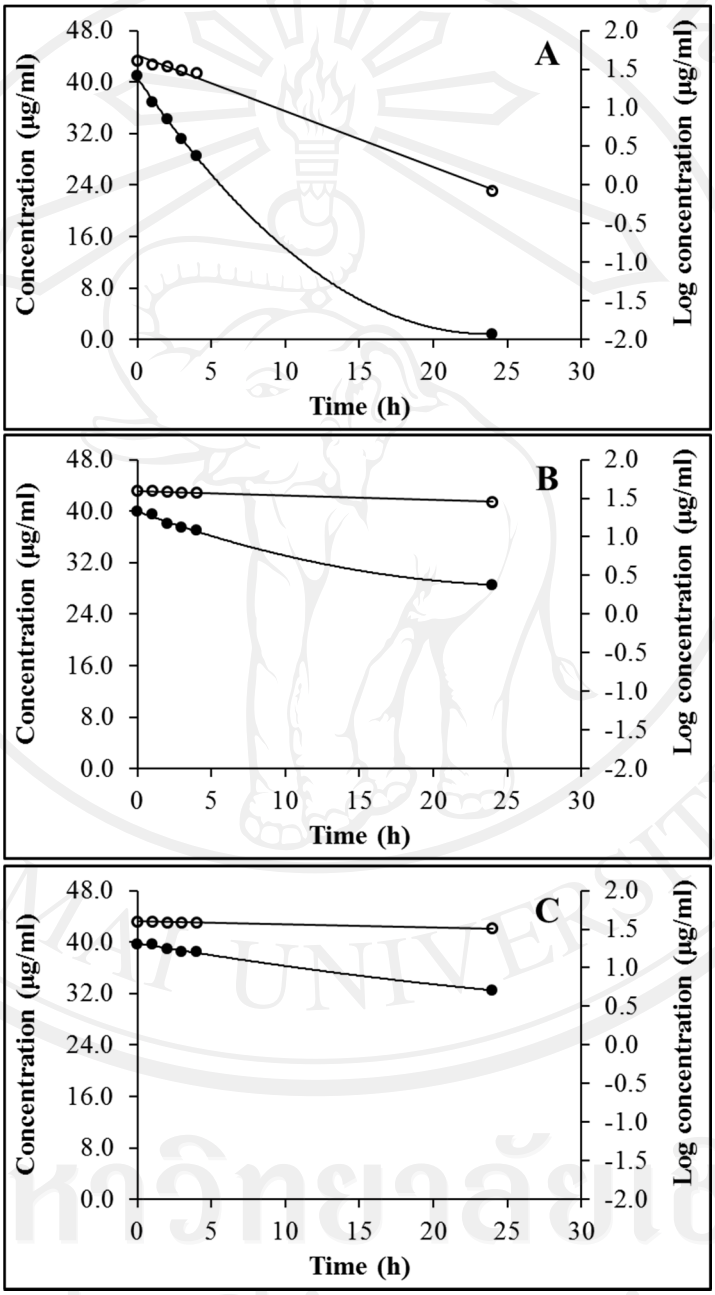

Figure 4-2-7 Stability profiles of lycopene concentration (●) and log concentration (○) in solution (A), C-1216 (B) and Plantacare™ 1200 (C) NLC dispersions.

2. Effect of different solid lipids

Orange wax, mango butter and beeswax were selected to study on the influence of lipid type. All formulations were stabilized with Plantacare™ 1200. Figure 4-2-8 provides the summary on particle size and PdI values during the period of 14 days. It was found that using orange wax yielded significantly smaller particle size than that of using mango butter and beeswax. There is no significant difference of PdI values among 3 solid lipids used. All PdI values were below 0.2 which indicated a good narrow size distribution with spherical shape. The larger particles observed from LD were obviously detected from formulations using mango butter and beeswax, as seen in Figure 4-2-9. ZP was similar for formulations of orange wax and beeswax, as demonstrated in Figure 4-2-10. Therefore, orange wax was selected for further investigation.

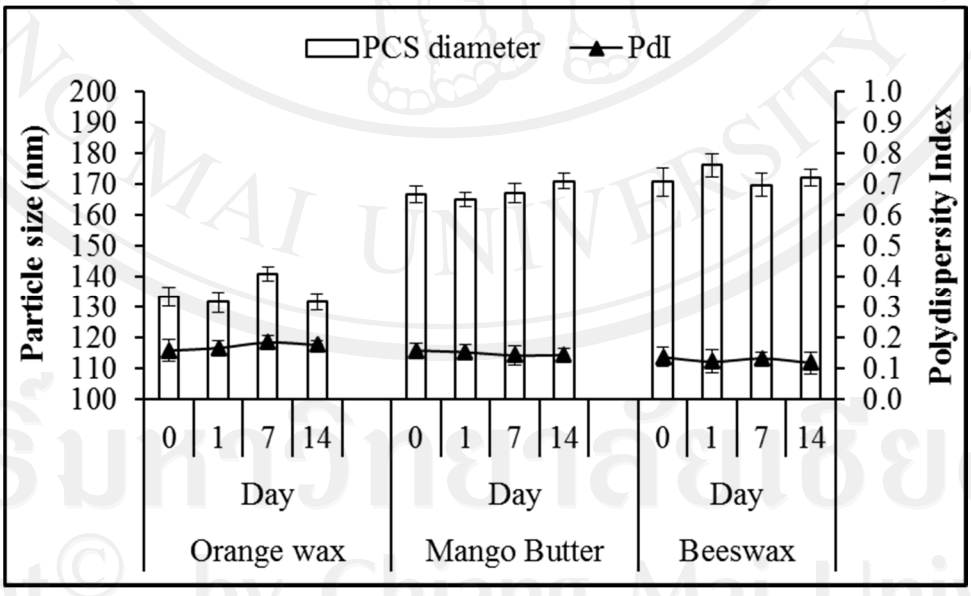

Figure 4-2-8 Average PCS diameters and PdI values of formulations using three different solid lipid types (orange wax, mango butter and beeswax) during the period of 14 days.

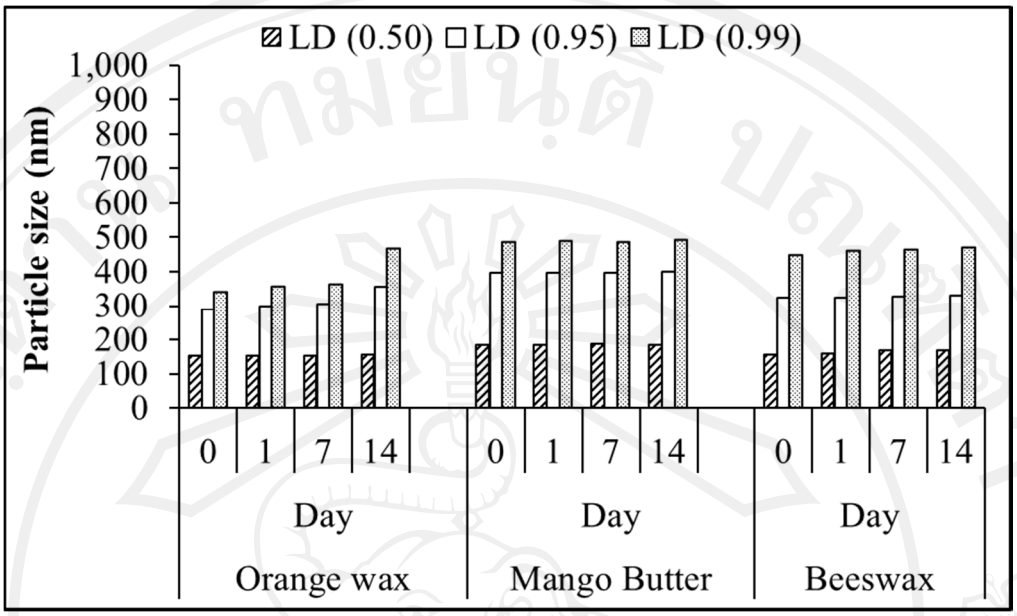

Figure 4-2-9 LD (0.50), LD (0.95) and LD (0.99) diameters of formulations using three different solid lipid types (orange wax, mango butter and beeswax) during the period of 14 days.

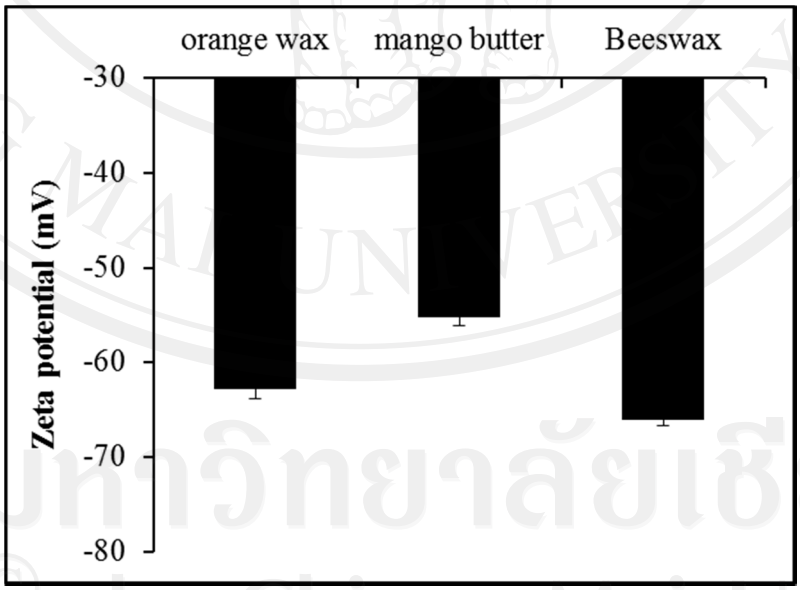

Figure 4-2-10 ZP values of formulations using three different solid lipid types (orange wax, mango butter and beeswax) using four different surfactants during the period of 14 days.

3. Effect of the amount of cycle and pressure

Figure 4-2-11 shows the average particle size and PdI measured by PCS. At 500 bar, the average particle diameter after cycle 1 was decreased about 25.2% and about 26.9% at 800 bar. Between cycle 2 and 3 a reduction of the particles size by 9 nm was found for 500 bar and 12 nm for 800 bar. After cycle 3 the particle remained constant for both formulations. With increasing cycle number, the PdI decreased. After 3 cycles a PdI of 0.1339 and 0.1342 was obtained for 500 and 800 bar, respectively. This indicated a narrow particle size distribution. The homogenization process reduced the mean particle size and simultaneously narrowed the width of the size distribution. During the homogenization process particles break at imperfections of their crystal structure. With a decreasing particles size, the number of imperfections is reduced. Therefore, the force required to break the particles increases with a decreasing particle size. This can be observed by a rather exponential decrease in particle size than a linear decrease in Figure 4-2-11. If the forces in the homogenizer are equal to the interaction forces in the crystal, no further decrease in particle size will be observed, even when additional homogenization cycles are applied. Figure 4-2-12 provided a summary of the LD (0.50), LD (0.95) and LD (0.99) values obtained after each production cycle for both pressure. With increasing cycle number a decrease in the LD values can be observed whereby the particle size decreased more between cycle 1 and 2 than between cycle 2 and 3. After 2 homogenization cycles the particle size of both pressure was well within the nanometer range. The presence of microparticles can be excluded (LD (0.99) = 0.535 μm for 500 bar; LD (0.99) = 0.510 μm for 800 bar). At 800 bar and 500 bar, the possessed identical particle sizes after 3 homogenized cycles were applied (Figures 4-2-11 and 4-2-12).

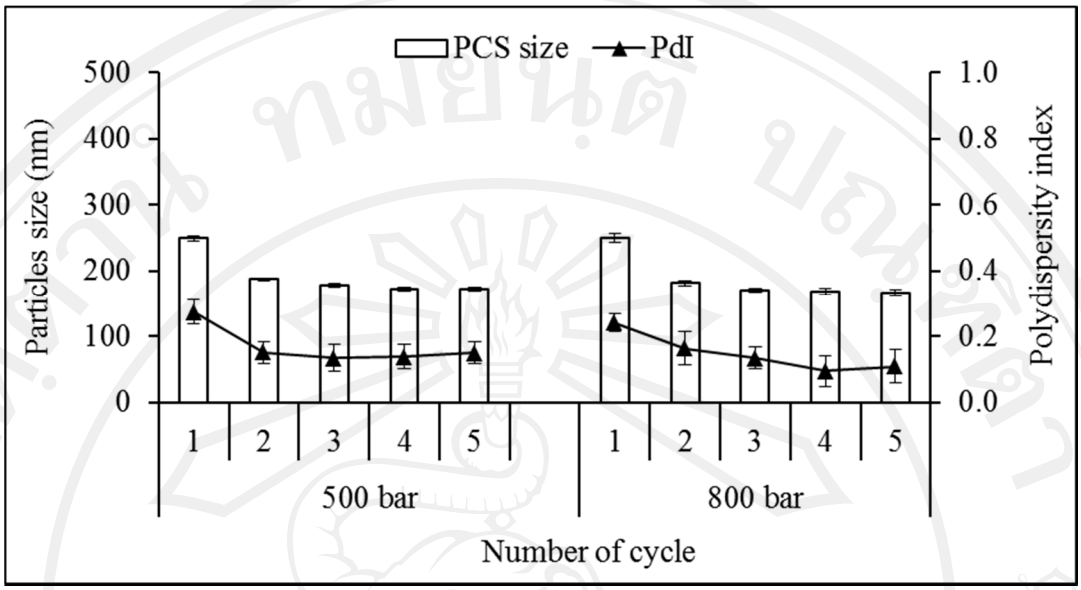

Figure 4-2-11 Average PCS diameters and PdI values of formulations after 1, 2, 3, 4 and 5 cycles at 500 bar and 800 bar.

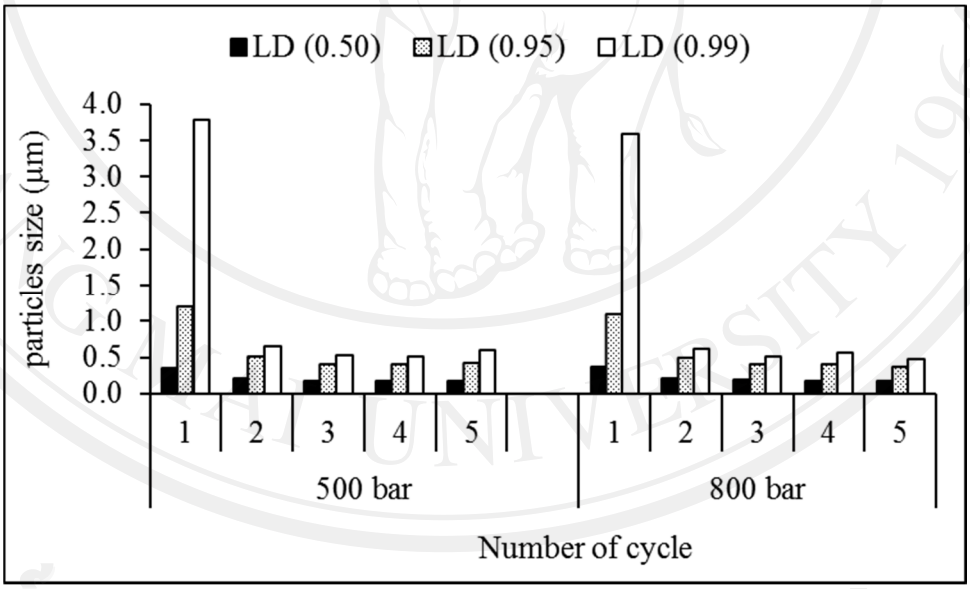

Figure 4-2-12 LD (0.50), LD (0.95) and LD (0.99) diameters of formulations after 1, 2, 3, 4 and 5 cycles at 500 bar and 800 bar.

Figure 4-2-13 shows the PCS mean diameter and the PdI of formulations measured at 3 different time points during 14 days. The LD mean diameters for those systems measured at the same time points as the PCS values were displayed in Figure

4-2-14 and 4-2-15. After applying both pressures for 1 homogenized cycle, the LD (0.95) and LD (0.99) showed the size larger than 1 μm and increased after 14 days indicating unsuitable production conditions. After 2 until 4 homogenized cycles, all LD diameters showed the particle smaller than 1 μm. Their particles size was identical and remained constant during 14 days. The result indicated optimum range of energy to apply to particle. In a meanwhile, after applying 5 homogenized cycle for both pressures, the LD (0.95) and LD (0.99) showed the particle lower than 1 μm. However, the slightly increasing of those values was observed after 14 days indicating too much of the energy input to the particle. Therefore, agglomeration was likely to occur. Increasing number of homogenization cycle up to 5 cycles did not cause a big reduction in particle size. Moreover, the formulations prepared under this condition were unstable and slightly of particle growth occurred after 14 days. To reach a balance between the efficacy and economy of the homogenization process, 3 cycles at 500 bar was chosen to be the homogenization parameters.

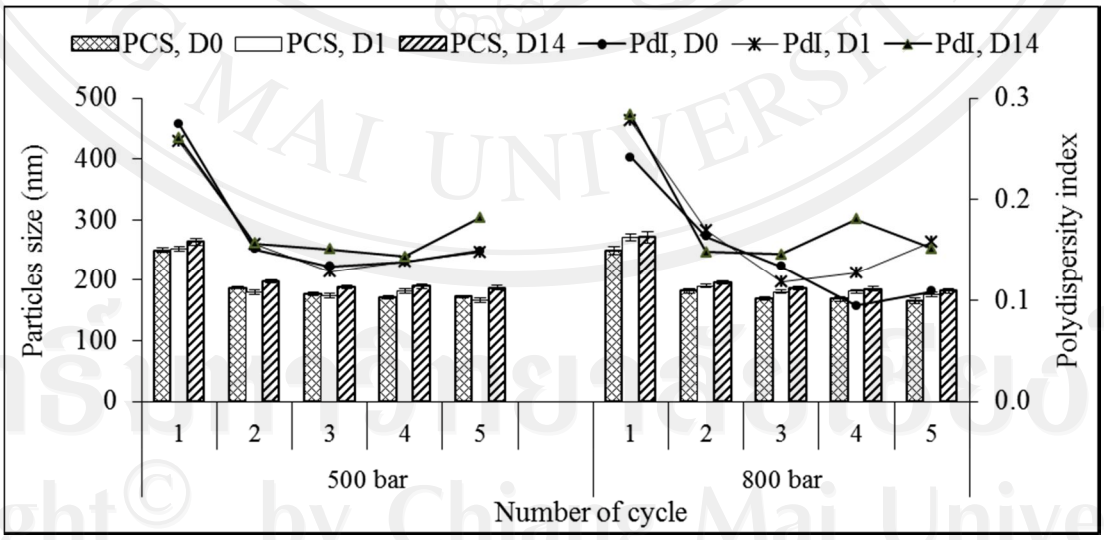

Figure 4-2-13 Average PCS diameters and PdI values of formulations after 1, 2, 3, 4 and 5 cycles at 500 bar and 800 bar at during the period of 14 days.

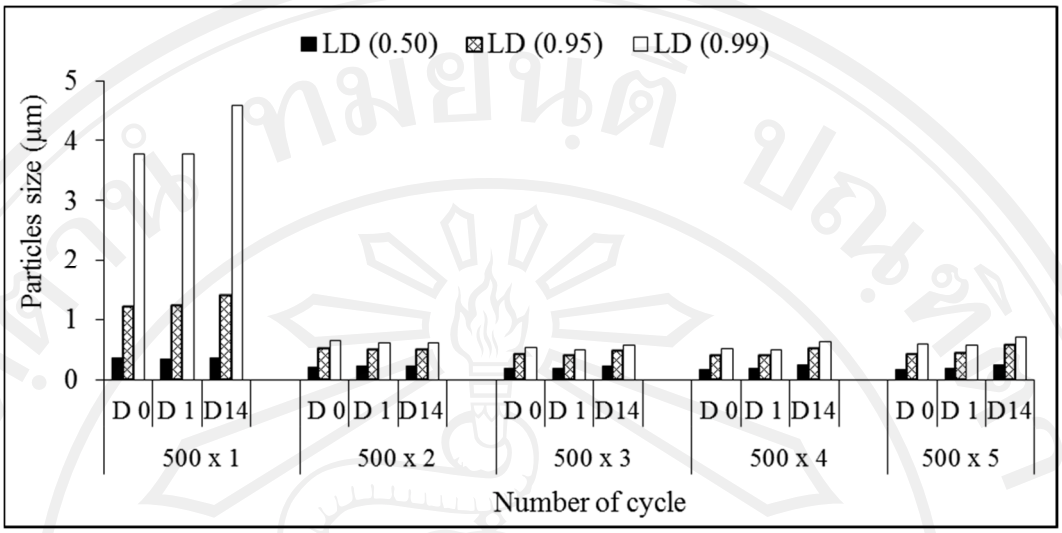

Figure 4-2-14 LD (0.50), LD (0.95) and LD (0.99) diameters of formulations after 1, 2, 3, 4 and 5 cycles at 500 bar during the period of 14 days.

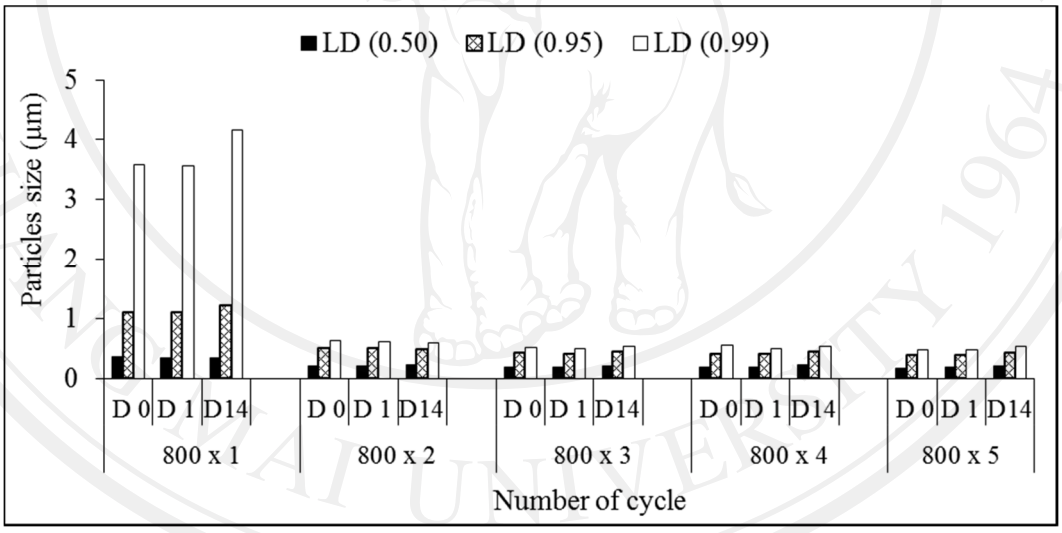

Figure 4-2-15 LD (0.50), LD (0.95) and LD (0.99) diameters of formulations after 1, 2, 3, 4 and 5 cycles at 800 bar during the period of 14 days.

4. Effect of different liquid lipids

The result from the contact angle study demonstrated that the small particle size was obtained from the small surfactant molecular size (C12) but the lack of preserving integrity of formulation could be resulted from using only 1 surfactant.

The NLC system consists of both lipid and aqueous phase. Stabilization of those two phases will gain high benefits. Tegocare^{TM} 450 is a small lipid soluble surfactant, whereas Tween^{TM} 80, Plantacare^{TM} 1200, and Inutec^{TM} SP 1 are water soluble surfactants. Therefore, 3 pairs of surfactant combination were selected. The 1st surfactant combination is between Tegocare^{TM} 450 and Tween^{TM} 80 at the same weight ratio (1:1). Smallest particle size was obtained when using rice bran oil as demonstrated in Figure 4-2-16. PdI values below 0.3 indicate narrow size distribution with spherical shape. After 90 days, very large particle was observed from lipid blends with sesame oil and pomegranate seeds oil which indicated poor stabilities of those systems.

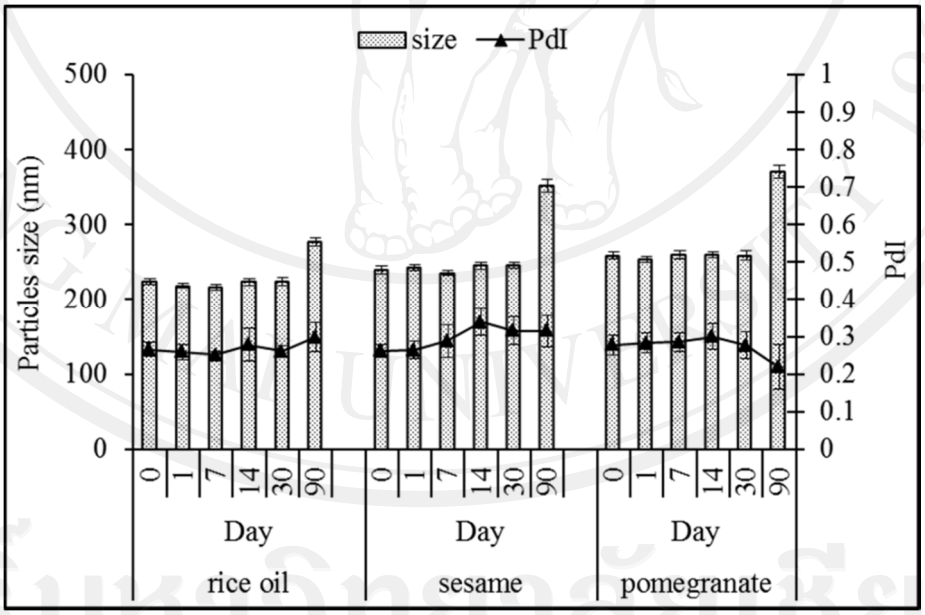

Figure 4-2-16 Average PCS diameters and PdI values of formulations using different liquid lipids; rice bran oil, sesame oil, and pomegranate seeds oil, stabilized with surfactant combination between Tegocare^{TM} 450 and Tween^{TM} 80 at ratio 1:1, respectively.

The 2nd surfactant combination is between Tegocare™ 450 and Plantacare™ 1200 at the same weight ratio (1:1). Figure 4-2-17 demonstrated the poor stability of formulation using sesame oil since the large particle size was observed after 14 days. The formulation using pomegranate seeds oil showed poor stability after 30 days, whereas the particle size remained constant with formulation using rice bran oil.

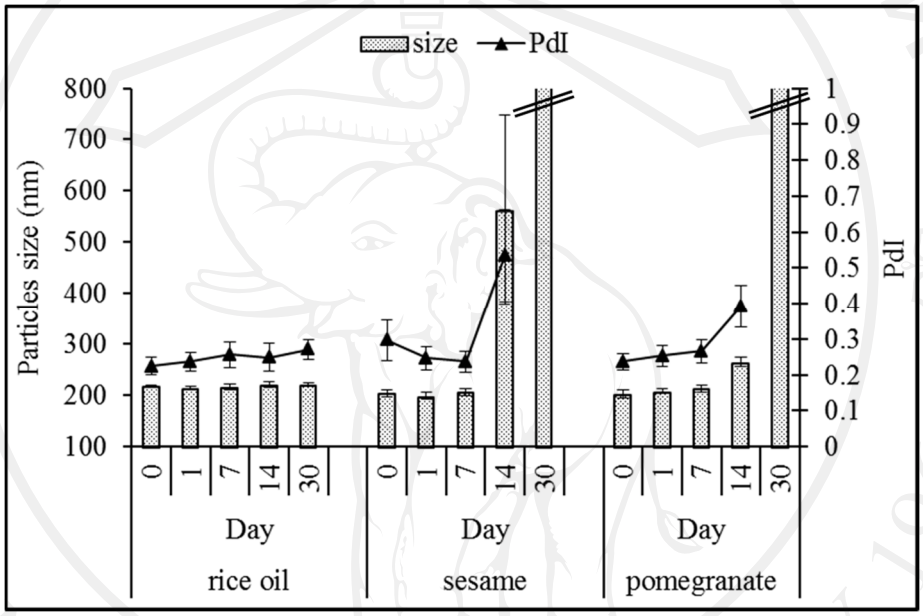

Figure 4-2-17 Average PCS diameters and PdI values of formulations using different liquid lipids; rice bran oil, sesame oil, and pomegranate seeds oil, stabilized with surfactant combination between Tegocare™ 450 and Plantacare™ 1200 at ratio 1:1, respectively.

The 3rd surfactant combination is between Tegocare™ 450 and Inutec™ SP 1 at the same weight ratio (1:1). Figure 4-2-18 demonstrated the smallest particle size was obtained from formulation using rice bran oil and maintained the particle size under 600 nm after 90 days, whereas the microparticle was detected for formulation using sesame oil and pomegranate seeds oil after 30 and 90 days, respectively.

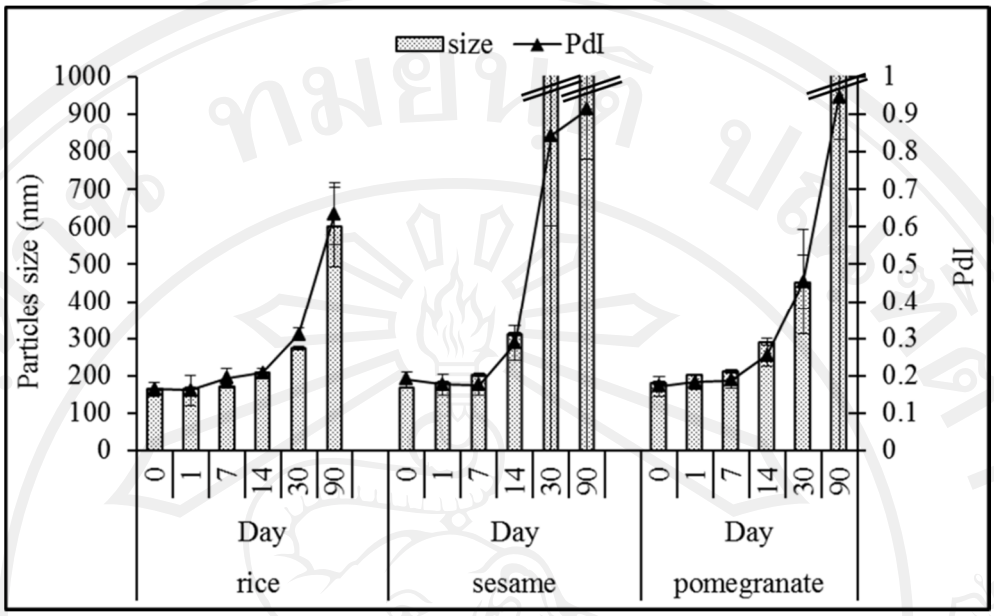

Figure 4-2-18 Average PCS diameters and PdI values of formulations using different liquid lipids; rice bran oil, sesame oil, and pomegranate seeds oil, stabilized with surfactant combination between Tegocare^{TM} 450 and Inutec^{TM} SP1 at ratio 1:1, respectively.

In Figure 4-2-19 from LD (0.95) and LD (0.99), the microparticle were only observed on day 90 for formulation using rice bran oil, but observed since day 30 for sesame oil and pomegranate seeds oil systems. Moreover, microparticle was detected for all LD diameters after 90 days involved with sesame oil and pomegranate seeds oil systems indicating the poorest stabilities of both systems.

From this study, using the blend of rice bran oil improves much better stability of NLC formulation and decreases particle size. Therefore, rice bran oil was selected for any further NLC development.

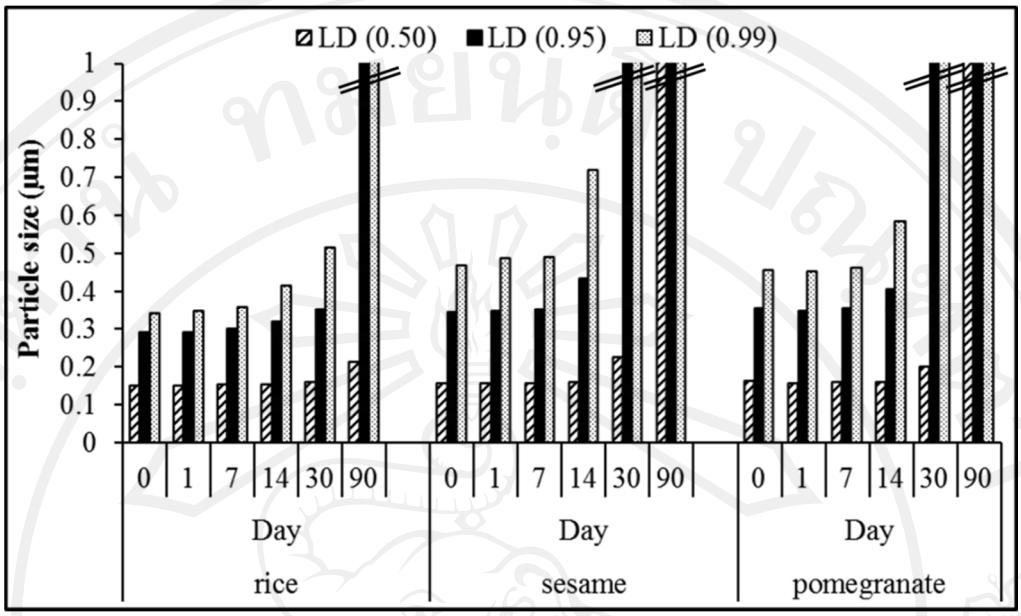

Figure 4-2-19 LD (0.50), LD (0.95) and LD (0.99) diameters of formulations using different liquid lipids; rice bran oil, sesame oil, and pomegranate seeds oil, stabilized with surfactant combination between Tegocare™ 450 and Inutec™ SP1 at ratio 1:1, respectively.

5. Comparison of NLC system *versus* NE system

5.1. The effect of lipid nanoparticle formulations on the particle size

Considering all 3 pairs of surfactant combination from the study of different liquid lipids, the surfactant combination between Tegocare™ 450 and Tween™ 80 provided the most benefits to success the small particle size and physical stability. This surfactant combination was used for this study. Formulations of NLC and NE with lycopene and without lycopene were prepared. Figure 4-2-20 shows the mean PCS diameters and the PdI values of 4 obtained formulations. All formulations show PCS diameters below 250 nm with the PdI values below 0.3 indicated a relatively narrow size distribution.

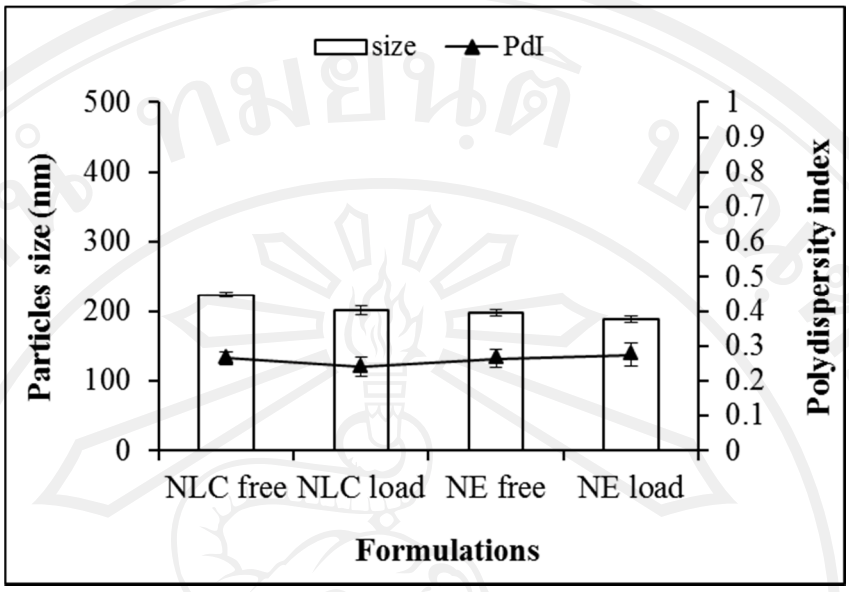

Figure 4-2-20 Average PCS diameters and PdI values of NLC and NE formulations with lycopene and without lycopene.

5.2. Entrapment efficiency

An appropriate standard calibration curve of lycopene by UV/Vis absorption was used for analysis. Since NLC and NE components do not absorb UV/Vis radiation when dissolved, the typical absorption peak at 475 nm for lycopene is clearly visible in the formulations which contain lycopene. The percentage of incorporated drug in the lipid matrix (entrapment efficiency) was evaluated immediately after production. Entrapment efficiencies of 97.63% and 67.85% were found for lycopene loaded NLC and NE, respectively. Incorporation of lycopene in NLC led to extremely high entrapment efficiency because of their lipophilic character and higher solubility in lipid mixture phase. Therefore, NLC formulation is responsible for a higher entrapment efficiency in comparison to NE formulations. Moreover, lycopene is unstable molecule because it is a highly unsaturated molecule, comprising many conjugated double bonds, it is very susceptible to oxidation when exposure to air and light (Sharma and Mague, 1996). However, the duration of the

thermal process has a serious effect on the degradation of lycopene. Shorter processing time is an important factor in reducing lycopene degradation. When coupled with exposure to oxygen and light, heating can result in not only the disintegration of tomato tissue, but also the destruction of lycopene (Shi and others, 2003). In this study, only short heating process used for dissolving lycopene into lipid phase as well as the wax content protect lycopene from degradation. Therefore, the utilization of NLC to increase the stability of lycopene is obtained.

5.3. Antioxidant activities

5.3.1. ABTS assay

As the scavenging activity of the NLC and NE on $ABTS^{\bullet+}$ free radical compared with a standard Trolox™, the TEAC is shown in Table 4-2-1. The different samples possessed the free radical scavenging properties in different degrees. The TEAC values ranged from 1.54 to 5.03 μM/mg. In comparing of TEAC values, the higher of TEAC value indicates the higher antioxidant capacity. The NLC load with lycopene exhibited the highest TEAC value of 5.03 ± 0.41 μM/mg, followed by that of unload NLC and NE load with lycopene with TEAC values of 4.71 ± 0.27 and 1.74 ± 0.28 μM/mg, respectively. The lowest TEAC value, which indicated the weakest antioxidant activity, was obtained from NE unload with lycopene. The result was later confirmed with DPPH results, NLC load formulations present the higher TEAC value than NE load formulation. The higher antioxidant capacities were in order from NLC load, and NE load, respectively. Therefore, the obtained results emphasize the utility of lycopene loaded NLC as a colloidal carrier system provided cosmeceutical benefits.

Table 4-2-1 TEAC values of NLC and NE samples by ABTS radical method.

Sample	TEAC (μM/mg)[a]
NLC free	4.71 ± 0.27
NLC load	5.03 ± 0.41
NE free	1.54 ± 0.54
NE load	1.74 ± 0.28

[a] Mean ± SD (n = 3).

5.3.2. DPPH assay

The DPPH method was used to confirm the results from ABTS test, since it is based on a similar antioxidant mechanism. The IC_{50} of all samples is shown in Table 4-2-2. Different kinds of nanodelivery system possessed obviously different antioxidant activities. The IC_{50} values widely ranged from 26.27 to 257.56 mg/mL. The lycopene loaded NLC showed the highest antioxidant activity with an IC_{50} of 26.27 ± 1.05 mg/mL, followed by unload NLC and NE load with lycopene with IC_{50} values of 49.19 ± 4.54 and 137.69 ± 2.18 mg/mL, respectively. The weakest antioxidant activity was obtained from unloaded lycopene NE. This result was in good agreement with that of the ABTS assay. The relationship between TEAC values and IC_{50} of the samples was non-linear, as shown in Figure 4-2-21. However, the plot of logarithmic values of IC_{50} against TEAC gave good linearity with R^2= 0.925, as shown in Figure 4-2-22, indicating similar trends in the free radical and hydroxyl radical scavenging activities. Regarding these results, it could be considered that the type of nanodelivery system potentially influenced on the antioxidant capacities of the

strong antioxidative agent, lycopene. The lycopene loaded NLC had the higher potential antioxidant activity than the lycopene loaded NE.

Table 4-2-2 IC_{50} values of NLC and NE samples by DPPH radical method.

Sample	IC_{50} (mg/mL)[a]
NLC free	49.19 ± 4.54
NLC load	26.27 ± 1.05
NE free	257.56 ± 0.94
NE load	137.69 ± 2.18

[a] Mean ± SD (n = 3).

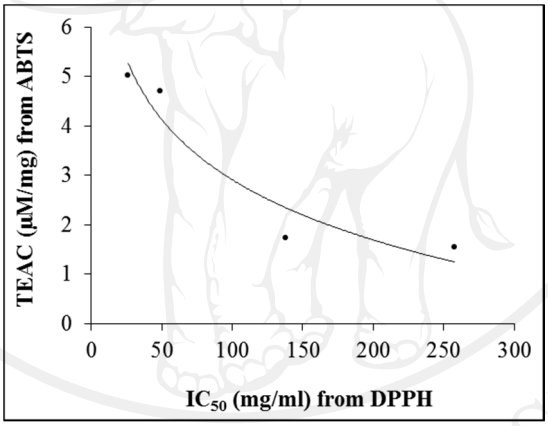

Figure 4-2-21 Correlation of antioxidant activities of samples from DPPH (IC_{50}) and ABTS (TEAC) assay.

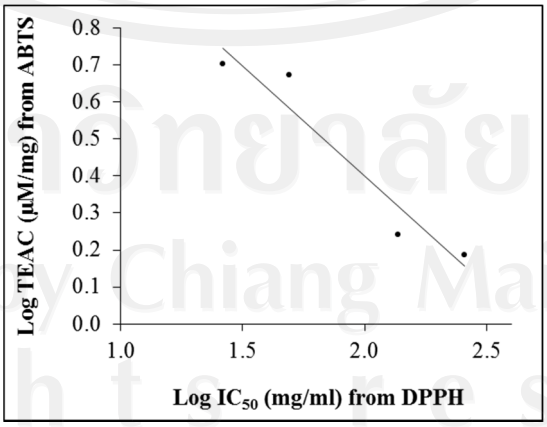

Figure 4-2-22 The linear relationship of logarithmic values of IC_{50} and TEAC.

5.4. Stability test

Figure 4-2-23 shows the stability data of samples for 30 days stored at room temperature. The PCS diameters for all formulations stayed practically unchanged and remained constant lower than 250 nm during 30 days after production. The PdI was almost constant at below 0.3 indicating a good narrow size distribution. NLC and NE had similar ZP values, as shown in Figure 4-2-24.

However, when observed by visualization found that the long-term stability of lycopene-loaded NLC stabilized by Tegocare^{TM} 450 and Tween^{TM} 80 combination-surfactant was poor. It lost the integrity and aggregated together after 4 months stored at room temperature. Therefore, more surfactants involved with steric and electrostatic effect were considered selection for the further study to provide a better long term stability.

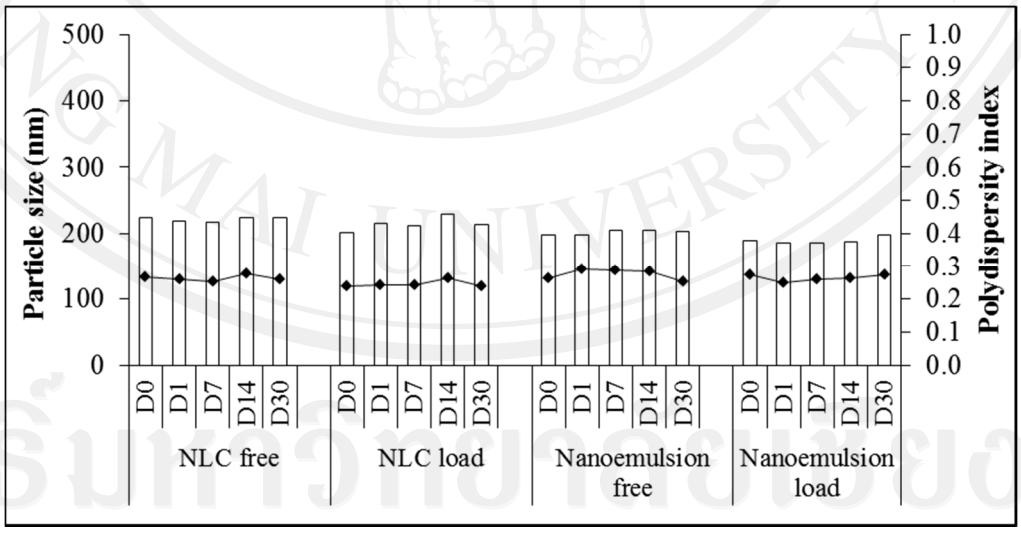

Figure 4-2-23 The PCS diameters and PdI values of NLC free, NLC load, NE free, and NE load dispersions stored at room temperature at a period of 30 days.

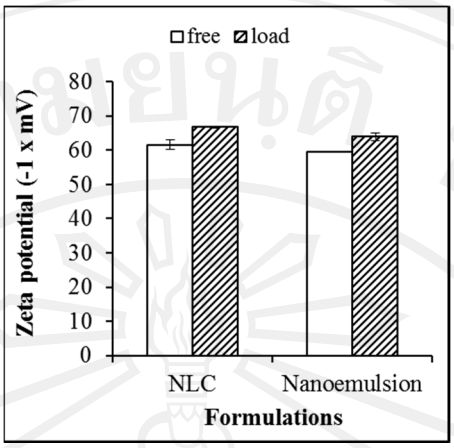

Figure 4-2-24 ZP values of NLC free, NLC load, NE free, and NE load dispersions measured on day 0.

6. Effect of surfactant on NLC stability

The factors that contribute for long term stability of lipid nanoparticles are their steric and/or electrostatic stabilization (Souto and Müller, 2009). As NLC are derived from emulsion system, hence they are mainly stabilized by a surface active molecule or a so-called surfactant. Therefore, these effects on NLC stability were investigated. The results are as following.

6.1. Steric effect

Poloxamers are poly(oxyethylene)-poly(oxypropylene)-poly(oxyethylene) series of block copolymer, as structures shown in Figure 4-2-25. Figure 4-2-26 shows the average PCS diameter and the LD (0.50), LD (0.95) and LD (0.99) values. The small particle size could be obtained by using Poloxamer^{TM} 188 and Poloxamer^{TM} 407. The properties of these 2 surfactants were shown in Table 4-2-3. However, some larger particle size was detected by LD (0.95) and LD (0.99) for formulation using Poloxamer^{TM} 188. Table 4-2-4 provides summary the stability of formulations using Poloxamer^{TM} 188 and Poloxamer^{TM} 407. It was found that the long-term stability on

particle size of formulations was limited only 2 months. After that, it lost the integrity and aggregated to become big particle.

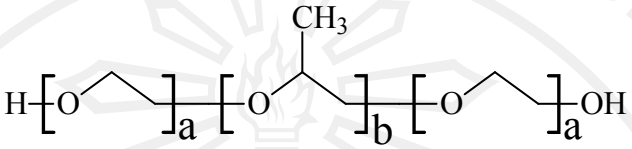

Figure 4-2-25 The chemical structure of Poloxamer™ surfactant.

Table 4-2-3 Physical properties of Poloxamer™ surfactants.

Poloxamer™	a	b	Average Molecular Weight
188	80	27	7680 to 9510
407	101	56	9840 to 14 600

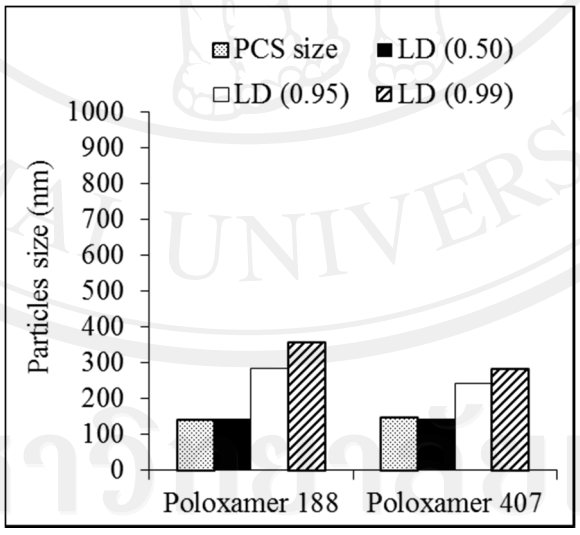

Figure 4-2-26 Average PCS diameters and the LD (0.50), LD (0.95) and LD (0.99) of formulations using Poloxamer™ 188 and Poloxamer™ 407.

Table 4-2-4 Stability on particle size (PCS and LD (0.99) diameter) and PdI of formulations using Poloxamer™ 188 and Poloxamer™ 407.

Trade name of surfactant	Day	PCS diameters (nm)	PdI values	LD (0.99) (μm)
Poloxamer™ 188	0	141.2 ± 2.1	0.146 ± 0.038	0.358
	1	145.7 ± 2.7	0.110 ± 0.027	0.318
	30	141.3 ± 3.2	0.127 ± 0.033	0.318
	60	143.3 ± 2.1	0.111 ± 0.039	0.313
	90	loss of integrity, aggregation		
Poloxamer™ 407	0	146.5 ± 2.9	0.109 ± 0.052	0.283
	1	149.3 ± 3.1	0.078 ± 0.032	0.283
	30	146.7 ± 2.1	0.101 ± 0.036	0.284
	60	150.2 ± 2.3	0.089 ± 0.051	0.283
	90	loss of integrity, aggregation		

6.2. Electrostatic effect

Electrostatic stabilization is owing to the presence of electric charge at the surface of the carriers. Surfaces of particles in suspension develop electric charge owing to the adsorption of ions or ionization of surface group, and the charge is correspondingly dependent on both the surface chemistry and the environment of the particles. The surface charge generates a potential surrounding the particle, which has a high value near the surface and decays with distance into the suspending medium. The same electrical charge repulses particle one another and therefore made a stable colloidal system. The result from the contact angle study demonstrated that the small particle size was obtained from the small molecular surfactant size. Dermofeel™ SL and Eumulgin™ SG were selected as represent small anionic surfactants which are available. These two surfactants had the same lipophilic tail (C18) but different in the hydrophilic head group size (Figure 4-2-27 (A)-(B)). Sodium stearoyl glutamate had a bigger head group size than that of sodium stearoyl lactylate. Figure 4-2-28 shows the

average PCS diameters and the LD (0.50), LD (0.95), and LD (0.99). Smaller head group of sodium stearoyl lactylate yields the smaller particle size observed from PCS, LD (0.50), LD (0.95) and LD (0.99).

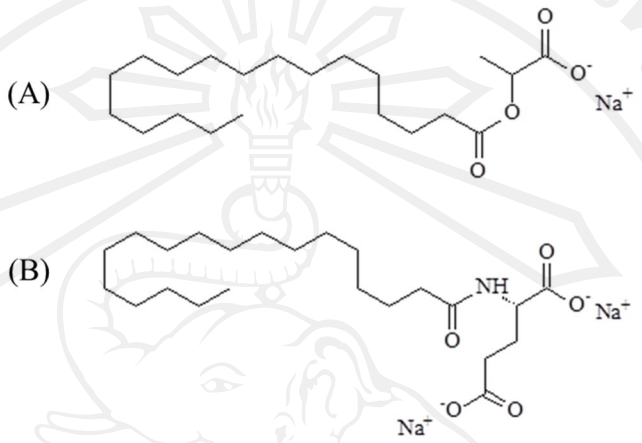

Figure 4-2-27 The chemical structures of sodium stearoyl lactylate (Dermofeel^{TM} SL) (A) and sodium stearoyl glutamate (Eumulgin^{TM} SG) (B).

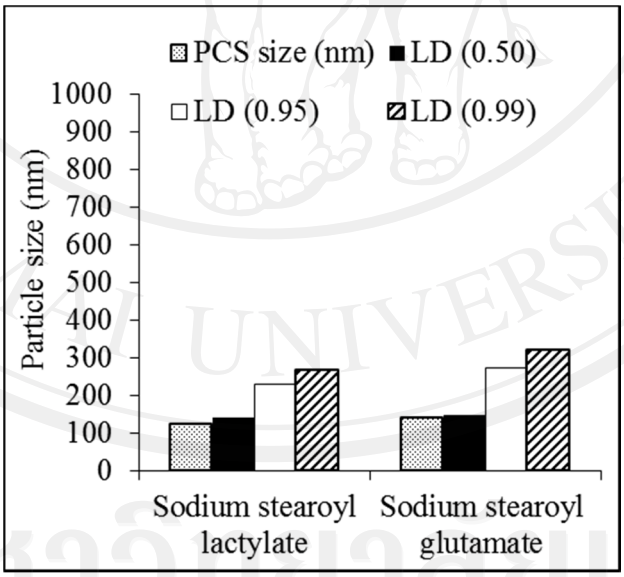

Figure 4-2-28 Average PCS diameters and the LD (0.50), LD (0.95) and LD (0.99) of formulations using Dermofeel^{TM} SL and Eumulgin^{TM} SG.

Table 4-2-5 provides summary the stability of formulations using Dermofeel^{TM} SL and Eumulgin^{TM} SG. It was found that the long-term stability on

particle size of formulation using Dermofeel™ SL was limited only 1 month. After that, it lost integrity and aggregated together. The long-term stability on particle size of formulation using Eumulgin™ SG was over 1 year and stayed practically stable.

Addition of the NLC to dermal formulations, the NLC is additionally stabilized by the high viscosity of the formulation. Despite this additional stabilizing effect, it is advantageous to incorporate a prior the most stable NLC, therefore also the long-term stability of the NLC themselves is important. NLC can be sold as concentrates for admixture to cosmetic and pharmaceutical products. Of course these products need to possess a sufficient shelf life. Eumulgin™ SG was chosen as the best promising surfactant to provide long term stability of NLC systems.

Table 4-2-5 Stability on particle size (PCS and LD (0.99) diameter) and PdI of formulations using Dermofeel™ SL and Eumulgin™ SG.

Trade name of surfactant	Day	PCS diameters (nm)	PdI values	LD (0.99) (μm)
Dermofeel™ SL	0	124.5 ± 3.1	0.149 ± 0.020	0.267
	1	122.6 ± 3.2	0.173 ± 0.027	0.271
	7	128.9 ± 1.2	0.155 ± 0.033	0.265
	14	124.0 ± 2.2	0.165 ± 0.029	0.265
	30	139.4 ± 2.4	0.184 ± 0.023	0.290
	90*	171.0 ± 47.4	0.269 ± 0.044	177.107
	180	large microparticle	0.887 ± 0.247	251.652
	*severe seperation, aggregation			
Eumulgin™ SG	0	143.0 ± 2.0	0.181 ± 0.024	0.323
	1	144.8 ± 2.0	0.185 ± 0.025	0.333
	7	153.5 ± 2.1	0.194 ± 0.016	0.300
	14	145.0 ± 1.1	0.187 ± 0.027	0.296
	30	150.9 ± 3.8	0.182 ± 0.034	0.325
	90	157.2 ± 4.1	0.134 ± 0.048	0.344
	180	165.1 ± 5.1	0.201 ± 0.038	0.413
	365*	156.2 ± 2.7	0.163 ± 0.053	0.408
	*practically stable			

<u>Part III</u> Preparation and physicochemical study of lycopene-loaded NLC

For people with sensitive skin, dermal application of skin products may result in problems such as acne, rosacea, burning and stinging, and high susceptibility to contact and irritant dermatitis. To avoid such problems, skin-friendly skin care ingredients or excipients are increasingly considered for topical formulations. In the present study, we demonstrate the development of a promising, skin friendly nanoparticle product by an emulsion technique using high pressure homogenization with skin friendly lipid materials, having lycopene as an active ingredient. The cosmetic industry nowadays moves away from ethoxylated surfactants and polymeric surfactants. PEG-free is becoming a quality criterion (Cosmetic Ingredient Reviews, 1999). Eumulgin^{TM} SG, an anionic and skin friendly emulsifier based on sodium stearoyl glutamate enables high efficiency emulsification tolerating electrolytes (Cognis corporation, 2009). Emulsification by this surfactant could be achieved at low concentrations. Skin pH of about 5 or lower usually limits the utilization of anionic surfactants; however, Emulgin^{TM} SG is superior to other anionic surfactants because it is effective over a wide pH-range, including pH values <5. Therefore, it was selected as the major emulsifier in this study. The lipid phase of the nanoparticles developed in the present study is mainly composed of orange wax, a solid biodegradable lipid from the fruit peel of Citrus. It is acceptable for cosmetic use in the United States, Europe, and Japan. It was reported to have many activities such as sunscreen-enhancing, antioxidant, antimicrobial and anti-inflammatory properties (Reynhardt and Riederer, 1991; Puleo and Rit, 1992). The main constituents of orange wax are the unsaturated monoesters, hydroxy-monoesters, free fatty acids (C12-C26), hydrocarbons (C21-

C33), sterol esters, free sterols, free alcohols, carotenoids, glycolipids, phospholipids, and flavonoids (Puleo and Peters, 1994). Orange wax can be classified as a skin friendly lipid material since its lipid composition is similar to that of skin. Rice bran oil is an edible natural fixed oil obtained from the bran of the rice kernel during the process of rice milling. It is composed of unsaturated fatty acids, triterpene alcohols, phytosterols, tocotrienols, alpha-tocopherol, gamma-oryzanol, squalene, and other nutrients (Orthoefer, 2005; Sugano and Tsuji, 1997). These components are useful in protecting cells against the effects of free radicals. They aid in slowing down the effects of aging, e.g. by slowing the formation of skin wrinkles (Santa-María and others, 2010). Gamma-oryzanol impedes the progress of melanin pigmentation and is effective in keeping skin smooth while squalene supports the collagen within the skin (Lerma-García and others, 2009). Moreover, the high content of fatty acids in rice bran oil is beneficial for mature, delicate and sensitive skin. Cholesterol is a lipid naturally produced by the body and is essential for the maintenance of healthy cell walls. It is one of three major lipid classes found in the skin (Bouwstra and others, 2001) that serve essential functions not only in terms of good skin health but also the health of the entire body. Skin cholesterol levels may decrease because of factors such as aging, various disorders, or use of certain drugs. Skin cells may deteriorate and perish due to lack of cholesterol. The stratum corneum becomes flaky, resulting in a severe dried skin condition called xerosis (Harding and others, 2000). Cholesterol imparts water-absorbing power with an emollient activity. Incorporation of cholesterol into topical products is necessary to soothe and plump up dry skin. Using only one lipid component like orange wax might be insufficient to meet the requirements of a desirable formulation. Therefore, rice bran oil and cholesterol were

incorporated as minor constituents of the lipid phase of orange wax. The effect of these two components was investigated on the size, size distribution and zeta potential as well as the stability of the obtained nanoparticles. Lycopene, an acyclic carotene with 11 conjugated double bonds found in tomato, watermelon, and pink grapefruit, was reported to possess pronounced antioxidant, anti-inflammatory, anti-cancer, and anti-mutagenic properties (Giovannucci, 1999; Heber and Lu, 2002; Stahl and Sies, 1996). However, its therapeutic usefulness is limited by certain disadvantages. Lycopene is water insoluble and hardly diffusible *via* the transdermal pathway when applied topically. Moreover, it is unstable and highly susceptible to oxidation when exposed to air or sunlight (Shi and others, 2003). It was reported that the stability of many active ingredients such as vitamin A, coenzyme Q10, ascorbyl palmitate, and vitamin E is increased after incorporation into lipid nanoparticles (Dingler and others, 1999; Jee and others, 2006; Teeranachaideekul and others, 2007a; 2007b). The utilization of lipid nanoparticles to increase the stability of lycopene by using skin friendly materials as lipid carriers is considered a worthwhile challenge and has not yet been reported elsewhere. The aim of the present study was to develop suitable skin friendly NLC for entrapment of lycopene. The effects of the lipid materials on the characteristics and stability of the lycopene loaded nanoparticles were explored.

1. Development of skin friendly lycopene-loaded NLC

1.1. Morphology and re-crystallize of lipid matrix

As the crystalline nature of the lipid mixture is an important characteristic link to the solid state and their benefits. A mixture of orange wax and lycopene was created to predict the re-crystalline characteristic after sample preparation. The outer

texture of the mixture containing orange wax and lycopene presented in Figure 4-3-1 (A) showed the spherical granule-like texture but the size of granules was slightly larger than that of the pure orange wax. This larger size was considered to be due to solubilized lycopene in the mixture. The sparkle crystalline nature of this mixture was observed from PLM as shown in Figure 4-3-1 (B). The results indicated that after melting and solidifying process, the internal structure of this solid lipid mixture was still in crystalline form, not became an amorphous or a supercooled melt state. The crystalline appearance of this mixture was more similar to that of the pure orange wax than of lycopene. Therefore, it was considered that the crystalline characteristic of the mixture was of orange wax. Since this, it was proposed that the lipid mixture in the SLN dispersion can also be solidified as well after heating. Besides, it should provide the crystalline characteristic (not amorphous or even a supercooled melt state).

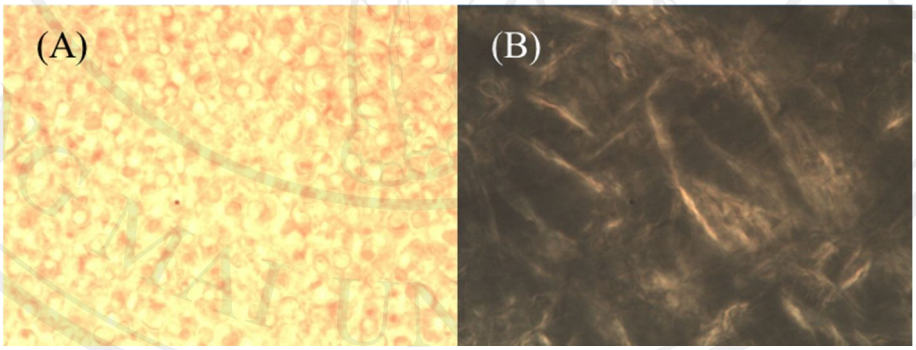

Figure 4-3-1 LM picture (A) and PLM picture (B) of mixture of orange wax 99.9 %w/w and lycopene 0.1 %w/w with magnification of 100x10 folds.

Rice bran oil is miscible well with the melted orange wax. The external structure of the mixture containing orange wax and rice bran oil observed by LM was demonstrated in Figure 4-3-2 (A). A granule-like texture with a small size spherical shape was clearly seen. It was noted that the size of granular shape was slightly

smaller than that of the pure orange wax. This was considered to be due to the effect of rice bran oil to the wax structure. The structure of this mixture was observed by PLM and demonstrated in Figure 4-3-2 (B). Interestingly, it was found that the crystalline characteristic of orange wax was still existing but less than that of the pure wax. It was considered that adding small amount of rice bran oil to orange wax could cause the decrease in crystalline characteristic of the wax.

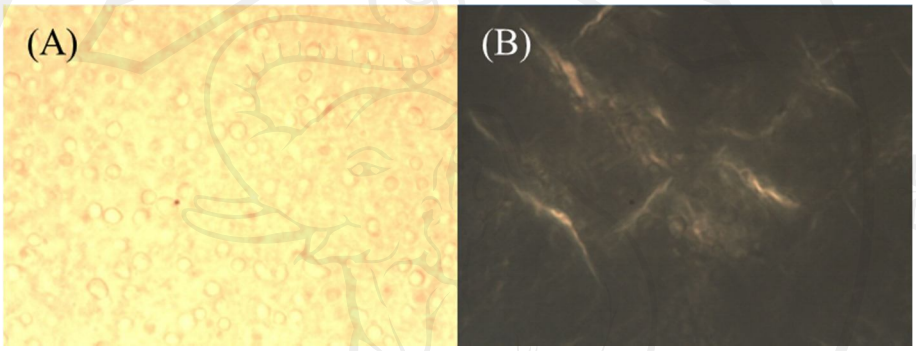

Figure 4-3-2 LM picture (A) and PLM (B) of mixture of orange wax 90 %w/w and rice bran oil 10 %w/w with magnification of 100x10 folds.

The external structure of the mixture containing orange wax, lycopene, and rice bran oil observed by LM was demonstrated in Figure 4-3-3 (A), the color of lipid mixture became red corresponding to the color of lycopene. A texture of various spherical granular shapes was seen. It was noted that the size of granular shape was similar to that of the mixture containing orange wax and rice bran oil. This was considered to be due to the effect of rice bran oil that interfere the wax structure and its ability to dissolve lycopene before entering to the wax structure. The structure of this mixture observed by PLM demonstrated the crystalline structure of the mixture as the sparkle crystalline nature as demonstrated in Figure 4-3-3 (B). This result confirmed that after blending of rice bran oil to the mixture of orange wax and

lycopene, the crystalline characteristic of the solidified wax after melting was still obtained.

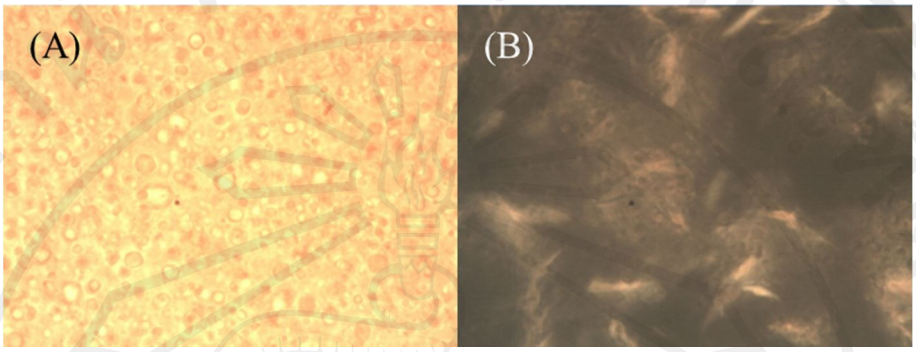

Figure 4-3-3 LM picture (A) and PLM picture (B) of mixture of orange wax 89.91 %w/w, rice bran oil 9.99 %w/w, and lycopene 0.1 %w/w with magnification of 100x10 folds.

After the lipid mixture of orange wax 72 %w/w, cholesterol 18 %w/w, rice bran oil 10 %w/w was mixed up, the crystalline characteristic was clearly observed by LM as shown in Figure 4-3-4 (A). Under PLM (Figure 4-3-4 (B)), which reveals bigger crystals, demonstrates the highly order degree of crystallization due to superimpose with the highly crystalline characteristic of cholesterol.

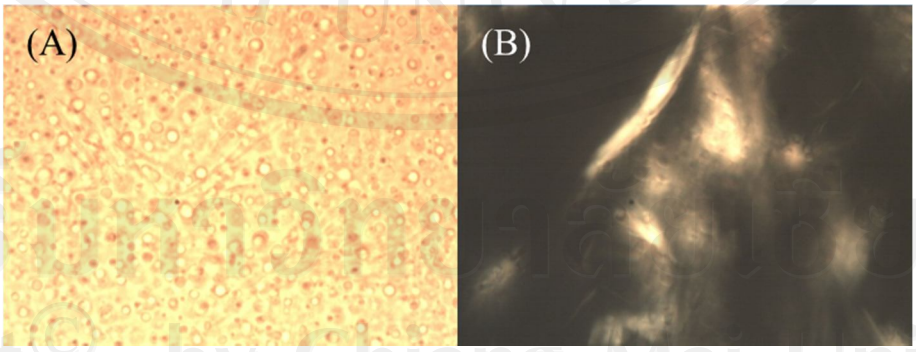

Figure 4-3-4 LM picture (A) and PLM picture (B) of mixture of orange wax 72 %w/w, cholesterol 18 %w/w, rice bran oil 10 %w/w with magnification of 100x10 folds.

Finally, the mixture was added up with lycopene (Figure 4-3-5 (A)), after the heating supplied, the lipid mixture solidified at room temperature and showed many crystals which indicated crystalline characteristic (Figure 4-3-5 (B)). Therefore, it was proposed that all lipid mixtures which were investigated by this step can also be solidified as well after SLN/NLC producing. Besides, it should also provide the crystalline characteristic as observed from PLM. The results from this experiment suggested an appropriate amount of the oil and wax for preparation of lycopene loaded NE, SLN, and NLC.

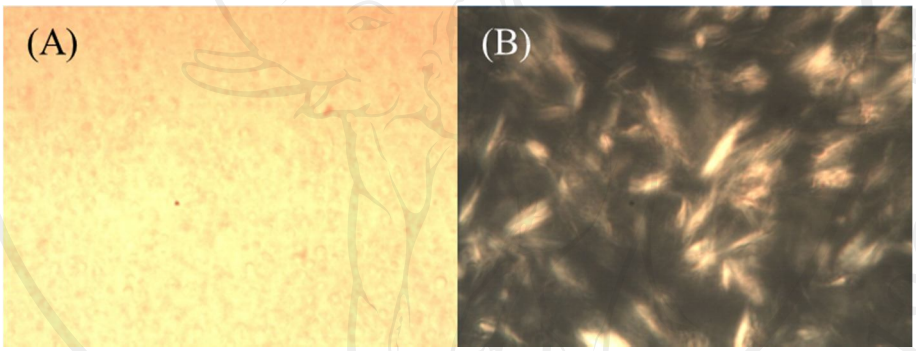

Figure 4-3-5 LM picture (A) and PLM picture (B) of mixture of orange wax 71.93 %w/w, cholesterol 17.98 %w/w, rice bran oil 9.99 %w/w, and lycopene 0.1 %w/w with magnification of 100x10 folds.

1.2. Effect of lipid combination

Materials of brown, homogeneous texture were obtained from the mixtures of rice bran oil and orange wax containing 10% and 20% oil as seen in Figure 4-3-6. Small fragments of separated solid lipid could be seen in the mixtures containing 30-50% oil, indicating incomplete miscibility of the wax and oil. The thermograms obtained by differential scanning calorimetry (DSC) of these mixtures running from 35 to 65°C are shown in Figure 4-3-7. The melting point of orange wax was observed at 57.8°C. Adding 10% or 20% of rice oil results in decreased melting temperatures of

the wax of 56.6°C and 56.3°C, respectively. Orange wax is composed of C21-C33 hydrocarbons, sterol esters, free sterols, glycolipids, phospholipids, carotenoids, and flavonoids. These compounds were well arranged with limited imperfection holes (Puleo and Peters, 1994). Adding of certain oils might distort the formation of perfect lipid crystals of the wax by incorporation into these holes as a monolayer film and interaction with the molecules of wax substances resulting in imperfections of the crystal lattice of the mixtures and slightly decreased the melting point of the wax. The endothermic peaks of the mixtures containing 30%, 40%, and 50% oil were found to be 57.6, 57.5, and 57.4°C, respectively. These peaks were considered to be the melting peak of the pure orange wax. These results could be explained that the oil at first might spread through the surface of the wax and modified the interfacial tension to, at equilibrium, a lower value than that of the pure wax. The residual oil hence would gather together in a completely separate phase from the wax and cover the wax surface in a monolayer film. On the basis of these results, the completely miscible lipid mixtures containing rice bran oil and orange wax of 1:9 and 2:8 were selected for further study.

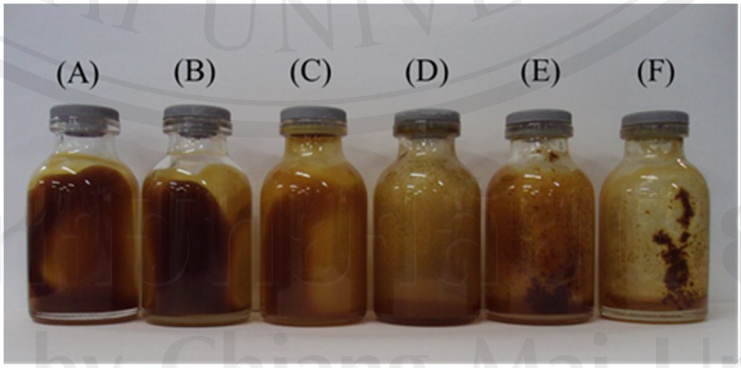

Figure 4-3-6 The physical appearance of the melted orange wax (A) and orange wax - rice bran oil mixtures containing oil of 10% (B), 20% (C), 30% (D), 40% (E) and 50% (F).

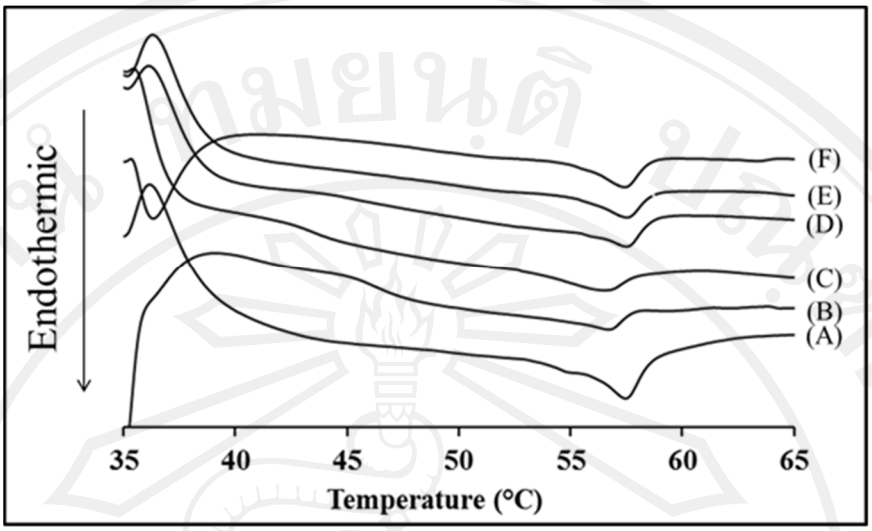

Figure 4-3-7 DSC thermograms of the melted orange wax (A) and orange wax – rice bran oil mixtures containing 10% (B), 20% (C), 30% (D), 40% (E) and 50% oil (F).

Considering the skin friendly effects of cholesterol, we attempted to incorporate as much cholesterol as possible in the formulations. The miscibility between orange wax and cholesterol was investigated prior to formulation. A heterogeneous texture with separated lipid matter distributed through the system was found in the mixture of wax/cholesterol, 7:3 as seen in Figure 4-3-8. Pale brown homogeneous texture was obtained from the mixtures of 4:1 and 3:1. Hence, mixing quantities of orange wax and cholesterol in these ratios was considered to result in homogeneous miscibility. The mixtures of 4:1 and 3:1 were selected for further investigation by DSC. The thermograms of these mixtures shown in Figure 4-3-9 revealed that the melting peak of cholesterol at 147.9°C was absent while melting endothermic peaks were observed at 48.1°C and 48.3°C for mixture ratios of 4:1and 3:1, respectively. These endothermic peaks are similar in shape to the melting peak of

orange wax at 57.8°C. These data suggested that cholesterol could completely dissolve in the melted orange wax. Considering the most suitable ratio, the mixture at a ratio of 4:1 was selected and used for further experiments.

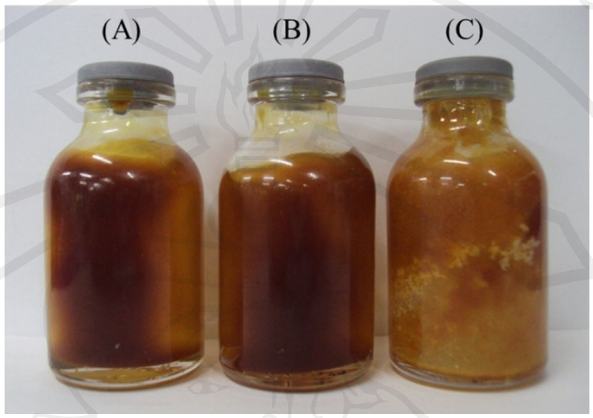

Figure 4-3-8 Physical appearance of the melted orange wax/cholesterol mixtures of 4:1 (A), 3:1 (B), and 7:3 (C).

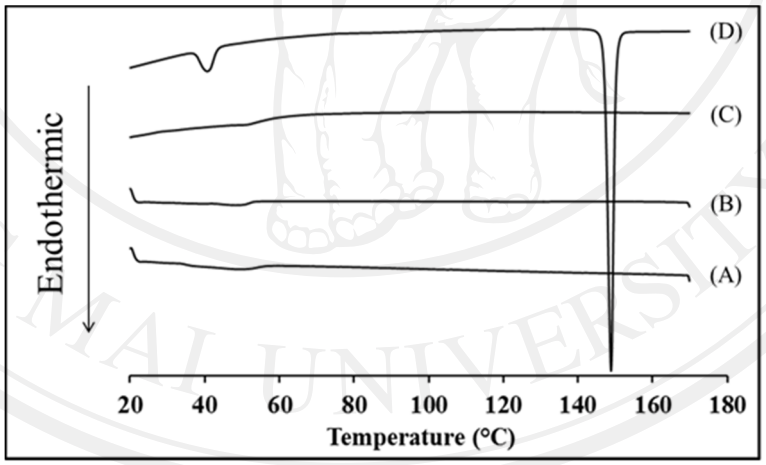

Figure 4-3-9 DSC fusion curves for the mixtures of orange wax and cholesterol at ratios of 4:1 (A) and 3:1 (B), orange wax (C) and cholesterol (D).

1.3. Preparation and characterization of the investigated formulations

Lipid nanoparticle bases composed of ingredients as shown in Table 4-3-1 were prepared. Formula 1 yielded SLN whereas in Formula 2 and 3, lipid phases containing 1:9 and 1:4 weight ratios of rice bran oil to orange wax, respectively, were

used to form NLC formulations. These formulations were obtained in the form of homogenous, viscous pale yellowish liquids as shown in Figure 4-3-10. Particle size analysis indicated that Formula 2 yielded the lipid nanoparticles of the smallest size as shown in Figure 4-3-11. Moreover, after 1 day at room temperature (25°C), the SLN (Formula 1) and NLC (Formula 2) were unchanged whereas solid lipid fragments had obviously been formed from Formula 3, indicating the separation of the ingredients in this formula (Figure 4-3-12). Formula 2 and 3 correspond to NLC products and differ from each other by the quantity of rice bran oil. These results suggested that, in order to obtain homogenous formulations, the rice bran oil loading in the NLC should be not more than 10%. It was known that incorporation of oil into the solid lipid could reduce the degree of organization of the lipid matrix (Müller and others, 2002a). Lipid mixtures incorporating an optimum quantity of rice bran oil facilitated particle size reduction. The smaller particle size obtained was therefore considered to be due to the effect of rice bran oil incorporated into the system. However, increasing oil content to more than 20% resulted in bigger particles. The larger particle size could be mainly due to particles aggregation.

Table 4-3-1 Composition of ingredients used in the lipid nanoparticle bases.

Material	Amount of ingredients (% w/w)		
	Formula 1	Formula 2	Formula 3
Orange wax	5.0	4.5	4.0
Rice bran oil	0.0	0.5	1.0
Eumulgin™ SG	1.0	1.0	1.0
Milli Q water qs.	100	100	100

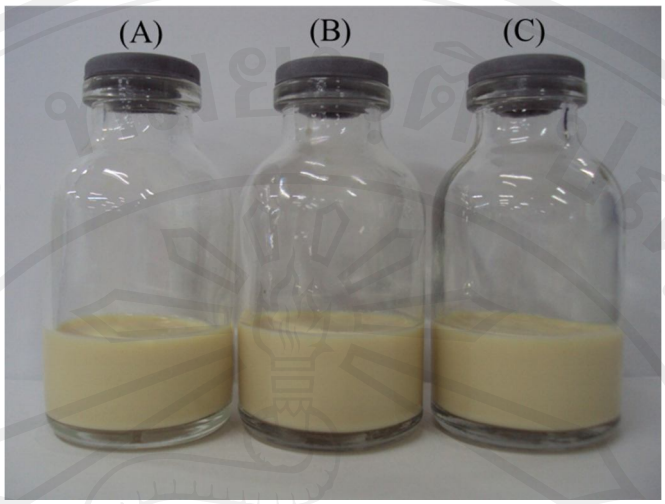

Figure 4-3-10 Outer appearance of Formula 1 (A), Formula 2 (B) and Formula 3 (C).

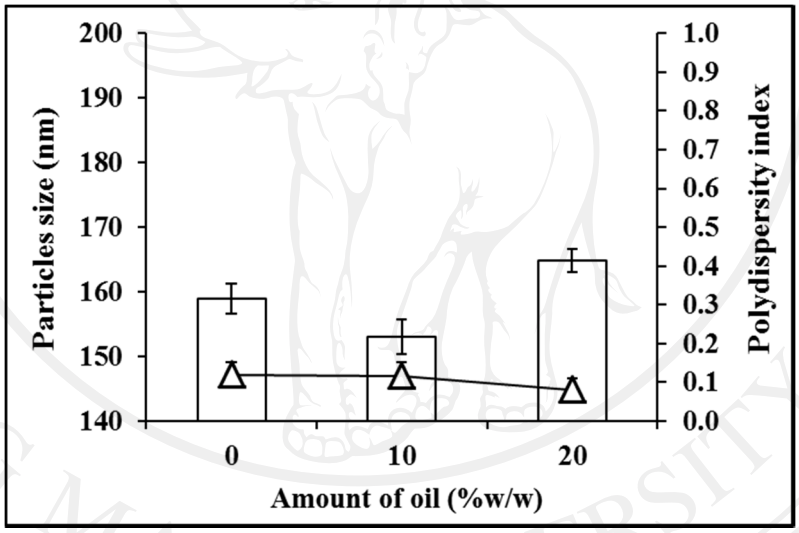

Figure 4-3-11 The PCS diameters and PdI values of Formula 1 (A), Formula 2 (B) and Formula 3 (C).

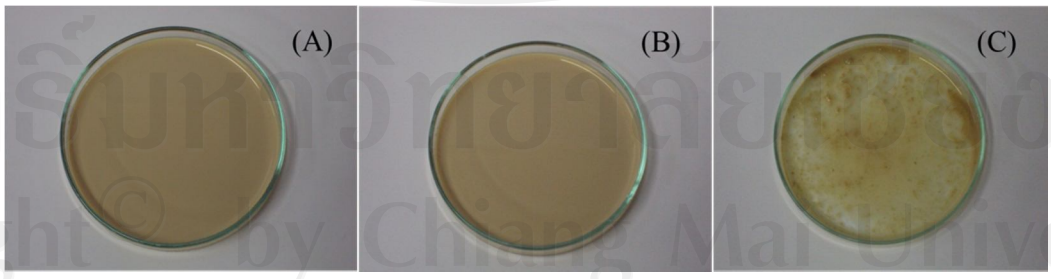

Figure 4-3-12 Outer appearance of Formula 1 (A), Formula 2 (B), and Formula 3 (C) after 1 day's storage at room temperature.

In order to obtain the maximum therapeutic efficacy via the transdermal route, the size of the carrier plays the most important role. With the extremely small size of the NLC, the amount of encapsulated drug reaching the site of action will be increased because the particle ensures close contact to the stratum corneum and thus, the bioavailability of drugs penetrating into viable skin can be enhanced (Souto and others, 2007). In the present study, we therefore focused our attention on the particle size of the products. According to our results, four lycopene loaded lipid nanoparticle formulations composed of the selected lipid combinations and ratios as shown in Table 4-3-2 were prepared. It was found that the outward appearance of the four emulsions obtained was that of opaque liquids with yellowish orange color corresponding to the color of lycopene. The emulsion type was tested by the dye-soluble method and conductivity measurements. All emulsions were miscible with the water soluble dye and showed conductivity values higher than 100 μS/cm as shown in Table 4-3-3. This result indicates that all emulsions obtained were of the o/w type.

Table 4-3-2 Composition of ingredients used in lycopene loaded lipid nanoparticle formulations.

Material	Amount of ingredients (% w/w)			
	Formula 4	Formula 5	Formula 6	Formula 7
Lycopene	0.005	0.005	0.005	0.005
Orange wax	0.0	5.0	4.5	3.6
Cholesterol	0.0	0.0	0.0	0.9
Rice bran oil	5.0	0.0	0.5	0.5
Eumulgin™ SG	1.0	1.0	1.0	1.0
Milli Q water qs.	100	100	100	100

Table 4-3-3 Conductivity values of lycopene loaded lipid nanoparticle formulations.

Formula	Conductivity (μS/cm)
4	1208.33 ± 17.21
5	2060.05 ± 20.01
6	1851.00 ± 13.45
7	1293.67 ± 11.93

1.4. Effect of lipid on the state of the internal phase

DSC provides information on the thermal behavior of a compound by measuring the heat loss or gain resulting from physical or chemical changes within a sample as a function of temperature. In order to investigate the state of the internal phase, the products were subjected to DSC and the results are shown in Figure 4-3-13. Formula 4 and 5 were compared as they differ from each other by one lipid component, the liquid state rice bran oil and the solid state orange wax, respectively. The DSC thermogram of Formula 4 shows no endothermic peak or melting point as seen in Figure 8(A) whereas an endothermic peak was observed at 54.4°C for Formula 5 as seen in Figure 8(B). This result confirms that the state of the internal droplets of Formula 4 is liquid whereas that of Formula 5 is solid. As expected, the state of the lipid raw material used in the formula determines the state of the internal phase of the product.

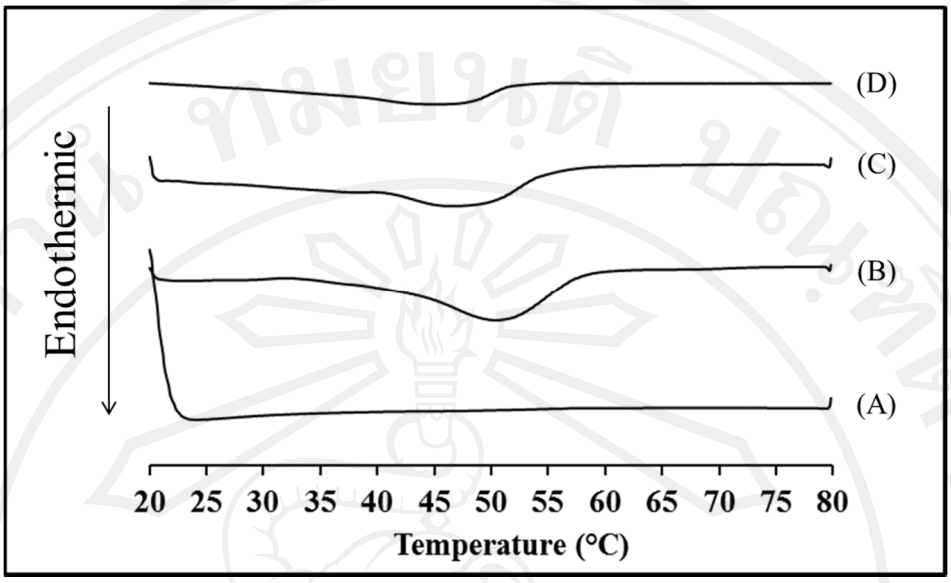

Figure 4-3-13 DSC thermograms of Formula 4 (A), Formula 5 (B), Formula 6 (C) and Formula 7 (D).

1.5. Effect of rice bran oil and cholesterol on the state of the internal phase

To investigate the effect of rice bran oil, Formula 5 was compared with Formula 6, and Formula 6 was compared with Formula 7 when the effect of cholesterol was investigated. The DSC thermograms of Formula 6 and 7 exhibited melting peaks at 48.4°C and 46.1°C, respectively, as shown in Figure 4-3-13 (C) and 4-3-13 (D). This result clearly indicates that the internal phases of these emulsions are solid state. Replacement of some solid orange wax with liquid rice bran oil reduced the melting point of the internal phase. Further replacement of some orange wax with cholesterol led to further reduction of the melting point. According to the solid lipid nanoparticle classification (Müller and others, 2006), the lipid particle internal phase of Formula 5 is classified as a simple SLN whereas that of Formula 6 and 7 is categorized as NLC.

1.6. Effect of rice bran oil and cholesterol on particle size of the internal phase

In order to obtain maximum physical stability and skin penetration, the particle size of the internal phase should be extremely small and homogeneous without any aggregation (Mäder and Mehnert, 2005). The small size (<1 μm) of the internal phases of all formula was determined by PCS whereas the larger size (>1 μm) was measured by LD. The PCS yielded the mean particle size (z-ave) and the PdI which indicates the width of the size distribution. The LD data of 50%, 90%, and 99% cumulative undersize of median volume weighted diameters expressed as LD (0.50), LD (0.90), LD (0.99), respectively, indicate the percentages of particles possessing a diameter equal to or lower than the given value. Mie theory was used for LD data evaluation. The real refractive index and the imaginary refractive index were set as 1.456 and 0.01, respectively. These values were assessed to be valid for our lipid nanoparticle formulations by using the methods and equipment cited in previous reports with similar oil variation (Müller and Schuhmann, 1997; Kovacevic and others, 2011). There are slight variations in the indices depending on the nature of matrix lipid and stabilizer used, but for the envisaged development of a dermal formulation with lipid variation as in our study range, these effects can be neglected (Muchow and others, 2011; Pardeike and others, 2010). The PCS diameter of Formula 4 was 170 nm as shown in Figure 4-3-14. The LD diameters of all formula were found to be less than 1 μm. According to the state of the internal phase and droplet size, Formula 4 is classified as nanoemulsion. The PCS diameters of the SLN (Formula 5) and NLC (Formula 6) were insignificantly different, amounting to 160-162 nm. The NLC of Formula 7 is slightly smaller with a diameter of 156 nm.

Considering the LD diameters at LD (0.95) and LD (0.99) of solid particles in each system, it was found that the lipid particles of the NLC (Formula 6 and 7) are significantly smaller than those of the SLN (Formula 5). The incorporation of liquid lipid into the solid lipid could reduce the degree of organization of the lipid matrix as described above. The resulting smaller particle size obtained in both NLC formulations was therefore considered to be due to the incorporation of rice bran oil. The effect of rice bran oil could be seen clearly when Formula 5 was compared with Formula 6. The rice bran oil disrupts the structure of the orange wax and facilitates size reduction by high pressure homogenization. This result is in accordance with Mitri *et al.* (2011) who have reported that the incorporation of oil into solid lipid results in smaller particle size. In Formula 7, some more orange wax was replaced with cholesterol but the particles obtained were still classified as NLC. The effect of cholesterol can be seen when comparing the LD (0.95) and LD (0.99) diameters of Formula 6 (without cholesterol) and Formula 7 (with cholesterol). Addition of cholesterol significantly reduces the LD diameters of the NLC. Cholesterol is composed of hydrophilic and lipophilic parts, enabling it to act as a surface active agent. Its use was reported as co-emulsifier in a bioactive delivery system (Mu and Feng, 2001). Therefore, the small particle size obtained with Formula 7 was considered to be due to the surface active function of cholesterol. The results of the present study confirm the ability of cholesterol to facilitate emulsification. The PdI values for all formulations were below 0.16, indicating a good narrow size distribution. Figure 4-3-15 reveals that the mean PCS diameters of the three batches of each formula were insignificantly different ($p<0.05$). This result illustrates the high batch-to-batch reproducibility of the formation of small size particles. The LD

diameters of each formula shown in this figure suggest that good reproducibility of the production process can be achieved with Formula 4, 6, and 7.

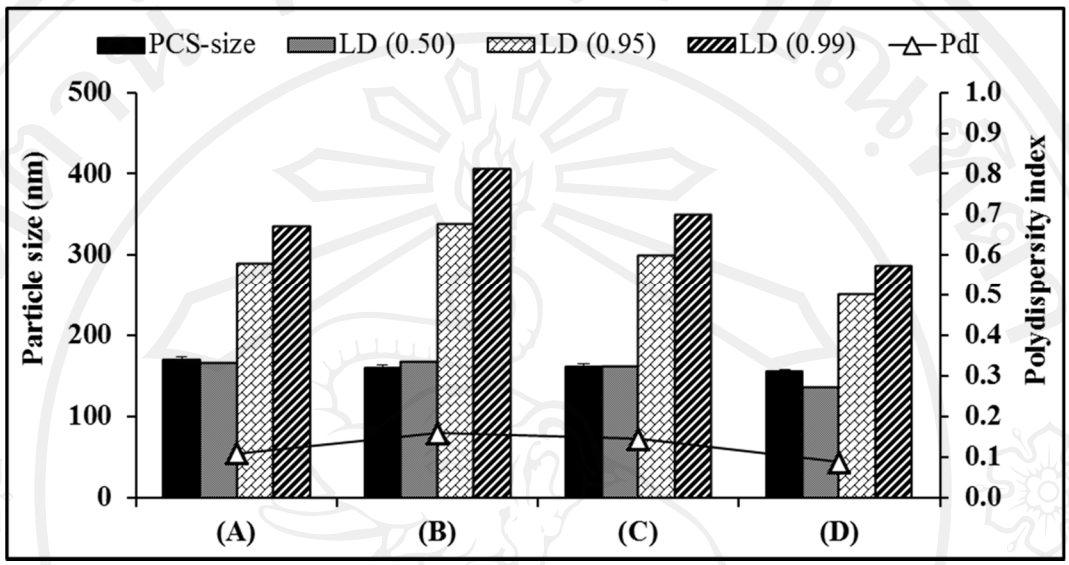

Figure 4-3-14 The particle size and size distribution of Formula 4 (A), Formula 5 (B), Formula 6 (C) and Formula 7 (D).

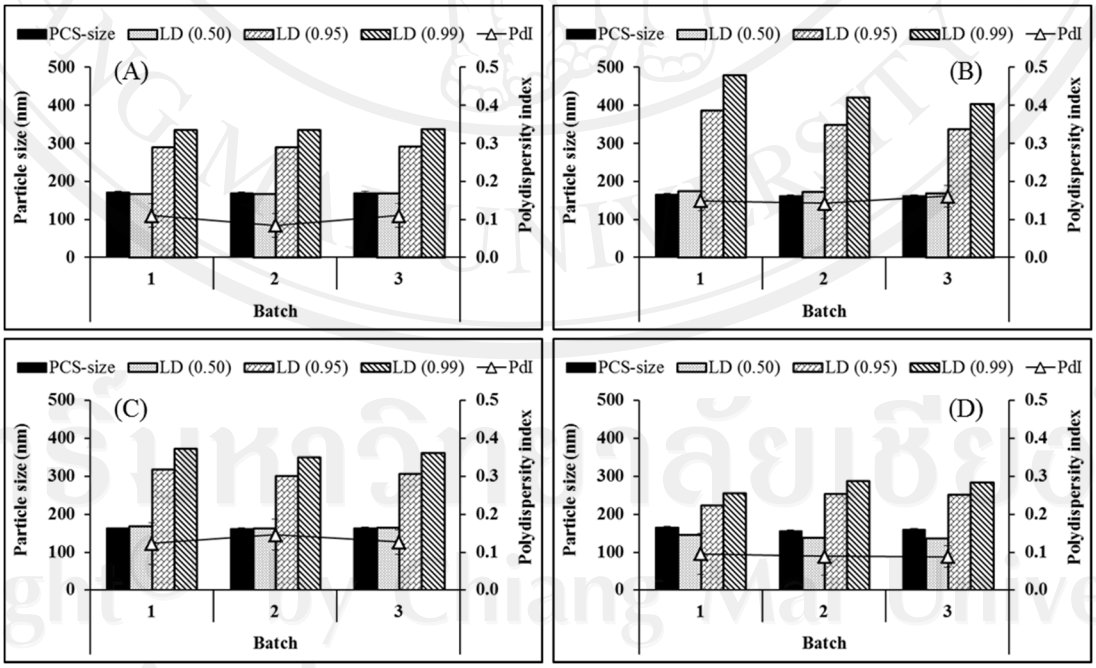

Figure 4-3-15 The particle size and size distribution of the three batches of Formula 4 (A), Formula 5 (B), Formula 6 (C) and Formula 7 (D).

1.7. Effect of rice bran oil and cholesterol on zeta potential of the internal phase

Zeta potential plays an important role in the prevention of particle agglomeration. Figure 4-3-16 shows that the zeta potentials of all formula are not significantly different. Therefore, rice bran oil or cholesterol has no influence on the zeta potential of the internal phase. Zeta potential values below -30 mV indicate good physical stability of lipid nanoparticles. The zeta potential values measured ranged from -66 mV to -74 mV. These high zeta potential values are considered to be due to the anionic groups of the surfactant used.

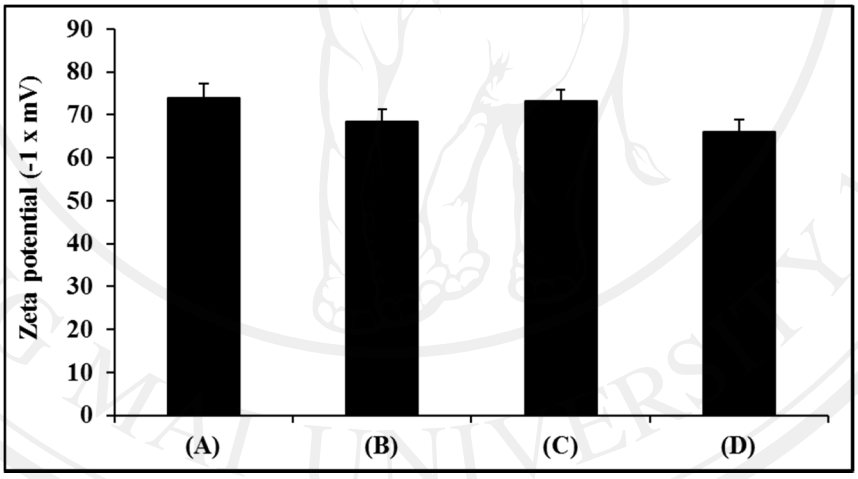

Figure 4-3-16 Zeta potential of Formula 4 (A), Formula 5 (B), Formula 6 (C) and Formula 7 (D).

1.8. Stability

The developed formulations showed constant particle size during 45 days of storage at 25°C as shown in Figure 4-3-17. This is considered to be due to the high zeta potential causing the particles to repel each other, resulting in a stable colloidal

system. According to the small particle size, Formula 6 and 7 were selected for further stability study at different temperature settings.

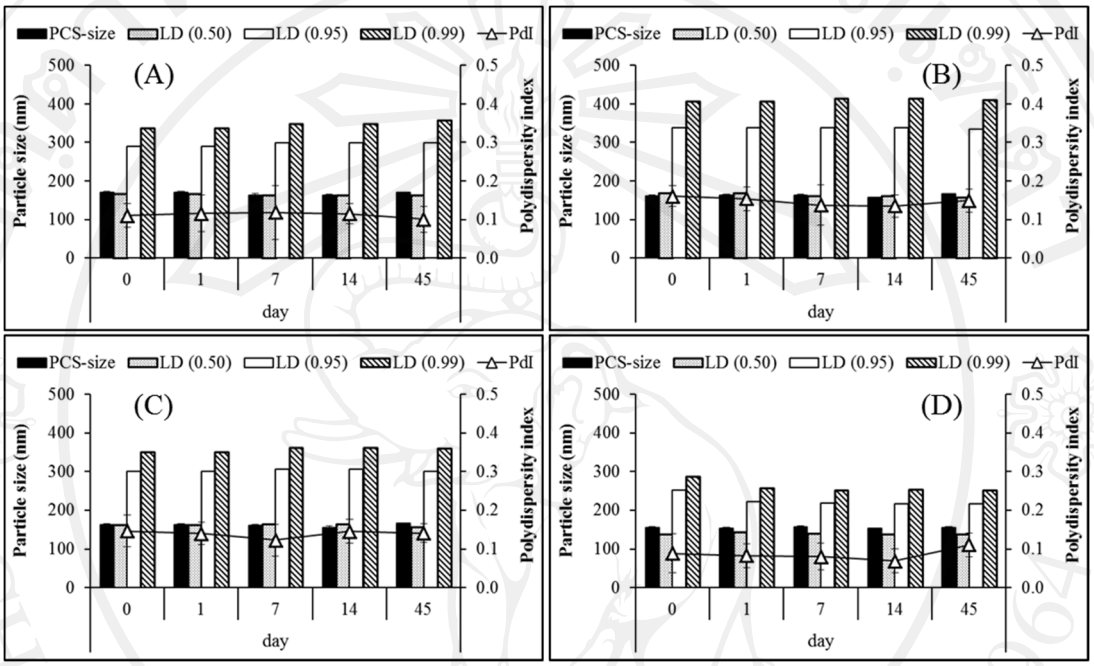

Figure 4-3-17 Particle size and size distribution of Formula 4 (A), Formula 5 (B), Formula 6 (C) and Formula 7 (D) during stored at 25°C for 45 days.

The color of the formulations was found to change from pale yellow to brown after 14 days' storage at 40°C and became dark brown at the end of the test period (45 days). The determinations of size and zeta potential for the formulations kept at 40°C after 14 days were omitted in view of the obvious degradation of the products. The particle size of Formula 6 which was kept at 4°C and 25°C stayed almost constant at 158-163 and 156-162 nm, respectively, as seen in Figures 4-3-18 (A) and 4-3-18 (B), whereas that of Formula 7 kept at both temperatures stayed at 156-163 and 152-156 nm, respectively as seen in Figures 4-3-18 (D) and 4-3-18 (E). The PdI values of the two formulas kept at 4°C and 25°C are below 0.2. Formula 6 and 7 exhibited stable

zeta potential values at ca. -73 and -66 mV, respectively during the study period (Figure 4-3-19).

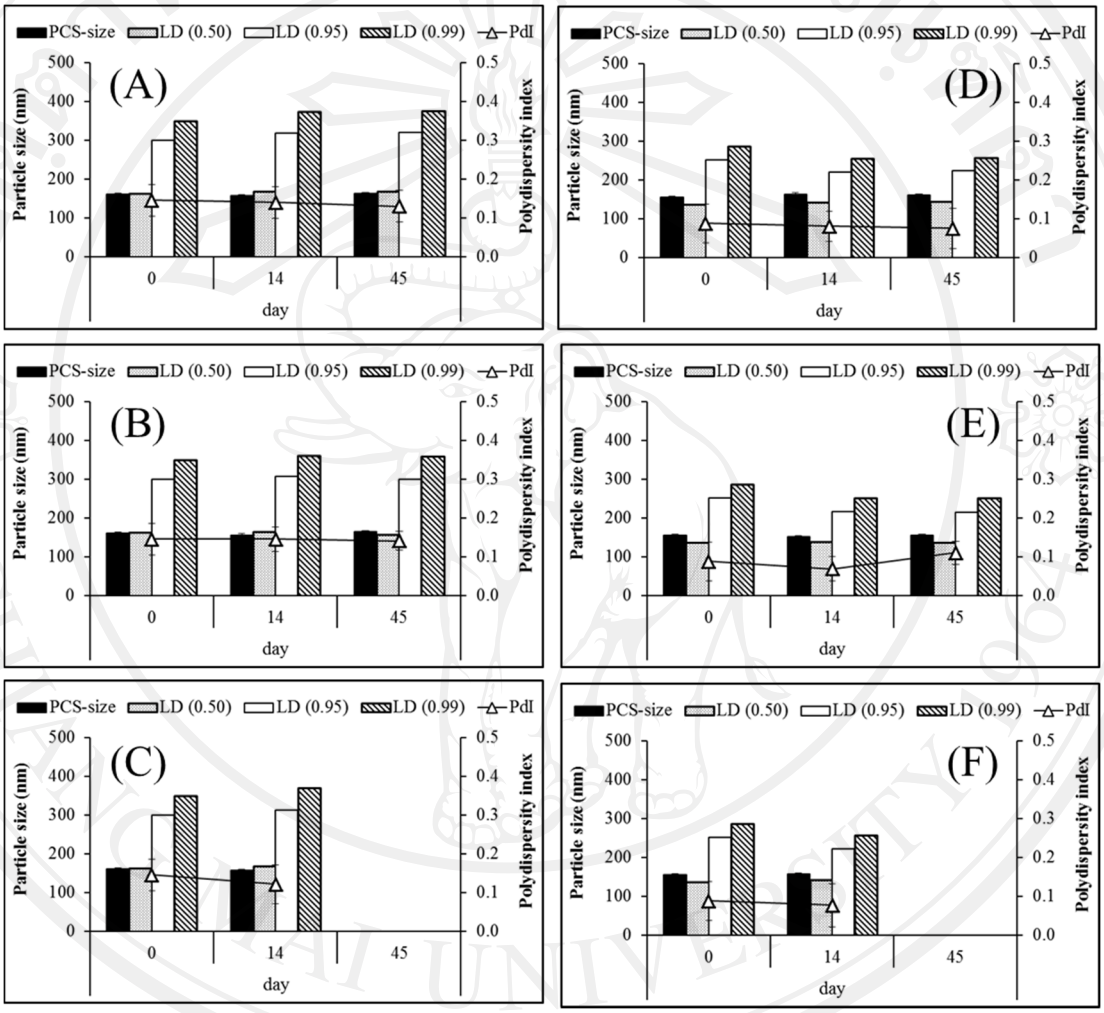

Figure 4-3-18 Particle size and size distribution of Formula 6 stored at 4°C (A), 25°C (B), and 40°C (C) and Formula 7 stored at 4°C (D), 25°C (E), and 40°C (F).

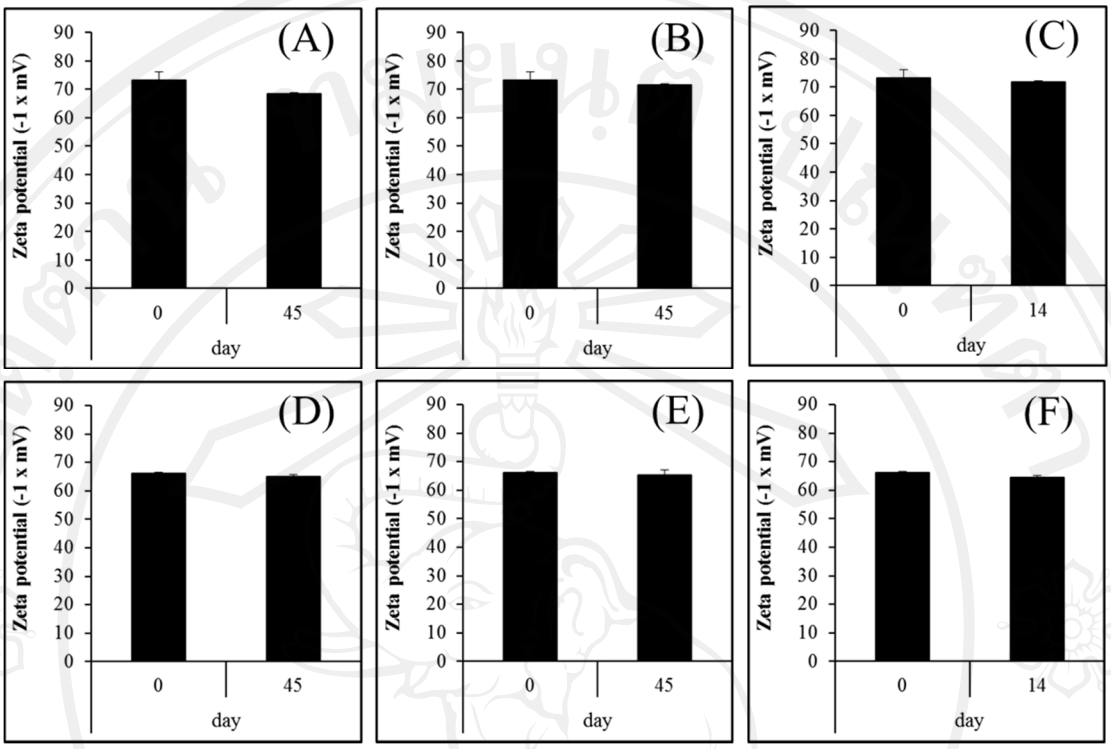

Figure 4-3-19 Zeta potential of Formula 6 stored at 4°C (A), 25°C (B), and 40°C (C) and Formula 7 stored at 4°C (D), 25°C (E), and 40°C (F).

Lycopene is an unstable molecule. It was reported that more than 95% of lycopene is degraded from a lycopene oil solution stored at room temperature for 24 h (Riangjanapatee and Okonogi, 2012). In the present study, lycopene loaded nanoemulsion, SLN, and NLC formulations were kept at 25°C for 45 days and compared with that of a lycopene oil solution. No color change was observed in the SLN and NLC formulations while the color faded rapidly in the nanoemulsion and oil solution, indicating the loss of lycopene content in these systems. This result underscores the potential of lipid nanoparticle systems for protecting lycopene from degradation in skin formulations. Chemical stability profiles of lycopene in the NLC formulations are shown in Figure 4-3-20. Formula 6 were kept at 4°C and 25ºC

showed high stability of lycopene compared with that at 40ºC as shown in Figure 4-3-20 (A). This result is in agreement with a previous study of the effect of thermal processing on lycopene degradation (Stahl and Sies, 1992). Müller *et al.* (2011) reported that the addition of oil to a solid lipid can prevent or retard the recrystallization of the lipid to form a less stable modification. Hence, over time, no changes or fewer changes in modification occur in NLC and thus no or minimized drug expulsion is observed. This can explain the retention of lycopene inside the nanoparticles of Formula 6, resulting in high chemical stability. Formula 7 was kept at 4ºC could protect lycopene from degradation for a week. However, lycopene was almost totally degraded after 3 weeks in all tested conditions of 4°C, 25°C, and 40ºC as shown in Figure 4-3-20 (B). Considering the components in Formula 7 which include the highly crystalline cholesterol, it must be assumed that after preparation, at least a part of the particles crystallizes in a higher energy modification (α or β′). During storage, these modifications can revert to the low energy, more ordered β modification. Due to its high degree of order, the number of imperfections in the crystal lattice is reduced. The drug can therefore be expelled from the nanoparticles, leading to a large quantity of drug in the water phase where it is easily degraded. The results of this study suggest that the suitable storage temperature for the developed NLC systems should not be above 25°C.

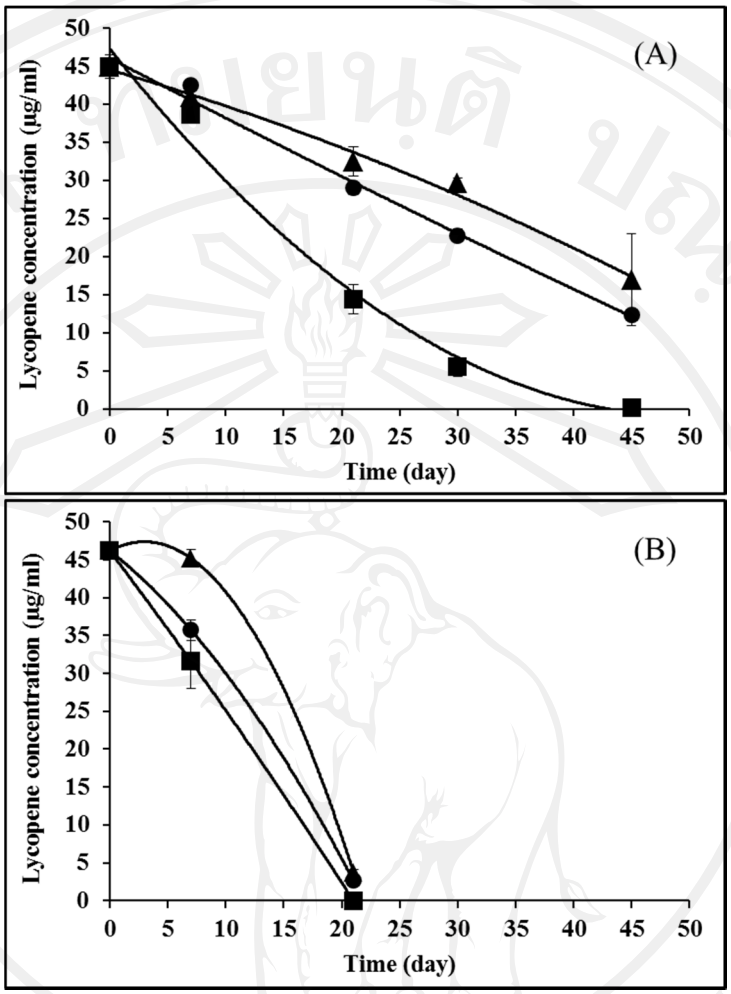

Figure 4-3-20 Effect of temperature on lycopene stability of Formula 6 (A) and Formula 7 (B)

1.9. Occlusive property

Figure 4-3-21 shows the F values of formula 4-7. The occlusion factors of lipid nanoparticle formulations (formula 5-7) were much higher than the occlusion factor of the NE (formula 4), although they had the equivalent lipid content. Formula 5-7 had melting point during 46-54°C, therefore, they are still solid at both room and skin temperature. From the literature reviews, after the water is evaporated from the SLN and NLC dispersions, only the solid particles stay on the skin. The capillary

force of the nanometer pores between the SLN/NLC particles are contractive, which promotes fusion and dense film formation. Thereby, formula 5-7 could be applied with and showed the higher occlusion factors than formula 1. Considering the dependency of the occlusion factor upon particle size of formula 2-4, formula 2 obtained the largest mean diameters observed from LD, whereas formula 4 obtained the smallest mean diameters. There is an evident correlation between occlusion and particle size. This is due to the fact that the larger particles form a film on the filter paper with larger pores. Water evaporation takes place through the pores, and if the pore diameter is increased, water evaporation takes place more readily. Moreover, film formation of smaller particles can take place more easily. Consequently, it has been found that smaller particles show higher occlusion factors. Regarding the time dependency of the occlusivity, it can be seen that for particles between 200 nm and 400 nm, the occlusion factor remains fairly constant after 24 hours. This was supposed that film formation completely took place after 24 hours. After film formation is completed, water evaporation should remain at a constant rate, as found in this study

Besides dependency of the occlusion factor upon particle size, the crystallinity of the matrix material also plays an important role for the occlusion of a system. A high degree of crystallinity of the lipid matrix leads to a high occlusive property. Therefore, the highest occlusive property of formula 4 was considered to be due to the highly crystalline cholesterol.

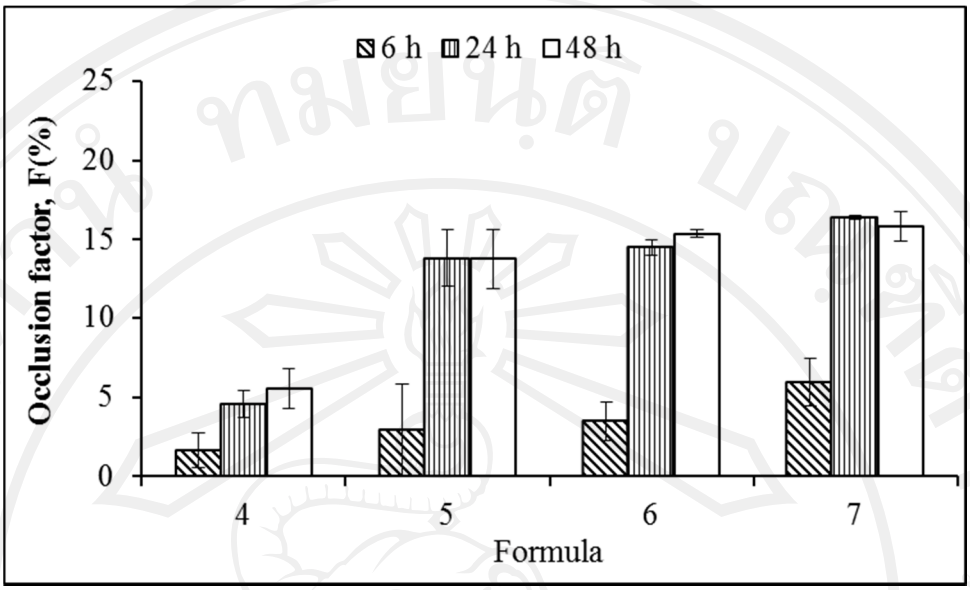

Figure 4-3-21 The occlusive properties of formula 4, 5, 6, and 7 observed at 6, 24, and 48 h.

2. The investigation on crystallization behavior of lycopene-loaded NLC

As for all drug delivery systems, detailed characterization is a major part of the research and development to ensure the generation of systems with the desired properties. In the work on lipid nanoparticle dispersions, the advantages of lipid nanocarriers (SLN and NLC) are essentially due to the solid state of the lipid matrix, the lipid crystallization is therefore an important point for the performance of the SLN and NLC carriers both *in vitro* and *in vivo* (Gonzalez-Mira and others, 2010; Mehnert and Mader, 2001). According to the low viscosity of the dispersed liquid phase, combined with the high specific surface area of colloidal dispersions, the traditional o/w emulsions cause rapid drug diffusion out of the droplet (Magenheim and others, 1993). In contrast the mobility of drug molecules is drastically reduced in a solid phase which should thus make it possible to reduce drug leakage or hydrolysis (Westesen and others, 1997). Therefore, the presence of a solid core brings many

advantages in comparison to a liquid core, that is, enhanced protection for chemically labile drugs. They also have many advantages like high adhesiveness, occlusive effects upon dermal application of which the occlusive character is based on film formation after application to the skin. The occlusion factor depends strongly on the degree of crystallinity of the lipid matrix. Noncrystalline lipid nanoparticles, i.e. supercooled melts have no occlusive properties. Moreover, the use of crystallized lipids instead of liquid lipids has been shown to increase control over release and stability of incorporated bioactives. This is because mobility of bioactives can be controlled by controlling the physical state of the lipid matrix. Therefore, to have these advantages, a crystalline status of the lipid particles is necessary. Moreover, the therapy of chronic diseases requires repeated drug administration. In the case of a short biological half-life, the drug has to be administered within short-time intervals up to several times daily. To reduce application frequency sustained formulations have been developed. Lipid nanoparticles are appropriate for this purpose because in a crystalline vehicle the drug diffusion is reduced by a factor of 10–1000 in comparison with a liquid vehicle such as a solution (Müller-Goymann, 2004; Souto and Müller, 2009,).

In fact, when some lipids (e.g. less crystalline lipids) are used for SLN production, the lipid matrix might not necessarily re-crystallize (Westesen and Bunjes, 1995). Moreover, due to the complexity involved in the crystallization process in SLN, transformation between the modifications may occur, and if the process is not carried out properly, even supercooled melts may also be obtained instead of solid particles (Weiss and others, 2008). A problem also associated with the formation of supercooled melts is usually encountered when the preparation process is

carried out by heat, such as during the preparation of SLN by melt emulsification or by hot o/w microemulsion method (Ali and others, 2010; Bunjes and others, 1998). Hence, the necessity to pay special attention to the physical state of lipid nanoparticle arises from these facts. The confirmation of the desired physical state of the matrix lipid is thus of crucial importance for the development of nanoparticles based on solid lipids. Among the multitude of analytical techniques employed for that purpose, DSC and XRD play a prominent role because they are able to provide structural information on the dispersed particles. Moreover, the use of these two techniques often leads to complementary information on the systems of interest. Unfortunately, the crystallization behavior of nanocarriers could sometimes not be or very hardly detected by the simple technique like DSC due to a very low lipid concentration or too much dilution of sample. The sensitivity of the XRD method is also low which means that an analysis of a component of less than 0.5 wt.% with respect to the total sample mass is also very difficult (Bunjes and Unruh, 2007). Therefore, the aim of this topic was to investigate and prove the crystalline status of the obtained nanocarriers.

2.1. Thermal analysis

DSC gives an insight into the melting and recrystallization behavior of crystalline material like lipid nanoparticles. The broken down of the crystal lattice by heating the sample yields inside information on, e.g. polymorphism, crystal ordering, eutectic mixtures or glass transition processes (Ford and Timmins, 1989). In the lycopene loaded NE, SLN and NLC, the drug was prior dissolved in the melted lipid phase before HPH. Therefore, the melted mixture of lycopene and lipid was analyzed by DSC to assess a possible melting point depression of the lipid and to evaluate the

crystalline character of the loaded drug (Figure 4-3-22). Since, the melting endothermic peak of lycopene around 171°C was not recorded, the complete solubilization of lycopene in the lipid matrix was then confirmed (Fang and others, 2008). Lycopene is entrapped and being molecularly dispersed (dissolved) in the lipid matrix (Souto and others, 2006).

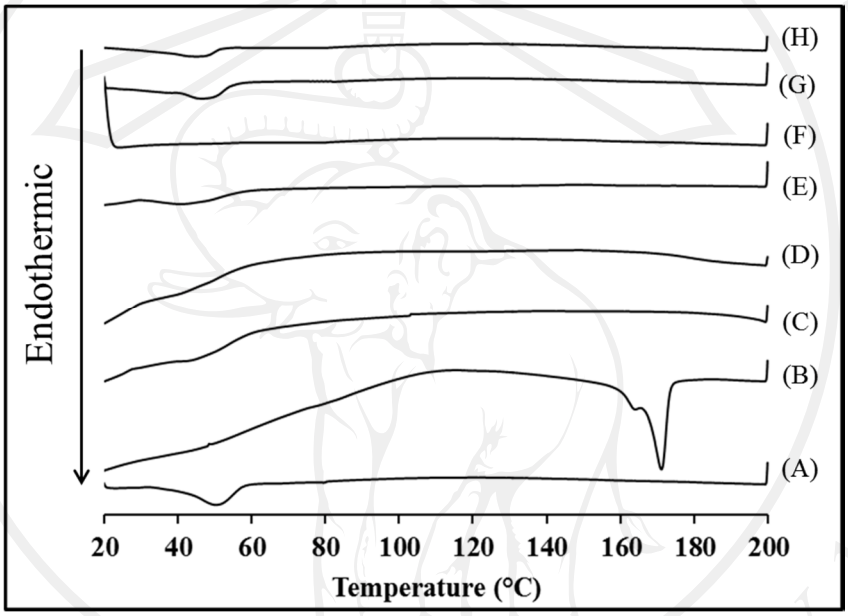

Figure 4-3-22 DSC thermograms of orange wax (A), lycopene (B), melted mixture of orange wax and lycopene (C), melted mixture of orange wax and rice bran oil (D), melted mixture of orange wax, rice bran oil, and lycopene (E), lycopene loaded NE (F), lycopene loaded SLN (G), and lycopene loaded NLC (H).

The DSC parameters from the thermograms of bulk orange wax and NE, SLN, and NLC formulations obtained are presented in Table 4-3-4. The percentage of crystallinity index (CI%) of aqueous dispersions was calculated. NE revealed no observed on melting temperature, enthalpy, and CI%. This can be assumed that this system consists of liquefied internal droplet phase or presents as an amorphous form.

The DSC analysis of bulk lipid, SLN, and NLC show a single broaden endothermic peak, with a maximum at 51.2, 49.4 and 48.4°C. Preparing the systems of SLN and NLC the CI values after 1 day of storage at room temperature found were 15.60 and 0.11% respectively. A supercooled melt might be excluded for SLN and NLC due to the presence of melting enthalpy (Teeranachaideekul and others, 2007a). However, the CI% for SLN and NLC were small (lower than 30%) meaning that lipid matrix might be in a supercooled melting state (Souto and others, 2005b). Supercooled melts are not lipid suspensions, rather systems similar to o/w emulsions (Mehnert and Mader, 2001). They describe a phenomenon that lipid crystallization may not occur, although the sample is stored at a temperature below the melting point of the lipid. Other possibilities of low CI values could be due to a very low lipid concentration and too much dilution of the sample. The physical state of nanocarriers was then very hardly detected by the simple technique like DSC. Subsequently, the calculated CI value is low. Special attention must be paid because the potential advantages of SLN and NLC over NE are linked to the solid state of the lipid. Therefore, the crystalline characteristics of lipid nanoparticle were then further investigated and clarified.

Table 4-3-4 The DSC parameters of orange wax, NE, SLN, and NLC formulations.

Sample name	Onset (°C)	Melting point(°C)	Enthalpy (J/g)	Area (mJ)	CI %
Orange wax	35.9	51.2	14.1000	19.43	100.0
NE	ND	ND	ND	ND	ND
SLN	36.5	49.4	0.1100	3.25	15.6
NLC	44.8	48.4	0.0007	0.02	0.1

(ND = not detectable)

2.2. Crystalline characterization

WAXS patterns demonstrate that orange wax possesses typical reflections at 2θ = 21.32º (d = 0.41 nm), and 2θ = 23.12º (d = 0.38 nm) as seen in Figure 4-3-23 (A). As previously described, orange wax corresponded to the β′ modification with orthorhombic perpendicular subcell unit. The WAXS pattern of lycopene (Figure 4-3-23 (B)) exhibits sharp peaks at 2 theta scattered angles of 2.64, 5.16, 21.44, 24.4, and 29.32°. Many diffraction peaks of lycopene in lycopene-orange wax mixtures are disappeared because the molecular dispersed state of lycopene in the mixture (Teeranachaideekul and others, 2007b). These results corresponded with the DSC results. However, the difference from DSC is that there is no heat supplied to the samples during WAXS measurement. Moreover, due to overlay with the peaks of lipid, the peaks of intensity occur at the interplanar distance of approximately 0.38 and 0.41 nm in the mixture were only observed as shown in Figure 4-3-23 (C). Incorporation of rice bran oil to the orange wax does not affect much on the wax crystalline structure as seen in Figure 4-3-23(D). In lycopene-orange wax mixture containing rice bran oil, the crystalline peaks are less intensity as demonstrated in Figure 4-3-23 (E), indicating that less crystalline lycopene existing in this wax-oil mixture than in the mixture without oil. The WAXS pattern of lycopene loaded NE reveals the halo pattern (Figure 4-3-23 (F)) indicating that all ingredients are in liquid or an amorphous form. The WAXS patterns of lycopene loaded SLN and NLC as shown in Figure 4-3-23 (G) and 4-3-23 (H), respectively, suggest that non-crystal materials are majority. The identical peaks of lycopene and orange wax cannot be seen. The absence of crystallinity of lycopene and orange wax in SLN and NLC dispersions is considered to be due to the major presence of water as dispersion

medium of the SLN or NLC samples. This caused the concentration of the solid ingredient to be too small or lower than the detection limit of the XRD instrument which is around 0.5-5% (Attama and others, 2008; Muchow and others, 2011). Therefore, the crystallinity of the lipid nanocarriers like SLN or NLC could hardly be detected by using WAXS. Further investigation using another higher potential instrument or technique is therefore required.

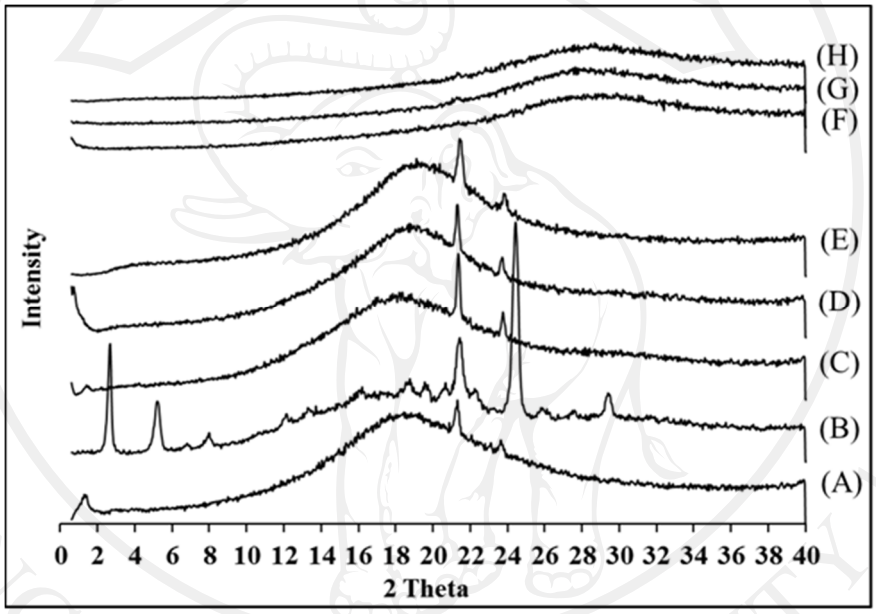

Figure 4-3-23 WAXS patterns of orange wax (A), lycopene (B), melted mixture of orange wax and lycopene (C), melted mixture of orange wax and rice bran oil (D), melted mixture of orange wax, rice bran oil, and lycopene (E), lycopene loaded NE (F), lycopene loaded SLN (G), and lycopene loaded NLC (H).

2.3. Electron diffraction mode of TEM analysis

TEM is conceptually similar to a normal microscope except that it uses electrons rather than light (photons). Electron wavelengths can be much smaller than

light wavelengths so it produces a greater magnification (Cockayne, 2007). By using the diffraction mode the obtained ED patterns from TEM yield information about the orientations and atomic arrangements in nanomaterials (Rao and Biswas, 2009). Previously, Pan *et al.* (2001) investigated nanobelts of semiconducting oxides using ED pattern to reveal single crystalline nanobelts. Zuo *et al.* (2003) showed that both high resolution and high contrast can be achieved by imaging from diffraction with a nanometer-sized coherent electron beam. These evidences show possibilities in using ED for detecting crystals. Therefore, this technique is considered to be possible in the detection of tiny crystalline in the systems like nanocarriers. The investigation on crystalline characteristics of lycopene loaded lipid nanocarriers hence was performed. The result of lycopene loaded lipid NE as in Figure 4-3-24 demonstrates only the large brighter centre dot which respects to the electron beam. There is no ED pattern of this system. This result relates to an amorphous structure of the liquid NE system. The TEM images of lycopene loaded SLN and lycopene loaded NLC are shown in Figure 4-3-25 and 4-3-26, respectively. It is found that the TEM images of these solid lipid nanocarriers are absolutely different from that of the liquid NE. The presence of diffraction spots is surely confirmed the crystalline characteristics of both SLN and NLC nanocarriers. Moreover, these specific patterns also reveal the internal structure of narrow regions of interest in nanomaterials. Many small crystals are exposed to the electron beam. The large brighter centre dot is the electron beam. Due to a variation in orientation of these crystals, the electrons follow Bragg's law and form circular patterns (rings) rather than spots; each ring corresponds to a specific lattice spacing of the nanomaterials. In the case of using polycrystalline materials in the TEM, a completely isotropic fine grained polycrystalline sample will give a diffraction pattern

of concentric rings in the zero order laue zone (ZOLZ). As the grain size increases, the rings within the diffraction pattern break up into discontinuous rings containing discrete reflections (Odo and others, 2012). The observed ED pattern of SLN and NLC are seen by the diffraction rings which are dealing with polycrystalline structure. These results clearly indicate that there is some small extent of crystalline structure in the lycopene loaded SLN and lycopene loaded NLC systems.

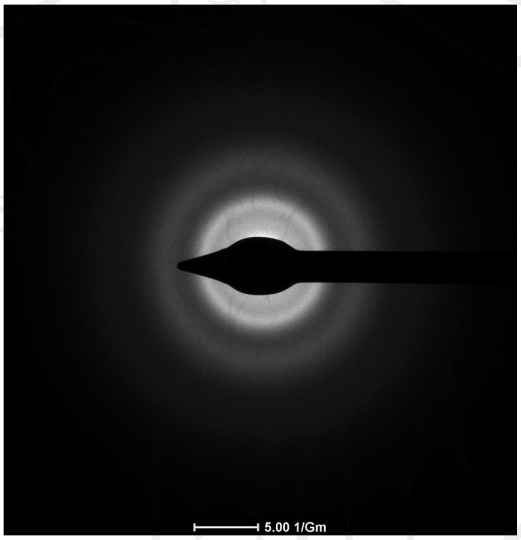

Figure 4-3-24 ED pattern of NE.

Figure 4-3-25 ED pattern of SLN.

Figure 4-3-26 ED pattern of NLC.

2.4. The bright field cryo-TEM analysis

Figure 4-3-27 shows cryo-TEM images of lycopene loaded NLC after 3 homogenization cycles at 500 bar at 75°C. On the picture the particle size range from 15-150 nm. This is well in agreement with the results obtained by PCS measurement. It was previously reported that nanoparticles with different shapes e.g. cube-shape, rode-shape and needle-shape were obtained by HPH (Müller and Peters, 1997). Lycopene loaded NLC with a spherical shape were obtained under this procedure.

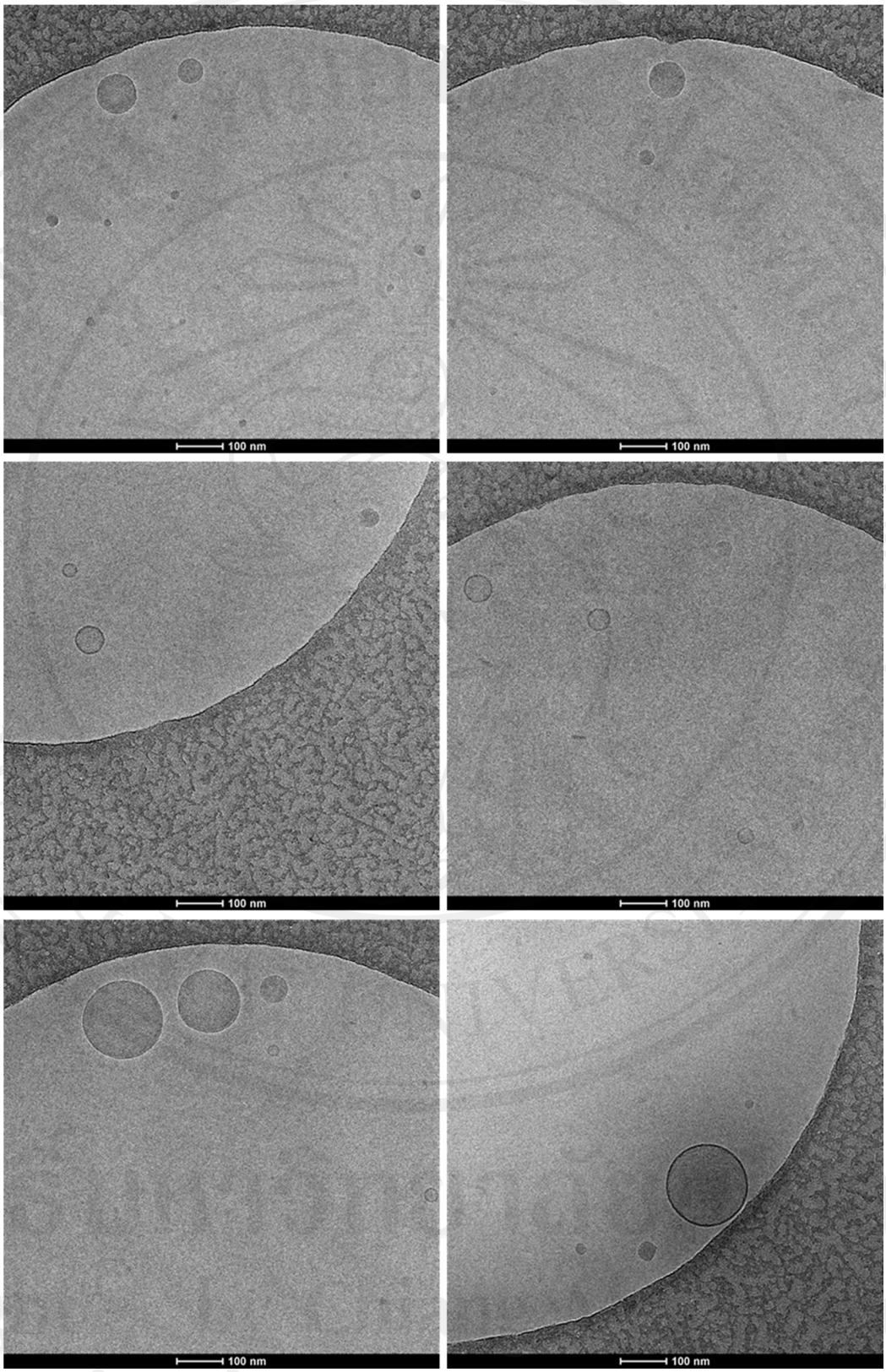

Figure 4-3-27 The bright field cryo-TEM images of lycopene loaded NLC.

<u>Part IV</u> Effect of lycopene concentration on lycopene-loaded NLC

1. Effect on the particle size and ZP

In this study, 4 different lycopene concentrations (0.000%, 0.005%, 0.025% and 0.050%) loaded NLC were prepared. It was found that the outer appearance of the four NLCs obtained were opaque liquid with yellowish orange color according to the natural color of lycopene (Figure 4-4-1). To obtain a maximum physical stability, Ostwald ripening should be avoided. Therefore, the NLC should be as homogeneous as possible and the amount of microparticles present in the formulation should be reduced as much as possible or absent (Müller and others, 1999b). The NLC samples with a particles size below 1 μm could be prepared using 3 homogenization cycles at 500 bar at 75°C. It is well known, that the achievable particle size reduction depends on the hardness of the material subjected to the homogenization process (Müller and others, 1999a). The average particle size, measured by PCS, was approximately 153.05 ± 2.66 nm for lycopene unloaded NLC dispersion. For 0.005% lycopene loaded NLC an average particle size 157.54 ± 3.37 nm was obtained using the same production conditions. Also at higher concentrations, i.e. 0.025% and 0.050% lycopene loaded, relatively small particles size were obtained under the same applied conditions, which provide evidence that lycopene nanocarrier is a soft material. The average particle size was approximately 160.07 ± 3.88 nm and 165.90 ± 4.32 nm for 0.025% and 0.050% lycopene loaded NLC, respectively. The increased diameters with higher concentration of the homogenized material can be explained *via* the power density (Krause and Müller, 2001). The production conditions were kept constant for the formulations with different concentrations, which means the energy to

disintegrate the particles was identical in all four productions despite the fact that the amount of material to be disintegrated was increased. All in all it could be shown that HPH applying 3 cycles at 500 bar at 75°C can be used to formulate lycopene loaded NLC with particles in the nanometer range and a narrow particle size distribution.

According to the DLVO theory the physical stability of a disperse system increases with increasing electrostatic repulsion energy. The electrostatic repulsion increases with increasing surface charge and increasing thickness of the diffuse layer. To investigate the surface properties of the NLC the ZP was measured. As a minimum ZP of |-30 mV| is required for a good physical stability (Müller, 1996), all NLCs under this investigation showed a ZP higher than |-30 mV| as shown in Table 4-4-1, and therefore expecting a good physical stability.

Figure 4-4-1 The outer appearance of the four NLCs obtained.

Table 4-4-1 PCS diameters, PdI and ZP values of NLC samples on freshly prepared (day 0) stored at room temperature.

Sample	Day 0		
	PCS diameters (nm)	PdI	ZP (mV)
0.000% lycopene loaded NLC	153.05 ± 2.66	0.12 ± 0.03	-73.80 ± 1.70
0.005% lycopene loaded NLC	157.54 ± 3.37	0.13 ± 0.02	-74.60 ± 1.31
0.025% lycopene loaded NLC	160.07 ± 3.88	0.14 ± 0.03	-74.17 ± 1.55
0.050% lycopene loaded NLC	165.90 ± 4.32	0.15 ± 0.05	-74.57 ± 1.95

2. Entrapment efficiency

Entrapment efficiency is defined as the percentage of drug incorporated into the lipid nanoparticles relative to the total drug added. It specifies the percentage of drug is included in the particles and how many percent of free drug are still present in the dispersion medium (Muchow and others, 2008). To assess the encapsulation parameters in colloidal carriers such as lipid nanoparticles, previous separation of the systems from the aqueous external phase is required. Once lycopene is not detected in the supernatant, it can be assumed that incorporation of lycopene into NLC was approximately 100%. In the present study, no lycopene was detected in the supernatant of all formulations. Moreover, the drug crystals could not be observed under PLM. Thus, it can be deduced that 100% EE was assumed in all formulations. This result is due to the high lipophilicity of lycopene, the high solubility of the active

both in the oil and wax, in addition to its low solubility in water. However, NLC loads with lycopene 0.005%, 0.025% and 0.050% showed an EE of about 99.81%, 99.15% and 99.39%, respectively, most likely due to only short heating process used for dissolving lycopene into lipid phase as well as the wax content protect lycopene from degradation. Therefore, small amount of lycopene was lost. From the obtained results, optimized NLC formulations were produced by HPH technique for the delivery of lycopene.

3. The *in vitro* release study

3.1. Membrane free release

This release test model allows to elucidate the mechanism of lycopene release from NLC independently of membranes. The diffusion of lycopene from NLC formulations into an oily phase was investigated over 24 h. Each sample was analyzed in triplicate. Lycopene loading might affect the release profile. It depends on the affinity of the lycopene to mix with the lipid and be enclosed in the matrix. Figure 4-4-2 shows the release profiles of lycopene from different formulations containing 0.005-0.050% of the lycopene. The biphasic release pattern was observed which revealed a fast release at the initial stage and followed by a prolonged release. The rate of release depends on the total concentration of lycopene in the formulation. A faster lycopene release was achieved by increasing lycopene concentration in the lipid phase. This is because lycopene was very well incorporated in the lipid matrix. When the lycopene enclosing capacity of lipid matrix was exceeded a faster release of the lycopene occurred.

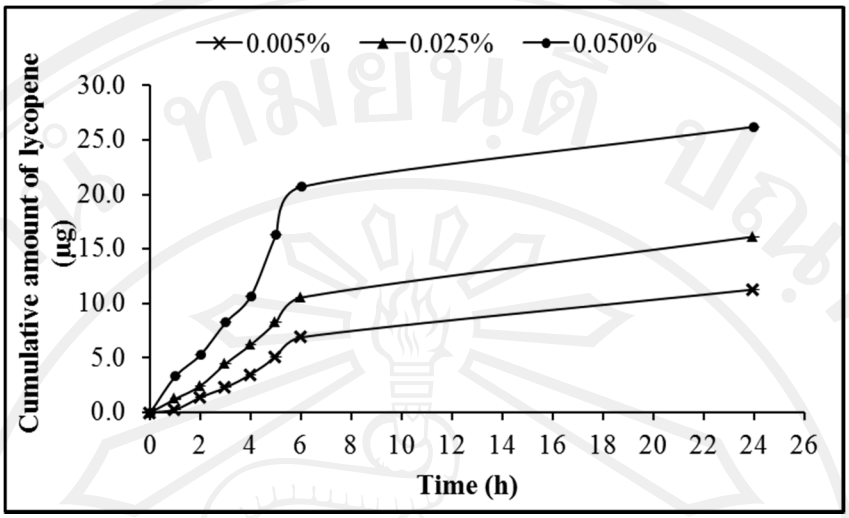

Figure 4-4-2 Cumulative amount of lycopene (µg) released from NLC over a period of 24 h independent of using membrane.

3.2. Release from membrane

According to the low solubility of lycopene in water and in buffer solution, in this study propylene glycol (PG) was selected as acceptor medium. Analysis of lycopene was performed over 24 h by spectrophotometry at 475 nm, where the peak of PG does not interfere with the peak of lycopene. In this study, sink conditions were maintained over the experiments. The release profiles obtained from different concentrations of lycopene incorporated in NLC were investigated (Figure 4-4-3). NLC dispersion containing lycopene 0.005% revealed a fast release at the initial stage, followed by a prolonged release. This biphasic release pattern was more pronounced with increasing amount of lycopene (0.025-0.05%). After 24 h, the cumulative amount released from NLC load 0.05% lycopene was higher than those from all NLC dispersions. The influence of particle size on the release profile of lycopene from NLC could be excluded because no major differences among the three NLC formulations were observed ($p > 0.05$). Furthermore, the EE of all formulations

was approximately 100%, and thus the occurrence of a fast release due to free active in the dispersion could also be excluded. The explanation might be the inhomogeneity of the oil distributed within the inner structure of lipid matrices. The different melting behavior of solid and liquid lipids can lead to accumulation of the liquid oil in the outer the shell of lipid nanoparticles after lipid crystallization. This oily layer contains also lycopene. As a result, a fast release at the initial stage of the assay has been observed (Hu and others, 2005). Factors contributing to a fast release are also the large surface area and a high diffusion coefficient due to small molecular size, and low viscosity in the matrix (Muhlen and others, 1998). The prolonged release in the second phase can be explained by slower diffusion of lycopene from the solid matrix of NLC. The solid lipid matrix has a higher viscosity, thus slowing down the release according to the law by Stokes–Einstein. The total amount release after 24 h increased from NLC containing lycopene 0.005% to 0.05%, which means with increasing amount of lycopene content.

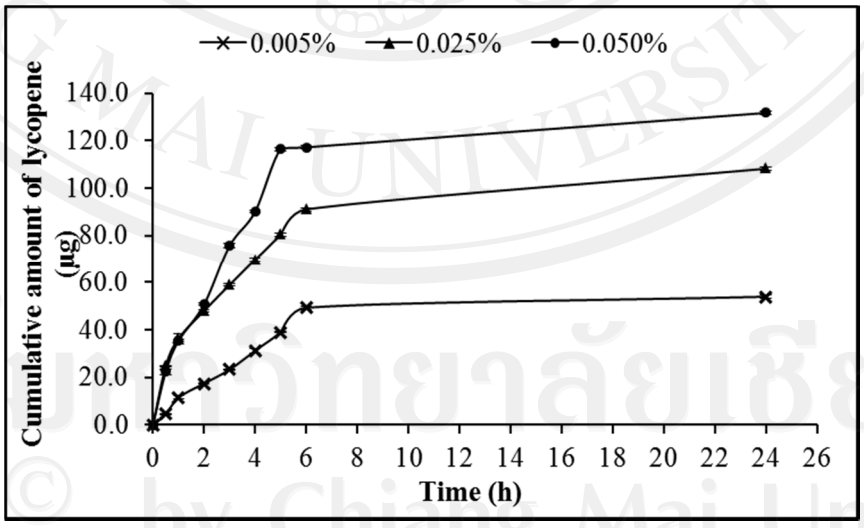

Figure 4-4-3 Cumulative amount of lycopene (µg) released from NLC over a period of 24 h using dialysis membrane.

4. Occlusive property

Increased adhesiveness to surfaces is a general property of ultrafine materials, the adhesiveness increases with decreasing particle size. That means all nanoparticles exhibit in general a distinct adhesiveness to surfaces. The lipid nanoparticles adhering to the skin lead to the formation of a film and subsequently to an occlusion effect. The occlusion effect could be proven *in vitro* by the occlusion test. From Figure 4-4-4, the occlusion factor increases by the increasing amount of lycopene incorporation. The highest occlusion factor was observed when incorporated high amount of lycopene up to 0.025-0.050%. The influence of particle size on occlusive property could be excluded because no major differences among these formulations were observed ($p > 0.05$). This high occlusion factor is considered to be due to the crystalline characteristics of lycopene in the system during the tested. When incorporate lycopene 0.005-0.05% the high occlusion value was observed during 6, 24 and 48 h could be due to the lipid film formation and the crystalline characteristics nature of lycopene. When applying the nanoparticle suspension to a surface/skin the pressure leads to fusion of the particles and finally to a dense film. This fusion is further promoted by capillary forces involved during the water evaporation process (similar to coating tablets with Eudragit @ nanoparticle dispersions) (Müller and others, 2005). Wising and Müller (2001) shows a SEM picture of such a nanoparticle film. Moreover, in Gasco *et al.* (1992) study, EM indicates that dense films are formed after drying (32°C) of SLN dispersions. This formation of the dense structure will favor occlusive effects on the skin. It is interesting to note that the films made from melts of the lipid bulk do not form close films as do dried SLN dispersions. Features of lipid nanoparticles well documented in the literature are: the film formation due to

particle adhesion (Souto and Müller, 2008; Souto and others, 2007), *in vitro* occlusion, *in vivo* increase of skin hydration as a result of occlusion (Wissing and others, 2001; Wissing and Müller, 2003a; 2003b), reduced wrinkle depth (Müller and others, 2000b), and increased penetration of actives (Chourasia and Jain, 2009; Jenning and others, 2000; Kim and others, 2009; Kuchler and others, 2009; Teeranachaideekul and others, 2008).

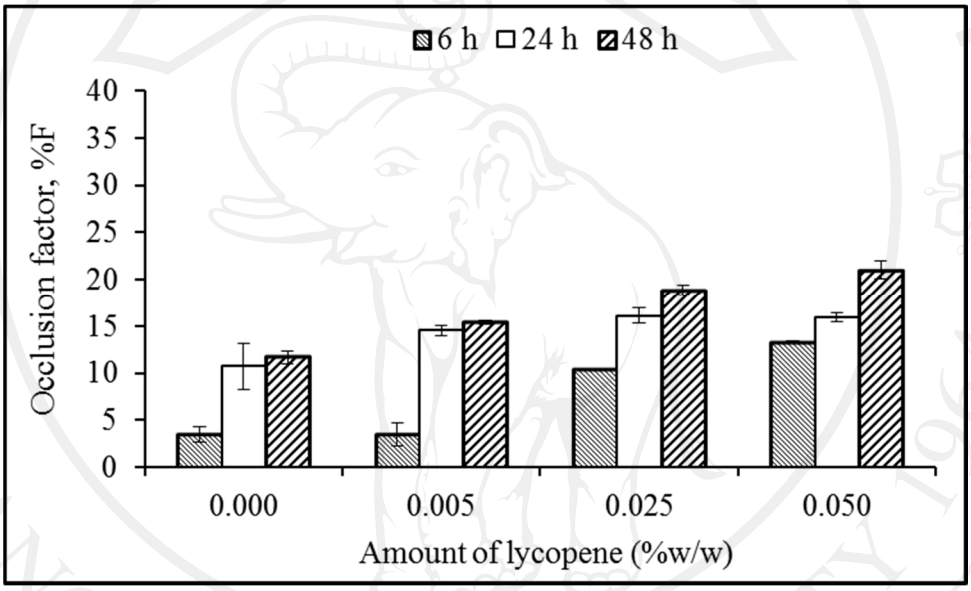

Figure 4-4-4 Occlusion factors of NLCs incorporated 0-0.05% of lycopene observed at 6, 24 and 48 h.

5. Biological action (antioxidant activities)

5.1. ABTS assay

The TEAC value is shown in Table 4-4-2. NLC samples possessed the free radical scavenging properties but in different degrees. The TEAC values ranged from 26.58 to 36.58 μM/mg. The NLC load with lycopene 0.050% exhibited the highest TEAC value of 36.58 ± 0.38 μM/mg, followed by that of 0.025 and 0.005% with

TEAC values of 33.34 ± 0.47 and 32.12 ± 0.30 μM/mg, respectively. The lowest TEAC value was obtained from NLC unload with lycopene.

Table 4-4-2 TEAC values of NLC samples by ABTS radical method.

NLC sample	TEAC (μM/mg)[a]
0.000% lycopene loaded NLC	26.58 ± 0.09
0.005% lycopene loaded NLC	32.12 ± 0.30
0.025% lycopene loaded NLC	33.34 ± 0.47
0.050% lycopene loaded NLC	36.58 ± 0.38

[a] Mean ± SD (n = 3).

5.2. DPPH assay

The IC_{50} of all NLC samples is shown in Table 4-4-3. They possessed obviously different antioxidant activities. The IC_{50} values ranged from 14.11 to 17.67 mg/mL. NLC load with lycopene 0.050% showed the highest antioxidant activity, with an IC_{50} of 14.11 ± 0.55 mg/mL, followed by NLC load with lycopene 0.025% and 0.005%, with IC_{50} values of 16.21 ± 1.21 and 16.47 ± 0.46 mg/mL, respectively. The weakest antioxidant activity was obtained from unload NLC with an IC_{50} of 17.67 ± 0.44 mg/mL. This was in good agreement with that of the ABTS assay. The relationship between TEAC values and IC_{50} of the samples gave good linearity with R^2= 0.89, as shown in Figure 4-4-5, indicating similar trends in the free radical and hydroxyl radical scavenging activities. Regarding these results, it could be considered that 0.050% lycopene loaded NLC had the highest potential.

Table 4-4-3 IC_{50} values of NLC samples by DPPH radical method.

NLC sample	IC_{50} (mg/mL)[a]
0.000% lycopene loaded NLC	17.67 ± 0.44
0.005% lycopene loaded NLC	16.47 ± 0.46
0.025% lycopene loaded NLC	16.21 ± 1.21
0.050% lycopene loaded NLC	14.11 ± 0.55

[a] Mean ± SD (n = 3).

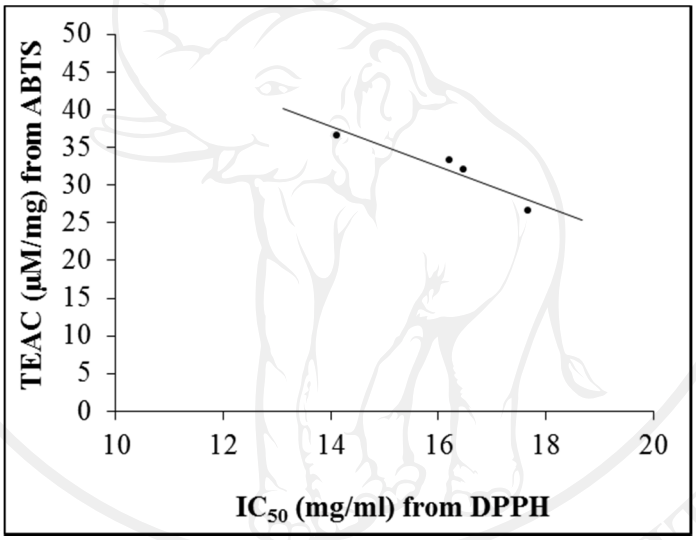

Figure 4-4-5 Correlation of antioxidant activities of NLC samples from DPPH (IC_{50}) and ABTS (TEAC) assay.

6. Stability test

The particle size and PdI values of the NLC samples stored refrigerated (4°C), at room temperature (30°C) and at 40°C was monitored up to 120 days. The particle size of NLC samples slightly increased at the end of the tested period (Table 4-4-4). The PdI values unchanged over the investigated period of time at all storage temperature (Table 4-4-5). The particle size and PdI values were stable over the investigated period of time when stored at all tested storage conditions. However, the

slightly decreasing of ZP values were observed for NLCs stored at 4°C and 30°C as shown in Table 4-4-6. The greater decreasing of ZP values were observed when stored NLCs at 40°C.

Table 4-4-4 PCS diameters of NLC samples over a period of 120 days stored at 4°C, 30°C and 40°C.

Sample	Day 0	Day 120		
	RT (30°C)	4°C	30°C	40°C
0.000% lycopene loaded NLC	153.05 ± 2.66	157.41 ± 3.01	162.22 ± 2.10	165.61 ± 3.40
0.005% lycopene loaded NLC	157.54 ± 3.37	161.65 ± 2.60	164.98 ± 2.77	169.21 ± 5.67
0.025% lycopene loaded NLC	160.07 ± 3.88	162.11 ± 3.01	163.55 ± 1.97	165.45 ± 2.41
0.050% lycopene loaded NLC	165.90 ± 4.32	167.21 ± 3.17	170.35 ± 2.91	170.31 ± 2.52

Table 4-4-5 PdI values of NLC samples over a period of 120 days stored at 4°C, 30°C and 40°C.

Sample	Day 0	Day 120		
	RT (30°C)	4°C	30°C	40°C
0.000% lycopene loaded NLC	0.12 ± 0.03	0.14 ± 0.05	0.14 ± 0.03	0.13 ± 0.03
0.005% lycopene loaded NLC	0.13 ± 0.02	0.16 ± 0.05	0.15 ± 0.03	0.15 ± 0.06
0.025% lycopene loaded NLC	0.14 ± 0.03	0.14 ± 0.03	0.13 ± 0.04	0.14 ± 0.03
0.050% lycopene loaded NLC	0.15 ± 0.05	0.15 ± 0.04	0.13 ± 0.05	0.15 ± 0.04

Table 4-4-6 ZP values of NLC samples over a period of 120 days stored at 4°C, 30°C and 40°C.

Sample	Day 0	Day 120		
	RT (30°C)	4°C	30°C	40°C
0.000% lycopene loaded NLC	-73.80 ± 1.70	-70.23 ± 2.02	-69.17 ± 1.62	-66.73 ± 1.61
0.005% lycopene loaded NLC	-74.60 ± 1.31	-72.37 ± 0.91	-71.70 ± 0.35	-68.40 ± 0.49
0.025% lycopene loaded NLC	-74.17 ± 1.55	-70.70 ± 0.92	-70.57 ± 0.75	-68.30 ± 0.10
0.050% lycopene loaded NLC	-74.57 ± 1.95	-72.03 ± 0.45	-70.00 ± 0.36	-67.83 ± 0.23

At the end of the tested period, the color of NLC stored at 30°C and 40°C was changed to dark brown. The color of NLC samples stored at 40°C started to become light brown on day 60. The color of NLC samples stored at 30°C started to become light brown on day 90. Since this, lycopene loaded NLCs were susceptible to degrade since 60 days stored at 40°C and 90 days stored at 30°C. Figure 4-4-6 (A-C) shows the chemical stability profiles of 0.005-0.050% lycopene loaded NLCs stored at 4°C, 30°C and 40°C. Since lycopene is very susceptible to oxidation when exposure to air and light resulting from many conjugated double bonds in its molecule (Sharma and Mague, 1996). NLC was reported to have an excellent protection of incorporated labile drugs from degradation (Wissing and others, 2004). Therefore, the utilization of NLC to increase the stability of lycopene is challenge. In this study, it was found that the degradation profile of lycopene was extremely retarded when stored at 4°C as

shown in Figured 4-4-6 (A-C). NLC dispersions loaded with 0.05% lycopene was selected for further incorporation into the base cream.

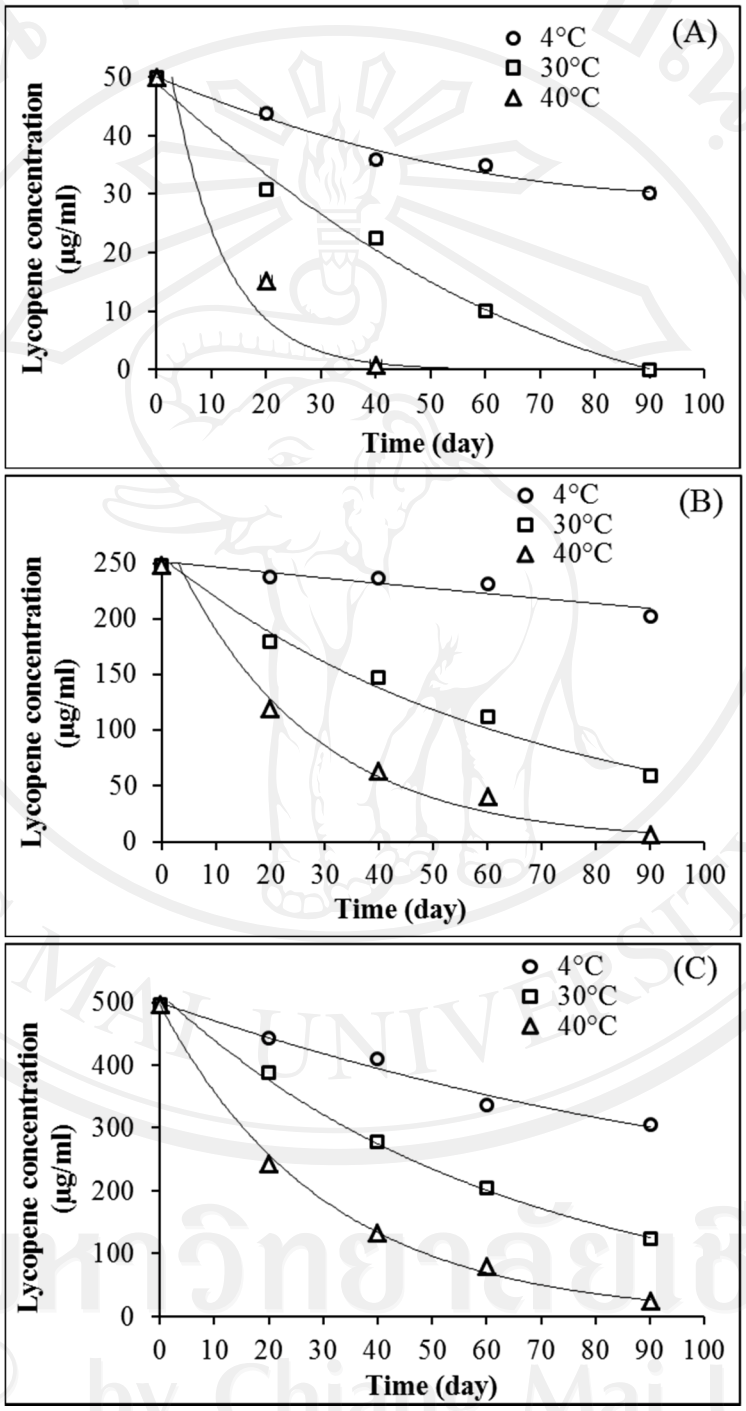

Figure 4-4-6 Stability profiles of lycopene concentration in NLC dispersions loaded with lycopene 0.005% (A), 0.025% (B) and 0.050% (C).

<u>Part V</u> Preparation and evaluation of topical dosage forms

The appearance of a cosmetic product is an important aspect that the pharmaceutical technologist or cosmetic formulator should keep in mind. In order to avoid particle aggregation one interesting approach, especially concerning the development of semisolid formulations, is the incorporation of lipid nanoparticles in base creams. The suitable selected NLC dispersion (10%) was added to yield the final preparations contained lycopene at a concentration of 0.005%. The goal is to obtain systems with long shelf life. In this section, the 7 semisolid cream formulations containing NLC dispersions were developed as seen in Figure 4-5-1. The details of formulations are shown in Table 4-5-1. The characteristic of NLC creams were described in Table 4-5-2.

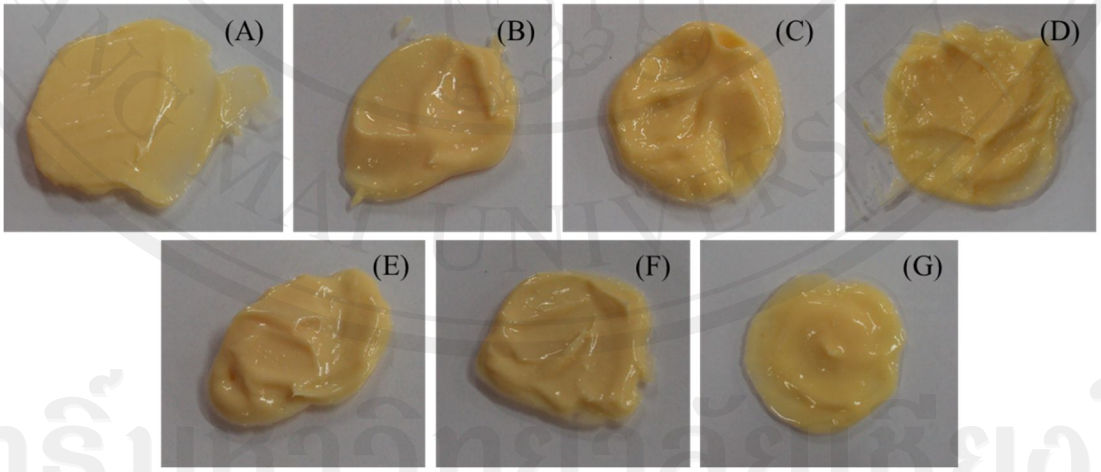

Figure 4-5-1 The physical appearance of 7 semisolid cream formulations containing NLC of which the composition of ingredients is detailed in Table 4-5-1.

Table 4-5-1 The amount of ingredients (%w/w) in 7 semisolid cream formulations containing NLC dispersion.

Ingredients	Formulations (% w/w)						
	1	2	3	4	5	6	7
Cetyl alcohol	7.00	7.00	7.00	7.00	7.00	7.00	7.00
Stearyl alcohol	3.00	3.00	3.00	3.00	3.00	3.00	3.00
Inutec^{TM} SP1	2.00	2.00	-	-	2.00	2.00	-
Montanov^{TM} L	1.00	-	1.00	-	1.00	-	1.00
Tegocare^{TM} 450	2.00	-	-	2.00	-	2.00	2.00
Rice bran oil	5.00	5.00	5.00	5.00	5.00	5.00	5.00
BHT	0.50	0.50	0.50	0.50	0.50	0.50	0.50
NLC dispersion	10.00	10.00	10.00	10.00	10.00	10.00	10.00
Salicylic acid	1.00	1.00	1.00	1.00	1.00	1.00	1.00
Propylene glycol	5.00	5.00	5.00	5.00	5.00	5.00	5.00
Concentration paraben	1.00	1.00	1.00	1.00	1.00	1.00	1.00
Sodium metabisulfite	0.01	0.01	0.01	0.01	0.01	0.01	0.01
Disodium EDTA	0.01	0.01	0.01	0.01	0.01	0.01	0.01
Glycerin	5.00	5.00	5.00	5.00	5.00	5.00	5.00
MilliQ water qs	100	100	100	100	100	100	100

Table 4-5-2 The texture of 7 semisolid cream formulations containing NLC.

Formula	Type	Physical appearance/texture	
		Day 0	Day 60
1	cream	smooth, soft, uniformity	uniformity
2	cream	smooth, soft, uniformity	uniformity
3	lotion	smooth, soft, uniformity	uniformity, white needle crystals remained after applied on the skin
4	cream	smooth, soft, uniformity	uniformity, white needle crystals remained after applied on the skin
5	cream	smooth, soft, uniformity	uniformity
6	cream	smooth, soft, uniformity	uniformity
7	cream	smooth, soft, uniformity, glossy	uniformity, glossy, white needle crystals remained after applied on the skin

1. Occlusive property

An occlusion effect is desired for cosmetic and also for pharmaceutical topical formulations. The occlusion of the skin increases skin hydration. This has a smoothing effect on wrinkles, due to the increased hydration, and the penetration of active ingredients is promoted. This can be beneficial for a skin caring effect and also for the therapeutic efficiency of dermal drugs. Occlusion can be obtained by applying a patch, which is not very practical. Occlusion effects can also be created by applying dense films of lipid or paraffin (e.g. petrolatum, vaselinum). There are undesired aesthetic effects, e.g. petrolatum is fatty and greasy on the skin. More suitable are lipid nanoparticle formulations, which have some occlusive effect due to the lipid film formation on the skin.

In order to assess the occlusion properties of cream containing NLC dispersions, an occlusion test was performed in which they were compared to an occlusive cream base system. Applying creams containing aqueous NLC dispersion yielded a higher occlusion effect with occlusion factors of about 26-50 after 6 hours compared with the base creams with occlusion factors of about 2-33, as can be seen in Figure 4-5-2. Particularly at this first time point after 6 hours, the higher occlusion effect of the 7 NLC creams compared to the base creams is pronounced. Even after 24 hours and 48 hours, the higher occlusion factor of the NLC creams is clearly visible. The highest occlusion effect was obtained from NLC cream formulation 1 followed by formulation 6, 5, 7, 2, 4 and 3. The higher occlusion effect of the NLC creams over the base creams can be attributed to the advantages from the dispersed lipid nanoparticles.

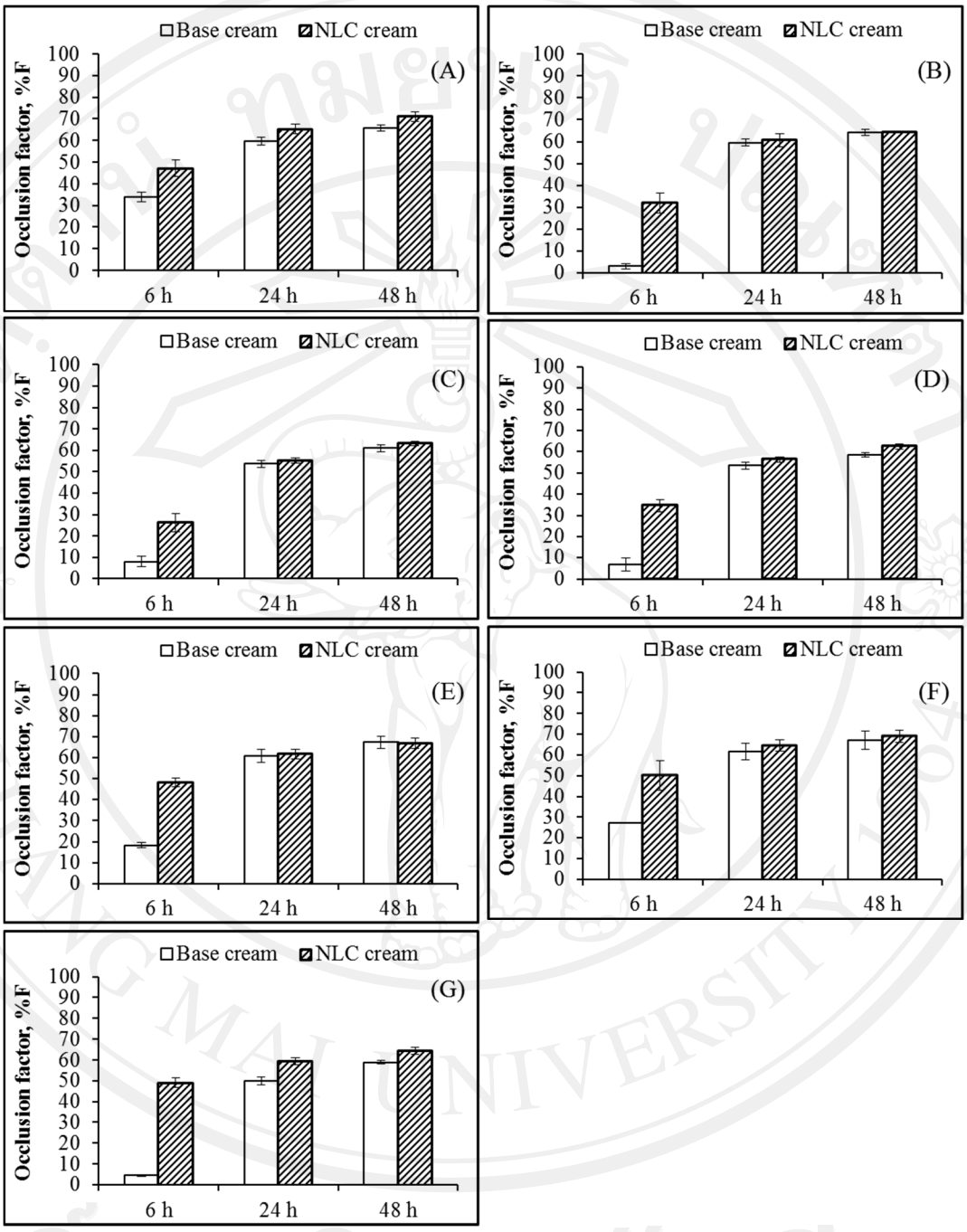

Figure 4-5-2 Occlusion factors of base creams and NLC creams of formulation 1 (A), formulation 2 (B), formulation 3 (C), formulation 4 (D), formulation 5 (E), formulation 6 (F) and formulation 7 (G) observed at 6, 24 and 48 h.

2. Stability test

Figure 4-5-3 shows the chemical stability of lycopene after incorporation in 7 base cream formulations. The good chemical stability of lycopene is proven by these stability measurements. Only 89.5% of lycopene concentration remained in NLC cream formula 3, whereas higher than 91% of lycopene concentration remained in the rest NLC cream formulations after 60 days stored at room temperature.

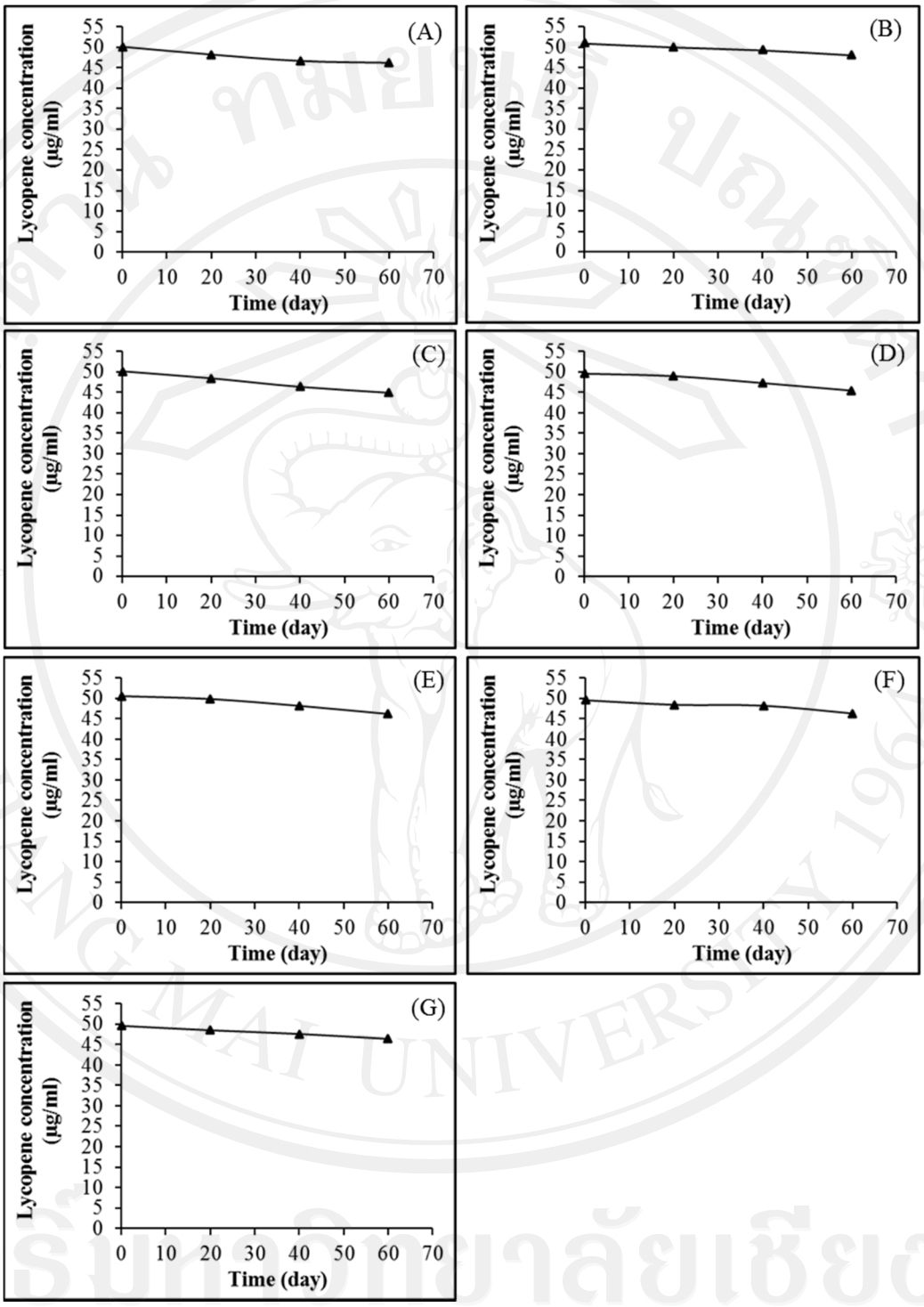

Figure 4-5-3 Stability profiles of lycopene concentration in NLC cream formulation 1 (A), formulation 2 (B), formulation 3 (C), formulation 4 (D), formulation 5 (E), formulation 6 (F) and formulation 7 (G) stored at room temperature.

3. Antioxidant activities

3.1. ABTS assay

TEAC values of base creams and NLC creams of formulation 1-7 were shown in Figure 4-5-4. The TEAC values of base creams ranged from 163 to 245 µM/mg, whereas the TEAC values of NLC creams ranged from 273 to 308 µM/mg. No significant difference of TEAC values among base creams and among NLC creams themselves. However, incorporation of NLC dispersion into cream bases significantly increased TEAC values of base creams.

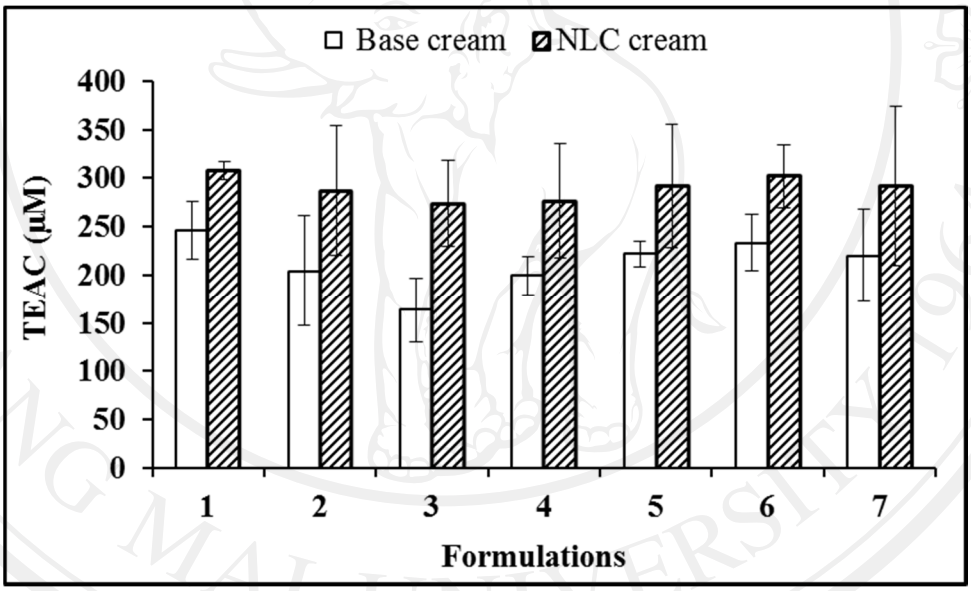

Figure 4-5-4 TEAC values of base creams and NLC creams of formulation 1-7.

3.2. DPPH assay

IC_{50} values of base creams and NLC creams of formulation 1-7 were shown in Figure 4-5-5. The IC_{50} values of base creams ranged from 0.19 to 0.24 mg/mL, whereas the IC_{50} values of NLC creams ranged from 0.14 to 0.18 mg/mL. No significant difference of IC_{50} values among base creams and among NLC creams themselves. However, the IC_{50} values of NLC creams were significantly lower than

base creams which indicated the improvement of antioxidant capacities. This was in good agreement with that of the ABTS assay. The relationship between TEAC values and IC_{50} of the samples gave good linearity with R^2= 0.94, as shown in Figure 4-5-6, indicating similar trends in the free radical and hydroxyl radical scavenging activities.

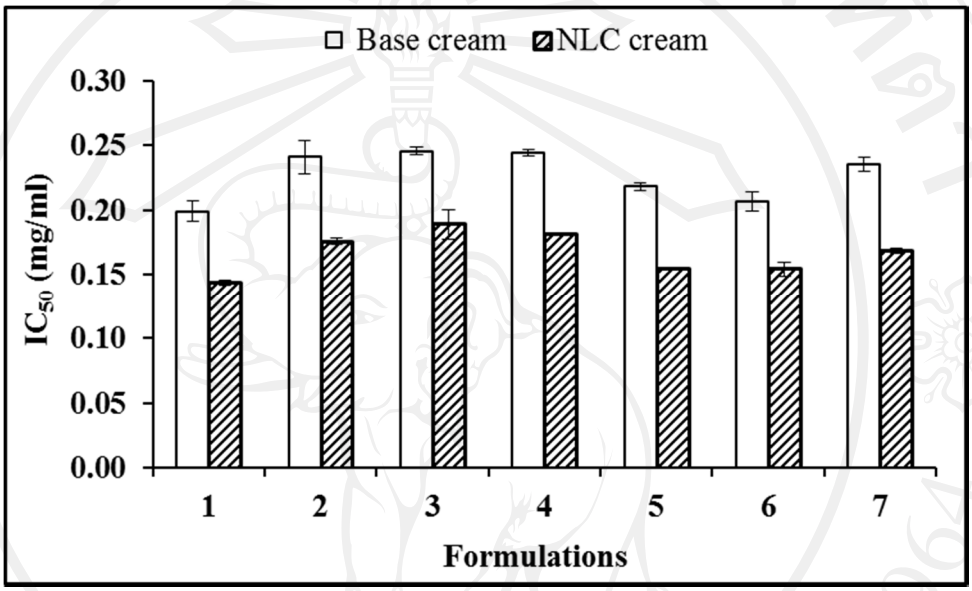

Figure 4-5-5 IC_{50} values of base creams and NLC creams of formulation 1-7.

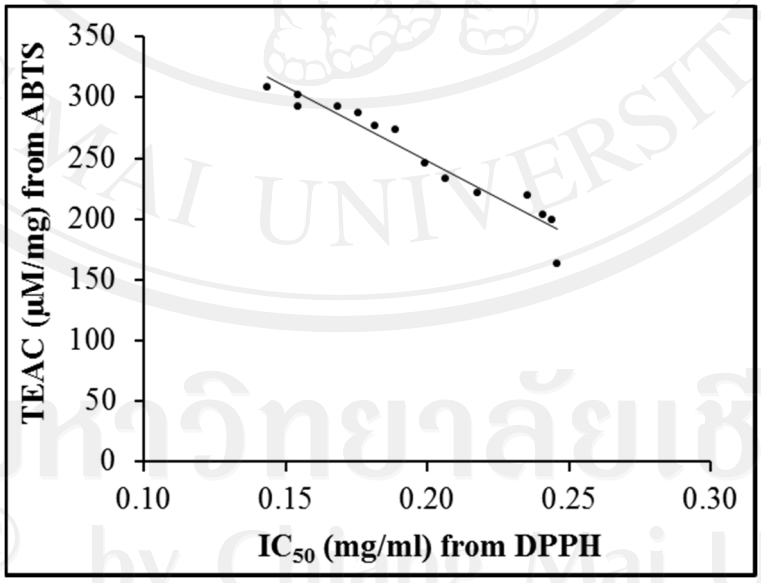

Figure 4-5-6 Correlation of antioxidant activities of base creams and NLC creams from DPPH (IC_{50}) and ABTS (TEAC) assay.